Characterization of the intraspecific variation within the nickel (Ni) hyperaccumulator species *Senecio coronatus* (Asteraceae):

A preliminary analysis of genetic population structure and shoot proteome expression

Michael Wolf

Supervisor:

Dr Robert Ingle (Department of Molecular and Cell Biology)

Co-supervisors:

Dr Jacqueline Bishop (Department of Biological Sciences)

Dr Muthama Muasya (Department of Biological Sciences)

Department of Molecular and Cell Biology

Faculty of Science

University of Cape Town

Thesis presented for the degree of Master of Science at the University of Cape Town

September 2013

Plagiarism declaration

"I, the undersigned, know the meaning of plagiarism and hereby state that all work presented in this document is my own, excepting studies and/or data properly acknowledged"

_____

Signature: Michael Wolf

_____

Date

Abstract

Heavy metal (HM) accumulator plants possess the ability to actively hyperaccumulate and detoxify exceptionally high concentrations of metals in their aboveground tissues, without exhibiting any apparent signs of toxicity. Despite nickel (Ni) hyperaccumulator plants representing the largest percentage of known metal accumulator taxa (over 75%), the underlying genetic and molecular basis of Ni accumulation remains unclear. A prominent difficulty in understanding Ni hyperaccumulation has been the severe lack of intraspecific variation in the trait. Hence, the study of a single species exhibiting a significant degree of variation is highly desirable, as it avoids the use of inter-species comparative studies mostly utilized to date. The Ni hyperaccumulator *Senecio coronatus* (Asteraceae) has been reported to contain a significant degree of phenotypic plasticity with respect to the amount accumulated and subsequent cellular distribution of Ni. This apparent intraspecific variation means that *S. coronatus* may represent a useful system in which to study Ni hyperaccumulation. No population genetics study has been carried out to date on this species, and the evolutionary relationships between hyper and non-accumulator populations were unknown. Here, results are presented from a genetic analysis of 15 naturally occurring *S. coronatus* populations. Analysis of molecular variance (AMOVA) and phylogenetic analysis (based on non-coding nuclear and plastid markers) suggest that Ni accumulation may have evolved twice within *S. coronatus*, as hyperaccumulator plants from site Kaapsehoop, cluster with non-accumulating serpentine populations and demonstrate distinct genetic differentiation from other accumulator populations. Four populations were selected for a preliminary comparative shoot proteome analysis by means of two-dimensional SDS-polyacrylamide gel electrophoresis (2D SDS-PAGE) to identify proteins potentially involved in Ni hyperaccumulation. This analysis identified nine chloroplastic proteins involved in plant energy production and metabolism as overexpressed in hyperaccumulator plants from Agnus Mine and Kaapsehoop, compared to hypertolerant non-accumulator and non-serpentine plants from Galaxy Mine and Pullen Farm, respectively. However, no difference in photosynthetic efficiency, as determined by chlorophyll fluorescence measurements, was detected between these populations.

Acknowledgements

I would like to recognize Prof Kevin Balkwill (University of Witwatersrand), whose hospitality; assistance in navigation and sample acquisition was invaluable to this study. Thanks must also go to Dr Jacqueline Bishop for her intellectual input towards our genetic structure analysis. Further, I would like to express thanks to Dr. Muthama Muasya who provided his intellectual input as well as the bulk of funding towards our DNA sequencing costs. I would also like to thank the National Research Foundation (NRF) and the University of Cape Town (UCT) for their generous financial support during my studies.

I would further like to thank all the members of my lab (430) past and present, namely; Lindsay, Delroy, Anastashia and Lance. And most notably, to my supervisor, Dr Robert Ingle, who gave me this opportunity to work on this project, I would like to express my sincere gratitude for all his knowledge, patience and guidance.

Finally, to all the people, friends and family that gave their support and encouragement, I cannot even begin to express my humility and appreciation. Specifically, to my Mother, Father, all my sisters, Uncle Richard, Erfan and Caroline, thank you all for everything big and small.

Table of contents

List of figures

List of tables

Chapter 1

Introduction

1.1 What constitutes plant heavy metal hyperaccumulation?

The vast majority of plant species worldwide are sensitive to elevated concentrations of trace elements, in particular heavy metals (HM) (Mithöfer *et al.,* 2004). From an elemental viewpoint heavy metals are defined as any transition metal with an atomic mass over 20 and a specific gravity greater than five (Parker, 1989; Lozet & Mathieu, 1991; Rascio & Navari-Izzo, 2011). In a biological context however, the use of the term HM has been both inaccurate as well as inconsistent. A prominent drawback with the term 'heavy metal' is that the physical properties (such as density) of a given metal have little or no bearing on the toxicity of the final compound formed after chemical transformation to a plant accessible nutrient (such as a salt). Nonetheless, many essential elements required for plant growth are often termed 'heavy metals'. Elements such as Co, Cu, Fe, Mn, Mo, Ni, and Zn are known to be essential micronutrients for proper plant growth and development. However, once the internal concentration of a micronutrient exceeds a certain threshold, said micronutrient is then considered toxic (Duffus, 2002; Appenroth, 2010).

Abiotic stress associated with excessive plant-metal uptake, often causes an accelerated production of reactive oxygen species (ROS) (Mithöfer *et al.,* 2004; Zhang & Qiu, 2007). The resulting oxidative damage to the plant's photosynthetic machinery and macromolecules such as DNA, proteins and lipids, disrupts regular tissue growth and cell maintenance (Cho & Seo, 2005; Cramer *et al.,* 2011). A relatively small number of plant species however, possess the ability to accumulate and detoxify exceptionally high concentrations of heavy metals in their aboveground organs, without exhibiting any apparent signs of toxicity

(Milner & Kochian, 2008). This group of extraordinary plants is known as heavy metal hypertolerant hyperaccumulators or simply hyperaccumulators.

1.2 Metal-rich soils provide an evolutionary pressure on local plant occurrences

Endemic hyperaccumulator occurrence on metal-rich soils has been documented for many decades, with hyperaccumulators predominantly restricted to natural metalliferous outcrops or sites enriched with HM due to anthropogenic activities such as mining (Lefèbvre & Vernet, 1990).

Naturally occurring metal-rich soils include serpentine soils derived from ultramafic rock types that are characterized by high divalent metal content (in particular Co, Cr, Ni), a low nutrient content (specifically K, P, N) and a high Mg/Ca ratio (Chiarucci & Baker, 2007; Galardi *et al*., 2007). Calcareous soils are similarly characterized by high divalent metal content (in particular Cd, Pb, Zn) and a low nutrient content, but differ to serpentine soils in that calcareous soils display a low Mg/Ca, and are often of an alkaline pH (Pawlowska *et al.,* 1996; Murphy, 2002). Due to the extreme cytotoxic potential of HM ions coupled with inadequate mineral content, metalliferous outcrops are hostile environments for most vascular plant taxa. Consequently, metalliferous outcrops seemingly provide a significant selective pressure on the evolution of hypertolerant species and further, appear to present restricted naturally occurring 'ecological islands', which could provide further insight into possible plant speciation mechanisms (Wild & Bradshaw, 1977; Lefèbvre & Vernet, 1990; Mengoni *et al.,* 2003).

Sources of anthropogenic metal contamination are both varied and globally widespread. The major cause of anthropogenic metal emission however, comes from mining activities together with downstream mineral processing techniques. For example, cadmium is often released as a by-product of zinc refining (Hutton & Symon, 1986; Nriagu, 1989). Mining processes can also result in metal emissions persisting in the environment for years after mining activity has ceased. Hard rock mines which usually take 5-15 years to deplete mineral sources, are reported to release metal contaminates for hundreds of years after

all mining has been stopped. A compounding problem with mining associated metal emission is that often the metals released leach into underground waterways or simply run-off into surface waters, resulting in rapid and widespread distribution of metal contaminants. This persistent metal emission consequently allows for HM hypertolerant plant colonization. Other activities connected to environmental metal emission include, disposal of cosmetics and manufacture of sodium hydroxide (mercury), smelting of metals, automobile exhaust fumes as well as paint degradation (lead-based) (Duruibe *et al.,* 2007).

1.3 A concentration criterion for defining heavy metal hyperaccumulation

The first instance of HM hyperaccumulation was described in 1865 (Sachs, 1865; Baumann, 1885) in the cadmium/zinc hyperaccumulator *Thlaspi caerulescens* J. & C. Presl [or *Noccaea caerulescens* (J. & C. Presl) F. K. Mey]. Sometime later (1948), nickel hyperaccumulation was discovered in *Alyssum bertolonii*, which together with *Thlaspi caerulescens* belongs to the family Brassicaceae (Minguzzi & Vergnano, 1948; Reeves & Baker, 2000). Currently, in the order of 400 - 500 plant species have been identified as hyperaccumulators, accounting for approximately 0.2% of all angiosperms (Verbruggen *et al.,* 2009). With respect to phylogenetic relatedness, evolution towards HM hyperaccumulation has occurred independently multiple times with the greatest occurrence within the Brassicaceae. The majority of Cd/Zn hyperaccumulators belong to Brassicaceae, and together with the Euphorbiaceae family contain approximately half of all know Ni hyperaccumulators (Krämer, 2010).

Markedly, Ni hyperaccumulating plant taxa account for approximately 80% of all hyperaccumulating species (table 1.1), which is likely a reflection of the global distribution and prevalence of Ni serpentine outcrops (Brooks *et al.,* 1974; Brooks, 1983; Reeves *et al*., 1983). However, while Ni hyperaccumulators are the most common group, relatively little is known about the molecular basis of Ni hyperaccumulation. In contrast, a number of key genes underpinning Cd/Zn hyperaccumulation have been identified in recent years (sections 1.7 & 1.9).

The concentration criterion used to define HM hyperaccumulation reflects the abundance and toxicity of the metal ion concerned, and typically ranges from 100 - 10 000 parts per million (on a dry biomass basis) in aboveground tissues (table 1.1). For example, less toxic metal ions such as Zn^{2+} are considered to be hyperaccumulated at concentrations exceeding 10 000 ppm, whereas a considerably more toxic metal ion such as Cd^{2+} is considered hyperaccumulated at concentrations as low as 100 ppm. Table 1.1 summarizes the concentration criterion for some of the more commonly accumulated metals. Only metals are shown in table 1.1, however, metalloids such as arsenic are classed under the same criterion. For example, in the case of arsenic, a concentration of 100 ppm in aboveground plant tissue is considered hyperaccumulated (summarised from Jaffré *et al*., 1976; Brooks *et al.,* 1977; Baker & Brooks, 1989; Baker & Walker, 1990).

Table 1.1: Concentration criterion presently used to define plant HM hyperaccumulation with respect to metal abundance and toxicity. Metal ion concentration in aboveground tissue types is shown in parts per million (ppm), where 1000 ppm is equivalent to 0.1 % total dry biomass.

Metal ion	Concentration criterion (ppm)	Number of taxa
Cadmium (Cd)	≥ 100	4
Cobalt (Co)	≥ 1000	26
Copper (Cu)	≥ 1000	35
Lead (Pb)	≥ 1000	14
Manganese (Mn)	≥ 10 000	10
Nickel (Ni)	≥ 1000	390
Zinc (Zn)	≥ 10 000	14

(Adapted from Verbruggen *et al.,* 2009)

1.4 Hypertolerance without hyperaccumulation

In addition to HM hyperaccumulators, another distinct group of plants is able to inhabit metalliferous outcrops without exhibiting the hyperaccumulation phenotype. Plant species found on metalliferous outcrops which do not contain elevated concentrations of metal ions in their aboveground tissues, are described as heavy metal hypertolerant non-accumulator plants (Pollard *et al.,* 2002; Verbruggen *et al.,* 2009). Although by definition HM hyperaccumulator plants are hypertolerant, hyperaccumulators and hypertolerant non-accumulator plants have adopted different physiological strategies to achieve HM homeostasis. An outline of the major mechanistic differences between hyperaccumulators and hypertolerant non-accumulators is shown in figure 1.1. The mechanisms involved in metal homeostasis within hyperaccumulators and hypertolerant non-accumulators work in somewhat of an opposite manner, as is reflected by different metal ion distribution and final storage sites between the two groups.

Hypertolerant plants are often termed 'excluders' owing to their ability to restrict metal ions from entering aboveground metabolically active tissue types. This group of plants exhibits an extreme metal-associated abiotic stress resistance by immobilizing metals into the root organ, in this way preventing metal ion movement into the shoot transpiration stream (Maestri *et al.,* 2010). While hypertolerant non-accumulators do show elevated concentrations of metals in their root organs, aboveground tissue metal concentration remains significantly below the surrounding substrate. Conversely, hyperaccumulating taxa typically display higher metal concentrations in their aboveground tissues compared to their root organs and surrounding substrate. The hyperaccumulation mechanism therefore centers on active metal ion movement towards aboveground organs against the concentration gradient, and hyperaccumulators typically display a shoot:root ratio in excess of 1 for the metal ion concerned (Pollard *et al.,* 2002).

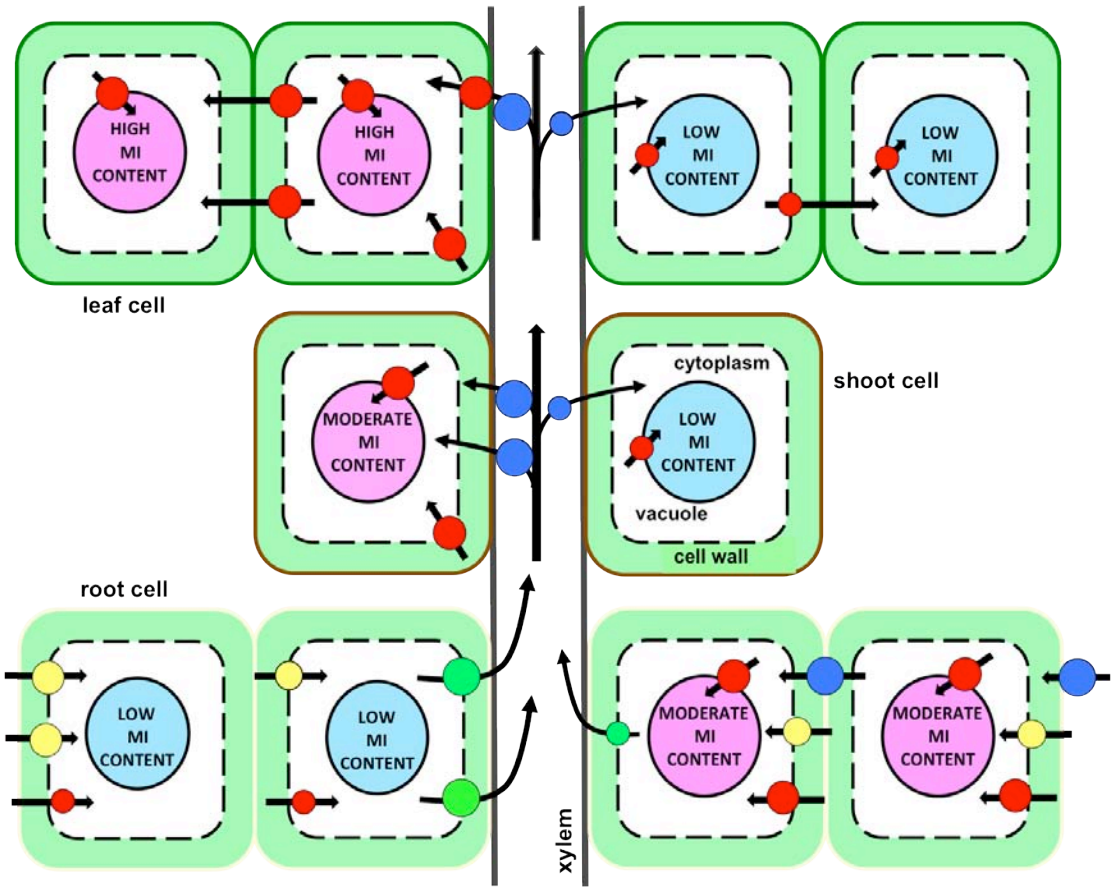

Figure 1.1: An outline of the different metal homeostasis strategies observed between HM hyperaccumulators (left of xylem) and HM hypertolerant non-accumulators (right of xylem). Black arrows indicate metal ion (MI) movement. Coloured spots indicate the locality of known physiological processes involved in MI homeostasis within the plant, and spot size indicates the relative degree of incidence of a specified process between hyperaccumulator and hypertolerant non-accumulator plants. Spot colour key: **yellow** – enhanced root uptake, **red** – HM ligand chelation into the cytosol and/or vacuole sequestration, **green** – enhanced rate of root-to-shoot loading for long-distance MI translocation, **blue** – HM binding to cell wall and/or intracellular antioxidants. Vacuoles within root, shoot and leaf cells are coloured to indicate presence of metal ions. **Purple** – moderate too high MI levels and **light blue** – low MI levels.

1.5 Ecological significance of heavy metal hyperaccumulation

The evolutionary fitness gain associated with plant HM hyperaccumulation remains unclear. Currently the most supported hypothesis centres around a proposed defense mechanism against intensive herbivory and/or pathogen attack (Behmer *et al*., 2005; Jhee *et al.,* 2005; Noret *et al*., 2005; Palomino *et al*., 2007; Fones *et al.,* 2010).

A choice feeding experiment utilizing the general herbivore *Helix aspersa* (brown garden snail) illustrates the 'elemental defense' hypothesis. Leaves from Ni hyperaccumulator and Ni hypertolerant non-accumulator *Senecio coronatus* (Asteraceae) ecotypes were given concurrently to *H. aspersa* snails as a sole food source. The study showed significantly more snails fed on hypertolerant non-accumulator leaves compared to hyperaccumulator leaves. Furthermore, *H. aspersa* species feeding on Ni amended cornmeal, displayed greater reduced body mass and/or mortality rates compared to snails on a control diet (Boyd *et al*., 2002).

It should however be noted, despite laboratory experimentation suggesting that HM accumulation is involved in defense against herbivory, no evidence has been found in the field to support laboratory findings (Noret *et al*., 2007). Furthermore, although some evidence has shown that elevated metal concentrations within plant-tissue types reduces a plants susceptibility to pathogen attack, no studies to date have shown that the hyperaccumulated metal(s) themselves are directly responsible for the perceived resistance to pathogenesis (Fones *et al.,* 2010). A recent paper published by Fones *et al.,* (2010) attempted to tie laboratory experimentation, *in planta* experimentation and fieldwork studies together. The study utilized the polymetallic (Cd, Ni and Zn) hyperaccumulator *Thlaspi caerulescens* and the pathogen *Pseudomonas syringae* pv. maculicola M4. The first strategy employed *P. syringae* infection of *T. caerulescens* plants treated with different concentrations of metal ions. As *P. syringae* proliferates in the apoplastic spaces between plant cells, the metal concentration within the apoplastic phase was determined in order to determine the effects of elevated metal levels on the growth of *P. syringae*. These

experiments supported the 'elemental defense' hypothesis *in vitro*. Secondly, by means of transposon insertion, mutants of *P. syringae* were created to have either increased or decreased Zn tolerance, and were subsequently shown to have an improved or reduced ability, respectively, to proliferate in high-Zn *T. caerulescens* plants. These experiments suggest that accumulated metals are indeed directly involved in pathogen reduction. Lastly, the Zn tolerance of naturally occurring endophytic bacteria (found on the leaves of *T. caerulescens* in the field) was tested to ascertain whether the elemental pathogen defense is effective under field conditions. The authors found that naturally occurring bacteria on leaves of hyperaccumulating *T. caerulescens* plants (from a site close to a former Pb-Zn mine) have a higher tolerance to Zn, as when compared to naturally occurring bacteria colonizing the leaves of non-accumulating *T. caerulescens* plants. This experiment has shown that high metal tolerance is required for bacteria colonizing hyperaccumulator *T. caerulescens* plants. These results support the 'elemental defense' hypothesis, and further, strengthen the hypothesis in the context of a natural environment (Fones *et al.,* 2010).

An alternative hypothesis proposes that hyperaccumulation can be used as a form of extreme allelopathy (Boyd & Jaffré, 2001; Pollard *et al*., 2002). For example, Ni hyperaccumulating taxa may increase Ni^{2+} ion phytoavailability in the surrounding soil through the decomposition of Ni-rich leaves. The 'allelopathy hypothesis' is supported by evidence of significantly elevated Ni^{2+} ion levels in surface soil surrounding Ni hyperaccumulator *Sebertia acuminata* (Sapotaceae) trees, compared to adjacent soil sites where most Ni is locked within ultramafic rocks (Boyd & Martens, 1998; Boyd & Jaffré, 2001).

1.6 A future geared towards engineered plants: the promise of phytoremediation

Plant HM hyperaccumulation has gained growing interest over the last decade for a number of reasons. Hyperaccumulator plants provide valuable genetic material to further develop our understanding of plant metal homeostasis and further our insight into plant adaptation to extreme environments. The practical

implications of the study of hyperaccumulation are focused on developing environmental phytoremediation, and to a lesser extent phytoextraction and food crop biofortification (Garbisu & Alkorta, 2001). Phytoremediation is defined as the use of vascular plants for *in situ* removal of toxic metal and/or metalloids contaminating soil outcrops (Chaney *et al*., 1997; Whiting *et al.,* 2004).

A number of hyperaccumulator taxa have been documented to not only accumulate HM to exceptionally high concentrations, but also grow to attain a relatively large final biomass. Most prominent is the constitutive Ni hyperaccumulating tree species endemic to the Pacific island of New Caledonia, *Sebertia acuminata* (Sapotaceae). This species can grow to a substantial size (15 meters) and total nickel content of a single mature tree is estimated at 37 kilograms (Sagner *et al.,* 1998). The Ni hyperaccumulator *Berkheya coddii* (Asteraceae) is also of particular interest as it is capable of reaching heights in excess of 1.5 meters, and is observed growing in large assemblages. Experimental plantations of *B. coddii* have demonstrated a substantial capacity for aboveground biomass production, producing up to 22 tons per hectare (Robinson *et al.,* 1997, 2003; Boyd *et al.,* 2006). Most metalliferous taxa however, are simply too diminutive in size for efficient soil decontamination. A full appreciation for the genetic and mechanistic physiology behind HM hyperaccumulation is therefore essential to the ultimate goal of transferring the hyperaccumulation trait to a suitable candidate plant species.

1.7 'Model plants' give first insight into molecular basis of heavy metal hyperaccumulation

Whilst biologists have been aware of the HM hyperaccumulation phenomenon for over a century, we still do not fully understand the underlying genetic and physiological bases. A major limitation in past studies has been the relatively low level of intraspecific variation in this trait displayed within hyperaccumulating taxa, making intra-species comparative studies problematic. All populations of a given hyperaccumulator species will typically accumulate a specified metal ion if it occurs in the surrounding substrate/soil, indicating the constitutive (or

species-wide) nature of HM hyperaccumulation. It should be noted however, that despite the constitutive nature of HM hyperaccumulation, some variation in whole-plant metal status has been observed within groups of hyperaccumulator plants of the same taxon. *Berkheya coddii* for example, is a constitutive Ni hyperaccumulator endemic to South African serpentine sites, and does display some variation in metal-status between groups on different Ni-rich outcrops. Although members of a *B. coddii* assemblage will always accumulate Ni if it occurs in the surrounding substrate, populations have been recorded accumulating Ni anywhere between 0.1 - 3.6 % (w/w) on a dry biomass basis (Mesjasz-Przybyłowicz *et al.,* 2001), where variation appears to correlate with soil Ni concentration (Anderson *et al.,* 1999; Robinson *et al.,* 2003). Nonetheless, the generally low levels of intraspecific variation observed in hyperaccumulator plants, has necessitated the use of comparative molecular approaches, often utilizing distantly related non-accumulator species.

As such, despite Ni hyperaccumulators accounting for the majority of all hyperaccumulator taxa, it is two Cd/Zn polymetallic hyperaccumulator species of Brassicaceae, *Arabidopsis halleri* and *Thlaspi caerulescens* that have been the focus of most HM hyperaccumulation studies. This is due to their relatively close evolutionary relationship to the model plant organism *Arabidopsis thaliana*, allowing for the use of many diverse molecular tools and genetic manipulations developed for this model organism (Roosens *et al.,* 2008).

Arabidopsis halleri last shared a common ancestor with the non-accumulator sister species *A. lyrata* approximately 2 million years ago (MYA) and with *A. thaliana* approximately 3 - 5.8 MYA (Clauss & Koch, 2006). *A. halleri* shares 94% nucleotide sequence identity (within coding regions) to *A. thaliana* (Clauss & Koch, 2006) and as is the case with most hyperaccumulator taxa displays constitutive Cd/Zn hyperaccumulation. All populations of *A. halleri* exhibit Cd/Zn hyperaccumulation irrespective of whether the surrounding substrate contains elevated or normal Cd/Zn soil levels; however, a significant degree of between-individual variation in Zn and Cd content has been reported (Bert *et al*., 2002). *T. caerulescens* which last shared a common ancestor with *A. thaliana* approximately 20 MYA, shares 88% nucleotide sequence (coding regions)

similarity to *A. thaliana* (Deniau *et al.,* 2006; Rigola *et al.,* 2006). As with *A. halleri*, Zn hyperaccumulation is exhibited constitutively amongst *T. caerulescens* populations (Martínez, *et al.,* 2006). However, in contrast to *A. halleri*, *T. caerulescens* displays greater between-population phenotypic variation with respect to whole-plant metal status, and demonstrates less metal-specific hyperaccumulation compared to *A. halleri*. The observed variation is shown to correlate with soil metal concentration and composition. For instance, *T. caerulescens* occurring on ultramafic outcrops will either hyperaccumulate Ni and Zn or Ni only. *T. caerulescens* will always hyperaccumulate Ni if present in the surrounding substrate, but does show a preference for Zn, suggesting Ni and Zn are accumulated through similar molecular systems (Reeves *et al.,* 2001; Koch & Al-Shehbaz, 2004; Assunção *et al.,* 2008; Krämer, 2010).

1.8 Comparative molecular studies - a starting place not without difficulties

Most molecular research on hyperaccumulator plants to date has mostly been carried out at a nucleic acid level (DNA/RNA). Specifically, interspecific variation between hypertolerant species has been elucidated predominately by homology studies, where the genetic profile of hyperaccumulator and distantly related non-accumulator species are compared to reveal any underlying differences. In particular, comparative microarray analysis has been extensively used to date (for example, Pence *et al*., 2000; Peer *et al*., 2003; Weber *et al*., 2004; Talke *et al.,* 2006). Given the constitutive nature of hyperaccumulation, microarray analysis has aided in identifying differentially expressed genes between hyperaccumulator and non-accumulator species. Consequently, expression profile comparisons between hyperaccumulator *T. caerulescens* and distantly related non-accumulators such as *T. arvense* have identified numerous genes constitutively overexpressed in the hyperaccumulator species compared to their non-accumulator counterparts (Filatov *et al.,* 2006; van de Mortel *et al.,* 2008; Küpper & Kochian, 2010). Similarly, comparisons between *A. halleri* and *A. thaliana* have identified numerous differentially expressed genes between the two species, however a number of factors complicate the identification of

potential candidate genes involved in hyperaccumulation (Becher *et al.,* 2004; Talke *et al.,* 2006; Weber *et al.,* 2006).

Complications associated with such comparative approaches arise, as differential gene expression between distantly related plant taxa does not necessarily implicate the genes involvement in HM hyperaccumulation. It is therefore difficult to ascertain which differences between the two plant species expression profiles are indeed attributed to an adaptive response to HM homeostasis or simply are a consequence of evolutionary divergence over time (Roosens *et al.,* 2008). Nevertheless, these comparative studies do provide support for the hypothesis that genes assumed to be involved in HM hyperaccumulation are not species-specific, but are rather under different regulation and control compared to non-accumulator taxa. The evolution towards HM hyperaccumulation therefore most likely involves the magnification or enhancement (such as metal-transporter gene multiplication or enhanced promoter activity) of a pre-existing function (section 1.9.2.1).

1.9 Metal-transport proteins identified highlight specific physiological processes

The key processes of HM hyperaccumulation involve proteins that facilitate enhanced metal ion root uptake, stimulated metal mobility from root-to-shoot tissue for long-distance translocation, and efficient metal ion cellular distribution and detoxification (Clemens *et al.,* 2002 and figure 1.1). Examples of extensively studied metal-transporter proteins described to date (figure 1.2) are discussed after each relevant physiological process.

1.9.1 Enhanced heavy metal root uptake

Metal transporter proteins facilitate metal influx from the surrounding soil substrate into the root cell plasma membrane. Both hyperaccumulator and non-accumulator taxa appear to regulate their cation-uptake rates with respect to whole-plant status, but differ in the manner and function of the regulation. For example the hypertolerant non-accumulator *T. arvense* increases its Zn-uptake as

the plant is subjected to conditions of sufficient to deficient Zn concentrations. In contrast the hyperaccumulator *T. caerulescens* maintains a consistent uptake rate, and only at very high Zn concentrations, does root Zn-uptake decrease (Klein *et al.,* 2008). This implies that within non-accumulating plant taxa HM uptake is regulated by differential gene expression under the control of whole-plant metal ion status. Significantly, this differs in hyperaccumulator taxa, which display constitutive gene expression with respect to whole-plant metal ion status. A recent study however, has shown that within the hyperaccumulating taxon, *A. halleri*, increased Zn accumulation is achieved by an upregulation of specific Zn transport proteins (compared to non-accumulator *A. thaliana*), apparently in response to constitutively high HMA4 activity [HMA4 has a high affinity for Zn loading into the xylem (see below)] that in essence starves the root organ of Zn (Hanikenne *et al.,* 2008; Klein *et al.,* 2008).

Molecular comparisons of HM hyperaccumulator and hypertolerant non-accumulator taxa have demonstrated overexpression of root transport proteins, in particular members of the ZIP family (see below), appear to be partly responsible for enhanced metal ion root uptake in the hyperaccumulator species (figure 1.1). A concentration-dependent root Zn-uptake kinetics study, demonstrated similar Zn-uptake efficiencies for *T. caerulescens* and *T. arvense*, which display K_m values of 6 μM and 8 μM, respectively. A considerable difference is observed in Zn-V_{max}, with *T. caerulescens* having approximately a six-fold greater Zn-V_{max} compared to *T. arvense*. As enhanced HM root uptake in hyperaccumulator taxa is driven by an increase in V_{max}, where K_m remains constant, this implies that transporters involved in HM uptake share a large degree of homology within non-accumulator and hyperaccumulator taxa, but are likely to be present in greater densities in the latter (Pence *et al.,* 2000; Weber *et al.,* 2004; Verbruggen *et al.,* 2009). *T. caerulescens* which demonstrates significantly greater whole-plant Zn levels compared to *T. arvense*, and subsequently displays a higher degree of radial metal movement from root-to-shoot tissue types, may explain the observation that *T. caerulescens* minimizes the amount of Zn chelation and subsequent root sequestration [possibly through enhanced HMA4 activity (Hanikenne *et al.,* 2008)]. Indeed a comparison of Zn ion

concentration in the root organs of *T. caerulescens* and *T. arvense* show the latter to contain up to two-fold more Zn within cellular vacuoles, highlighting *T. arvense* inability to translocate Zn away from the root organ (figure 1.1) (Lasat *et al.,* 1996, 1998, 2000; Pence *et al.,* 2000; Hammond *et al.,* 2006; Krämer *et al.,* 2007; Milner & Kochian, 2008).

1.9.1.1 ZNT1 – Zn Transporter

The ZNT1 or Zn transporter protein belongs to a large family of polypeptides, called ZIP (Zinc-regulated transporter, Iron-regulated transporter – related Protein). The ZIP Protein Family name is derived from the first members identified, ZRT and IRT-like Protein. ZRT1 and ZRT2 (zinc-regulated transporter) are high- and low-affinity zinc ion transporters, respectively, originally identified in yeast cells. Whereas, IRT1 (iron-regulated transporter) is a cation transporter expressed in the root cells of iron-deficient *Arabidopsis* plant species (Assunção *et al*., 2001; Papoyan *et al*., 2007; Hanikenne *et al*., 2008). *ZNT1* encodes for a putative Zn/Cd membrane transporter protein, and *TcZNT1* was first identified due to the relative abundance of transcript levels in *T. caerulescens* compared to a related non-accumulator species, *T. arvense*. TcZNT1 displays the greatest homology with AtZIP4. Microarray analysis has since exposed several highly expressed genes encoding ZIP Family members (such as ZIP3, ZIP6, ZIP9, ZIP10) within both *A. halleri* and *T. caerulescens* plants, while in the steady-state under Zn-sufficient growing conditions, as when compared to *A. thaliana* (Weber *et al.,* 2004). The majority of ZIP Family genes discovered thus far, are classified as part of the transcriptional Zn-deficiency response in *A. thaliana* and active in the effective uptake of metal ions (figure 1.2).

1.9.2 Root-to-shoot loading for long-distance metal ion translocation

An effective system for radial metal ion movement within the root symplasm towards active xylem loading is vital for HM hyperaccumulation. An efficient metal ion translocation mechanism is necessary in order to prevent HM ion build up in the root organ, which would lead to toxicity (Clemens, 2006). This is achieved by greatly enhanced rates of metal loading from the root symplasm into

the apoplastic xylem tissues. Metal ions are loaded into xylem vessels through an increased loading from xylem parenchyma tissue for long-distance translocation by means of the transpiration stream (Verbruggen *et al.,* 2009).

Several metal transporters have been implicated in enhanced xylem metal loading. FRD3, an antiporter protein of the multi-drug and toxic compound extrusion (MATE) membrane proteins is thought to facilitate citrate efflux into root tissue. Citrate is known to be required for iron (Fe) and possibly Zn cellular transport from root to shoot tissue types (Talke *et al.,* 2006). Microarray analysis has shown *FRD3* to be constitutively overexpressed in both *A. halleri* and *T. caerulescens* compared to *A. thaliana*, implicating FRD3 in Zn hypertolerance and cellular transport. HMAs (see below) form part of a P-type ATPases family of plasma membrane proteins capable of transporting specified HM ions against any electro-potential gradient using the energy provided by ATP hydrolysis (Garrett & Grisham, 2005). Expression of *AtHMA4* in *A. thaliana* appears to be restricted to xylem parenchyma tissues within the shoot. Whereas in *A. halleri* and *T. caerulescens HMA4* is seen highly expressed in xylem parenchyma tissues as well as root tissue types and has been shown to be involved in enhanced loading of HM into xylem vessels (figure 1.2) (Mills *et al*., 2003; Bernard *et al*., 2004; Hussain *et al*., 2004; Verret *et al*., 2004; Klein *et al*., 2008). Hyperaccumulators have been shown to contain elevated levels of metals in their xylem sap, likely as a consequence of enhanced xylem loading. X-ray absorption spectra analysis has demonstrated both elevated levels of Zn and Cd are predominately present in the free hydrated ionic form (Cd^{2+}/Zn^{2+}) within the xylem sap of *T. caerulescens* and *A. halleri* plants, respectively. Currently however, no clear system as to how metal ions are chaperoned from the root organ to a final storage site of hyperaccumulator taxa has been established (see sections 1.9.3 and 1.9.4 and sub-sections therein). In light of the apparent complexity associated with metal ion chelation and translocation, only a few examples will be discussed in the following text.

1.9.2.1 HMA – Heavy Metal ATPase

Gene knockout studies and molecular analysis of *A. thaliana* have shown AtHMA4 is involved in metal xylem loading and unloading, facilitating metal translocation from xylem parenchyma cells into the shoot xylem vessels (figure 1.2), and further is required for normal Zn homeostasis and Cd detoxification processes (Papoyan *et al.,* 2007). AhHMA4 has been implicated in Zn hyperaccumulation and normal levels of Cd accumulation in *A. halleri* plants, and the silencing of *AhHMA4* through RNAi interference demonstrated that *AhHMA4* is required for complete Cd hypertolerance, and to a lesser extent Zn hypertolerance (Ueno *et al.,* 2011). Similarly to TcZNT1, AhHMA4 has also been shown to confer increased Cd/Zn tolerance to transgenic metal-sensitive *Saccharomyces cerevisiae* yeast cells. Within the root organ of *A. halleri* plants, Zn concentrations are low compared to whole-plant status, highlighting a high degree of metal flux from the root organ to shoot tissues. This is in contrast to the root organs of *HMA4* RNAi *A. halleri* plants, which demonstrate between 49 to 134-fold higher Zn concentrations, (similar to non-accumulator *A. thaliana*) compared to wild-type *A. halleri* plants (figure 1.1). Currently there is no evidence to suggest any difference in protein function between AhHMA4 and AtHMA4. However, between a 6 and 53-fold increase in transcript number of *AhHMA4* has been observed in comparison to *AtHMA4* transcript abundance in *A. halleri* and *A. thaliana*, respectively (Talke *et al.,* 2006). Similarly, expression levels of *TcHMA4* in both root and shoot cells of *T. caerulescens* are significantly increased compared to *AtHMA4* expression in *A. thaliana*. The observed increase in transcript number is brought about as a result of gene triplication of *HMA4* in *A. halleri*, with three almost identical *AhHMA4* gene copies present in the genome compared to *A. thaliana*. Increased gene copy number is paired with an enhanced promoter activity brought about by *cis*-regulatory mutations in *A. halleri* lineages. Recent transgenic studies have shown that when any of the AhHMA4 promoters are introduced into *A. thaliana* or *A. halleri*, a corresponding increase in transcript expression levels is observed, compared to reporter genes under control of the AtHMA4 promoter (Hanikenne *et al.,* 2008; Krämer, 2010). This therefore further advocates a crucial step towards the evolution of HM

hyperaccumulation involves the enhancement of gene function activity of an already existing process in a recent ancestor.

1.9.3 Aboveground tissue metal ion movement and subsequent detoxification

Cellular metal uptake rates are increased in aboveground tissue types, allowing for an effective system for cell-to-cell metal distribution. An active metal influx occurs across shoot/leaf plasma membranes, moving metal ions into the cell. Further, an increased efficiency in metal ion detoxification is achieved by ligand chelation, and subsequent vacuolar sequestration of reduced divalent metal ions (Krämer *et al.,* 1996; Lasat *et al.,* 1996, 1998; Verbruggen *et al.,* 2009).

1.9.3.1 MTP – Metal Transport/Tolerance Protein

Metal Transporter Proteins (MTPs, formerly known as ZAT or Zinc Transporter of *Arabidopsis thaliana*) are also referred to as Cation Diffusion Facilitators (CDFs). CDFs are a family of proteins involved in the transport of numerous metal ions including, Cd^{2+}, Co^{2+}, Fe^{2+}, Mn^{2+} and Zn^{2+}. As such, CDFs have been implicated in metal ion movement across a wide range of biological membranes including within root tissues, demonstrated by greater Zn tolerance and root accumulation in transgenic *A. thaliana* plants overproducing ZAT (Van der Zaal *et al.,* 1999). Significantly however, AtMTP1 was the first of these transporters to have been shown to facilitate both cytoplasm to organelle metal ion movement (apoplast transport), as well as metal ion transport from cytoplasm to the endoplasmic reticulum (Kim *et al.,* 2004; Peiter *et al.,* 2007). Accordingly, CDFs are observed primarily in metal partitioning within aboveground tissue cells types.

CDFs such as those identified in both the Ni/Zn hyperaccumulator *T. goesingense* (TgMTPs) and non-accumulator *A. thaliana*, have been suggested to facilitate metal translocation to the shoot and leaf cells for subsequent vacuolar sequestration (figure 1.2). Further, the capacity of *T. goesingense* to hyperaccumulate Ni seems to be in part dependent on the plants ability to

sequester Ni^{2+} ions into leaf vacuoles. Within *T. goesingense*, TgMTP1t1 and TgMTP1t2 (two variants which differ in a histidine-rich metal-binding domain) are proposed to be involved in metal ion vacuolar sequestration. Heterologous expression of *TgMTP1t1* and *TgMTP1t2*, within mutant yeast cells (deficient in the *TgMTP1* orthologues; *COT1* and *ZRC1*, respectively), show complementation in metal-sensitive yeast cells, where *TgMTP1t1* expression conferred greatest tolerance to Cd and Zn, and *TgMTP1t2* expression conferred the greatest tolerance towards Ni (Persans *et al.,* 1999, 2001). This is further supported by heterologous expression of either *AhMTP1* or *AtMTP1* in yeast cells (Kim *et al.,* 2004) and expression of either *AhMTP1* or *TgMTP1* in *A. thaliana*, which resulted in an increased Zn tolerance in both yeast cells and *A. thaliana* plants (Kim *et al.,* 2004; Krämer, 2005). Similarly, an overproduction of AtMTP1 in transgenic metal-sensitive *A. thaliana* plants was shown to increase Zn accumulation and tolerance (Kobae *et al.,* 2004). Furthermore, transcript levels of other genes encoding for vacuolar $Cd/Zn/H^+$ antiporter MTP-like proteins, are approximately 20-fold higher in leaf tissue types of *A. halleri* compared to *A. thaliana*, further implicating MTP-like proteins in leaf metal ion vacuolar sequestration (figure 1.2). In support of the proposed function of MTPs, *T. caerulescens* plants were shown to possess an *AtMTP1* homolog; *TcZTP1*. *TcZTP1* has subsequently been observed highly expressed ectopically in the leaf tissue of *T. caerulescens* plants (compared to expression in *A. thaliana*). Additionally, TgMTP1 appears to be localized at the plasma membrane in *T. goesingense* plants, suggesting a role in both Ni and Zn efflux from the cytoplasm (Assunção *et al*., 2001).

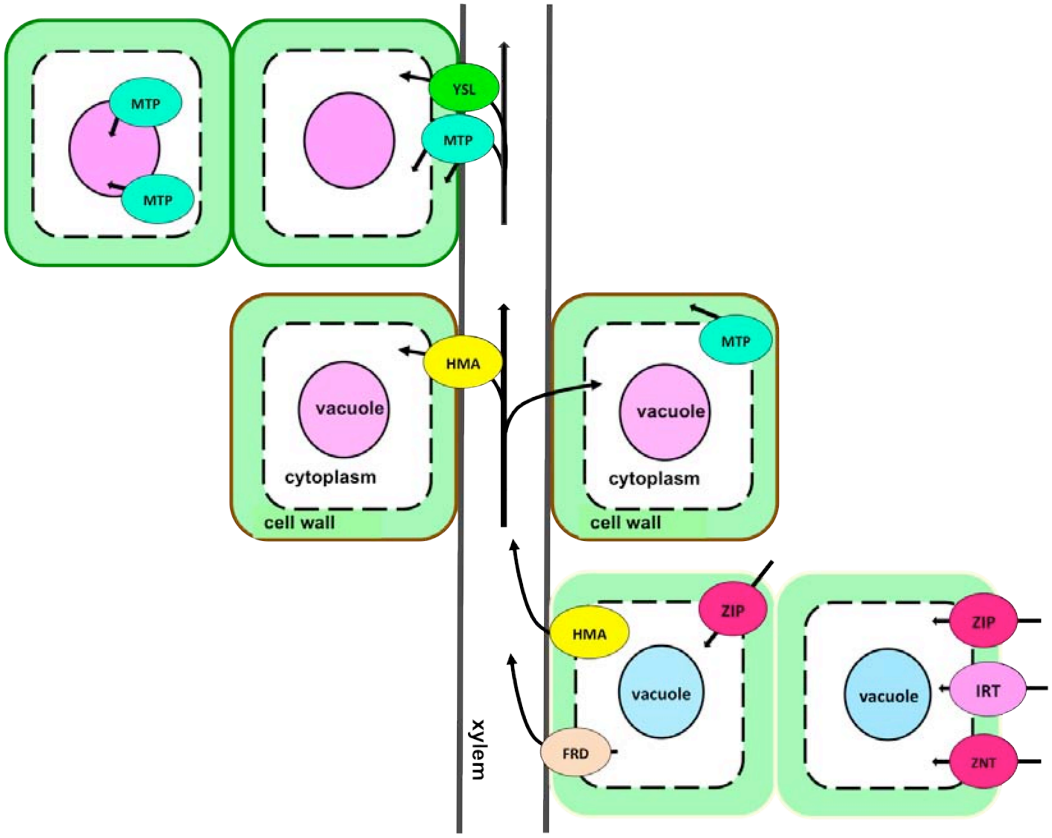

Figure 1.2: Identified metal-transport proteins involved in facilitating plant HM hyperaccumulation. Metal transport proteins are shown at the appropriate locality of function within the plant body. Black arrows indicate metal ion movement.

To further investigate whether the transport of metal cations (Ni in this case) by at least some CDF proteins [coupled to the movement of counter-ions, such as protons (Krämer, 2005)], Ingle et al. (2008) investigated the mechanism of Ni uptake into leaf vacuoles of the Ni hyperaccumulator *Alyssum lesbiacum*. Protoplast isolates from leaf tissue were used to monitor Ni uptake into individual vacuoles and visualization of cellular Ni was achieved with the metal-sensitive fluorescent dye, Newport Green. The vacuolar Ni uptake rate was accelerated through the stimulated energisation of vacuolar H^+-ATPase (V-ATPase) by addition of Mg/ATP. The ATP-induced Ni uptake was then successfully eliminated by addition of a V-ATPase inhibitor, bafilomycin, and dissipation of the trans-membrane pH gradient with the uncoupler ammonium sulphate. By illustrating the energetically active transport of Ni^{2+} into leaf cell vacuoles these experiments suggested a potential mechanism for metal ion vacuolar sequestration in plants (Ingle *et al.,* 2008).

1.9.4 Metal ion detoxification

1.9.4.1 Nicotianamine and mugineic acid

The capacity for mugineic acid (MA) to chaperone metals into a plants root organ has been reported in graminaceous plant species, such as barley, accumulating iron (Fe). MA is enzymatically synthesized in a step-wise process. The first step requires the condensation of three S-adenosyl-methionine (SAM) molecules, producing nicotianamine (NA), NA is then converted to a 3"-Oxo intermediate via the enzyme NA aminotransferase. The final step involves the conversion of the 3"-Oxo intermediate to MA with the use of deoxymugineic acid synthase (Haydon & Cobbett, 2007). Once produced, MA is then secreted from the root organ to bind Fe^{3+} ions in the rhizosphere. The metal-ligand complex is then moved into the root organ with the use of a specified metal-transporter. The first Fe-MA transporter was identified in mutant maize plants deficient in Fe-MA uptake, and was branded as yellow-stripe 1 or YS1 (Curie *et al.,* 2001, 2009). Nicotianamine is a non-proteinaceous amino acid synthesized by the condensation of three SAM molecules, via the enzyme nicotianamine synthase (NAS). NA is present in all plants. Unlike MA however, NA is not secreted into the root rhizosphere, and functions rather within the plant as a ligand (Haydon & Cobbett, 2007).

Microarray analysis between hyperaccumulator *A. halleri* and non-accumulator *Arabidopsis* accessions, has identified greater *NAS* transcript abundance within the hyperaccumulator species (in root and shoot tissue types) compared to non-accumulators, suggesting an overexpression of genes involved in NA biosynthesis is required for enhanced metal ion accumulation (Talke *et al.,* 2006). Additionally, the heterologous expression of *AhNAS2* and *AhNAS3* in yeast cells (*Schizosaccharomyces pombe* and *Saccharomyces cerevisiae*, respectively) confers an increased tolerance to Zn, suggesting a prominent role of NA in Zn tolerance *in vivo* (Becher *et al.,* 2004; Weber *et al.,* 2004; Haydon & Cobbett, 2007). NA has also been linked to an increased ability to tolerant Ni in accessions of *T. caerulescens*. The transgenic overexpression of *TcNAS* genes in either *Arabidopsis* or tobacco plants results in an increased resistance to Ni, whereby, a 2-fold increase in root NA pools is observed, compared to control *A. thaliana*

plants (Pianelli *et al.,* 2005). This was further supported by a Ni-dose time-course experiment, which demonstrated that when *T. caerulescens* is exposed to elevated Ni levels, an increasing concentration of NA accumulates in the plant roots (Curie *et al.,* 2001, 2009). Furthermore, with the use of HPLC coupled with inductively coupled plasma mass spectrometry (HPLC-ICPMS) as well as electrospray MS/MS, complexes of Ni-NA have been observed in the roots of *T. caerulescens* after exposure to Ni (Vacchina *et al.,* 2003). Interestingly however, the gene encoding TcNAS1 is not expressed in the root organ, and NAS activity is also absent within the root organ (Curie *et al.,* 2001). The accumulation of NA in the root organ after Ni exposure was seen to subsequently increase as a function of time, coinciding with a transient decrease in leaf NA concentration. The apparent coordination between leaf production of NA and root accumulation of NA was further confirmed by HPLC, capillary electrophoresis and mass spectroscopy, which exposed NA-Ni complexes present in the xylem vessels of Ni treated plants (Mari *et al.,* 2006). Conversely, distantly related non-accumulator species (of both *T. caerulescens* and *A. halleri*) were shown to lack Ni, NA and Ni-NA complexes in their xylem sap. These findings suggest the existence of a translocation system for mobilization of foliar NA to root NA pools and the subsequent re-cycling of NA-Ni complexes back to the plant leaves within hyperaccumulator taxa (Mari *et al.,* 2006; Milner & Kochian, 2008; Verbruggen *et al.,* 2009). The exact mechanism behind NA-Ni recycling remains unclear, however involvement of yellow stripe-like (YSL) transporters has been suggested. Expression of the gene *TcYSL3*, for example, has been shown to facilitate the transport of NA-Ni complexes from root-to-shoot tissue types in *T. caerulescens* plants (Curie *et al.,* 2001).

1.9.4.2 Histidine

Histidine (His) as a free amino acid is considered to be one of the major ligands involved in HM detoxification, and has been observed forming stable complexes with Cd, Ni and Zn (Verbruggen *et al.,* 2009). The first demonstration of histidine's involvement in HM hyperaccumulation/tolerance was in 1996 in the Ni hyperaccumulator *Alyssum lesbiacum* (Krämer *et al*., 1996). Exposing hyperaccumulator species of the genus *Alyssum* to Ni, results in the generation of

a significant and linear increase in free His levels within the xylem sap. The concentration of His detected within the xylem exudate of *A. lesbiacum* compared to distantly related non-accumulator *A. montanum*, was reported to be 36-fold higher in the hyperaccumulator plant, implicating His involvement in Ni xylem loading. In addition, the authors (Krämer *et al*., 1996) demonstrated that, within the non-accumulator *A. montanum*, supply of His elicits a large and proportional increase in Ni tolerance, as well as a greater capacity for Ni translocation to shoot tissue types. Further confirmation of His role in Ni tolerance is shown by utilization of X-ray absorption spectrometry, which has identified His-Ni complexes in the xylem sap as well as in the root and shoot tissue types of *A. lesbiacum*. This further suggests the complexation of Ni with His is required for Ni tolerance, and further, for facilitating the transfer of Ni from root to shoot tissue types (Krämer *et al*., 1996).

The 'Histidine Response' is supported by experiments (Ingle *et al.,* 2005a) demonstrating that, the constitutive overexpression of enzymes facilitating His biosynthesis is in part, responsible for Ni hyperaccumulation/tolerance. Exposure of Ni to hyperaccumulator *A. lesbiacum* and non-accumulator *A. montanum* did not however show any increase in transcript abundance of any of the enzymes required for His biosynthesis. Notably however, transcript abundance was seen to be constitutively greater in *A. lesbiacum* compared to *A. montanum*. Specifically, mRNA transcripts for the first enzyme in the His biosynthetic pathway, ATP-phosphoribosyltransferase (ATP-PRT), were constitutively greater in abundance as when compared to mRNA *ATP-PRT* transcripts of *A. montanum*. Consequently, it was demonstrated that up to a 15-fold increase in free His levels (in shoot tissue types) could be achieved in transgenic *A. thaliana* accessions overexpressing an *A. lesbiacum ATP-PRT* gene. This was further shown to correlate with an increased Ni tolerance. Interestingly, overexpression of *ATP-PRT* in *A. thaliana* (and corresponding His production) did not result in an equivalent increase in Ni levels within the xylem sap nor in shoot tissue types. This implies that constitutive overexpression of His is only part of the complete Ni hyperaccumulator phenotype (Ingle *et al.,* 2005a).

1.10 Proteomics over genomics?

Transcriptomic studies, such as microarray analysis, have aided in identifying potential candidate genes involved in HM hyperaccumulation. However, the relationship between mRNA and protein expression levels has been shown to be inadequate to confidently predict protein expression levels from corresponding quantitative mRNA data (Velculescu *et al.,* 1997; Gygi *et al.,* 1999; Ideker *et al.,* 2001). Processes shown to be responsible for weak correlation between mRNA expression and protein abundance possibly include post-transcriptional regulation and protein translation rates, protein and/or mRNA half-life status, as well as protein association with intracellular ligands which may increase or decrease protein stability (Varshavsky, 1996; Harford & Morris, 1997; Urlinger *et al.,* 1997). Hence, the study of an organism's proteome is clearly advantageous as it focuses on the actively translated portion of the genome, and has a greater potential to resolve properties of biological systems (such as HM hyperaccumulation) not apparent by transcriptomic study alone.

1.11 Evolutionary studies within *Alyssum* as an example of multiple independent evolution towards Ni hyperaccumulation

Ni hyperaccumulating taxa account for the majority of hyperaccumulating species described worldwide. Despite the diverse phylogenetic coverage represented in hyperaccumulator taxa, some families are seen to possess a high frequency of Ni hyperaccumulators, in particular the Brassicaceae (Krämer, 2010). Within Brassicaceae the greatest number of Ni hyperaccumulating taxa is found within the genus *Alyssum*. *Alyssum* contains approximately 180 species, found predominately in the Mediterranean Basin with occurrences of *Alyssum* species also documented in the Middle East (such as Iraq and Iran), Siberia, into the North-west of Northern America (such as Alaska) and North Africa. The genus is further subdivided into six sections, where the majority of species occur within *Odontarrhena* and *Alyssum*, while most Ni hyperaccumulating taxa occur within *Odontarrhena* (Mengoni *et al.,* 2003). Ribosomal internal transcribed spacer (ITS) sequences have been utilized extensively in plant systematics to

resolve evolutionary relatedness at fine-scale taxonomic levels (Baldwin *et al.,* 1995). Indeed, phylogenetic analysis of the *Alyssum* species complex revealed four main clades each containing both Ni hyperaccumulator and non-accumulator taxa. The phylogenetic grouping of *Alyssum* species suggests that the hyperaccumulator phenotype may have evolved independently multiple times and display a polyphyletic relationship with non-accumulator phenotypes. Additionally geographic distribution of *Alyssum* species does not correlate strongly with phylogenetic structure implying Ni tolerance has possibly been gained or lost, independently, by relatively few genetic changes (Pepper & Norwood, 2001; Mengoni *et al.,* 2003). Within the genus, it has however been demonstrated that populations of *A. bertolonii* show a significant degree of intraspecific genetic divergence, and comparatively (to other *Alyssum* species) a high degree of phenotypic heterogeneity (with respect to metal tolerance) exists within the species. Interestingly, for *A. bertolonii* a clear relationship between geographical isolation and genetic differentiation has been observed (Mengoni *et al.,* 2003; Galardi *et al.,* 2007).

These observations provide evidence of at least six independent evolutionary events towards Ni hyperaccumulation within the Brassicaceae (Krämer, 2010). Further, as Ni hyperaccumulation implies Ni hypertolerance, the presence of numerous Ni tolerant non-accumulating taxa living in close proximity to hyperaccumulating species, suggests that Ni hyperaccumulation and Ni hypertolerance are under different genetic control (Macnair *et al.,* 1999; Galardi *et al.,* 2007).

1.11.1 Population studies provide additional insight into genetic architecture

Research in plant adaptation to metal-polluted sites (naturally occurring or anthropogenic) has predominately taken a physiological approach, in particular transcriptomics. Transcriptomics studies have identified numerous metal-accumulation candidate genes, which are seen as ubiquitous to most vascular plant metal-homeostasis networks, but are under different regulatory control (Bernard *et al.,* 2004; Hammond *et al.,* 2006; Talke *et al.,* 2006). Identification of candidate genes has contributed greatly to the advancement of HM

hyperaccumulation studies; however, the genetic structural design of the HM hypertolerance/hyperaccumulation trait remains unknown (Pauwels *et al.,* 2008).

Consequently, to broaden the scope of experimentation, a combination of '-omics' based studies together with molecular ecology genetic methods such as within-species polymorphism and population differentiation for metal tolerance in a demographical framework, has been proposed, so as to identify any evidence for natural selection through patterns of genomic variation (Pauwels *et al.,* 2008). Examination of associations between identified candidate genes and the resulting phenotype (in controlled conditions) should then be considered. This could be achieved for example by, the study of individual wild populations that are structured by phenotypic plasticity or utilizing populations produced by quantitative-trait-locus (QTL) mapping. As such, inclusion of population genetic studies with '-omic' based experimentation has been proposed as a more effective way to fully elucidate the HM hyperaccumulation phenomenon (Purugganan & Gibson, 2003; Pauwels *et al.,* 2006, 2008).

For example, a recent paper by Pauwels *et al.,* (2008) on the constitutive Zn-hypertolerant model organism *Arabidopsis halleri*, revealed that within *A. halleri* individuals and populations across Western Europe, a large degree of plasticity in the Zn tolerance phenotype exists, contrary to the findings from most recognized hyperaccumulators. Further, significant population structure was observed (estimated by analysis of molecular variance, AMOVA), however variation in Zn tolerance did not correlate clearly with geographic distribution (besides a split into two groups, North and South by the Alps mountain range) but rather with HM soil concentration. Within the northern group, populations of Zn hyperaccumulator *A. halleri* were found to be more closely related to the geographically closest non-accumulator *A. halleri* populations, than to adjacent hyperaccumulators. These results support the hypothesis of the multiple independent evolution towards HM hyperaccumulation in this species (Pauwels *et al.,* 2005, 2008).

1.12 *Senecio coronatus*: a possible 'model organism' for Ni accumulation study

Ni hyperaccumulator species are typically restricted to Ni-rich outcrops, and characteristically display low intraspecific variation, where all individuals within a given taxon will actively accumulate Ni if it occurs in the surrounding soil substrate. *Senecio coronatus* (Asteraceae), however appears to be unique among described Ni hyperaccumulator taxa, in that distinctive mechanisms have been reported in different ecological conditions within the taxon (Hilliard, 1977; Mesjasz-Przybyłowicz *et al*., 1997; Comes & Abbott, 2001). On serpentine outcrops two different *S. coronatus* ecotypes have been described, a Ni hyperaccumulator and a Ni hypertolerant non-accumulator. Additionally, a third ecotype has been identified as a non-accumulator found on normal soil types. All three ecotypes are found throughout southern Africa (Mesjasz-Przybyłowicz *et al*., 1997; Boyd *et al*., 2002). Although populations of hyperaccumulating and hypertolerant non-accumulator *S. coronatus* plants are macro-morphologically identical, particle induced X-ray emission (PIXE) analysis and proton backscattering (BS) techniques have shown substantial differences in Ni cellular concentration and distribution between different *S. coronatus* ecotypes (Mesjasz-Przybyłowicz *et al.,* 1994, 1997, 2007). The concentration of Ni in the roots of hyperaccumulator and non-accumulator ecotypes differs significantly. The Ni concentration in hyperaccumulator ecotype roots was seen to be 60-fold greater in older root tissue types, and 10-fold greater in younger root tissue types, compared to equivalent root tissue types from non-accumulator ecotypes (Mesjasz-Przybyłowicz *et al.,* 2007). Further, within hyperaccumulator *Senecio* ecotypes, Ni is ubiquitously distributed within shoot tissue types, with the highest concentrations of Ni restricted to the epidermis, cortex and phloem. In contrast, within non-accumulating ecotypes Ni is seen restricted to the phloem only. For both hyperaccumulating and non-accumulating ecotypes, leaf Ni is seen concentrated in the epidermis, with hyperaccumulating ecotypes containing significantly greater Ni concentrations as reflected by a steep increase in Ni concentration from root to leaf tissue types (Mesjasz-Przybyłowicz *et al.,* 1994, 1997).

Occurrence of constitutive Ni hyperaccumulators, such as *B. coddii* alongside populations of both *S. coronatus* hyperaccumulator and non-accumulator ecotypes, suggests as variation is observed within *S. coronatus* and not within *B. coddii* populations, Ni accumulation is not influenced by Ni availability or concentration, but rather as a function of genetics within *S. coronatus*. In support of this hypothesis, individuals of Ni hyperaccumulators (removed from their natural environment), were shown to maintain their rate of Ni accumulation when grown on serpentine soil collected from sites where non-accumulator populations were present, whereas non-accumulator *S. coronatus* ecotypes transplanted to serpentine soil collected from sites with hyperaccumulating plants, were still unable to hyperaccumulate Ni (Mesjasz-Przybyłowicz *et al.,* 2007).

S. coronatus therefore displays marked intraspecific variation and appears to provide the whole spectrum of Ni responses within one taxon. This implies any variation observed in expression between *S. coronatus* ecotypes, is more likely as a consequence of the difference in hyperaccumulation phenotype, and not adaptation to other environmental factors.

1.13 Research objectives

Research on *S. coronatus* thus far has indicated that a large degree of intraspecific variation is present in this species Ni tolerance mechanism, and has been shown to display two distinct Ni accumulation phenotypes, namely hyperaccumulator and hypertolerant non-accumulator. As such, variation in *S. coronatus'* Ni accumulation phenotype may parallel a similar pattern and degree of genetic differentiation.

The aims of this study were to (i) evaluate genetic differentiation between Ni hyperaccumulator and non-accumulator populations of *Senecio coronatus* in the Mpumalanga province of South Africa and (ii) identify protein abundance differences between the hyperaccumulator and non-accumulator phenotypes from plants collected *in situ*. To do this sequence data from both the ribosomal internal transcribed spacer (ITS) and non-coding chloroplast markers (TrnfM)

were used to determine the evolutionary relationships among the sampled populations. The degree to which these populations were genetically differentiated was inferred by analysis of molecular variance (AMOVA). As a proof of concept, specific samples from the different evolutionary lineages revealed in the population genetic analysis, were chosen for an initial proteomic analysis. To infer any variation in protein abundance of total protein isolate, two dimensional SDS-PAGE and subsequent protein identification by liquid chromatography coupled mass spectrometry (LC-MS/MS) was utilized.

Chapter 2

Materials and Methods

2.1 Collection of *Senecio coronatus* plant material

Leaf samples and whole plants were collected from 15 different sites, including 12 serpentine and three non-serpentine ('normal') soil outcrops, in the Barberton region of Mpumalanga, South Africa (figure 2.1). Additionally, the sympatric species *Senecio conrathii* was collected from the Bulemba site as an outgroup population in subsequent genomic analysis.

To determine Ni accumulation phenotype, leaf samples were broken open and rubbed onto an indicator paper: Whatman paper (Whatman International Ltd., Maidstone, England) impregnated with dimethylglyoxime (DMG) as first described by Tschugaeff, (1905). The presence of Ni in leaf tissue is indicated by a strong pink-red colour, whereas paper exposed to plants without leaf Ni content showed no colouration, excluding a yellow-green colour, presumably from the leaf chlorophyll content (figure 2.2). No morphological differences were observed between hyperaccumulator and hypertolerant non-accumulator populations during sample acquisition.

At each site, leaf material was collected from ≥ 10 individual plants that were growing a minimum of 3 m apart. Leaf samples were desiccated with silica gel on site. Selected whole plants were excavated and potted on site, maintaining the soil-root structure. All sites (and abbreviations), co-ordinates and soil types are listed in table 2.1. At the Pullen Farm site, two different *Senecio coronatus* varieties (based on morphology) were collected, designated in this study as PF and PFX.

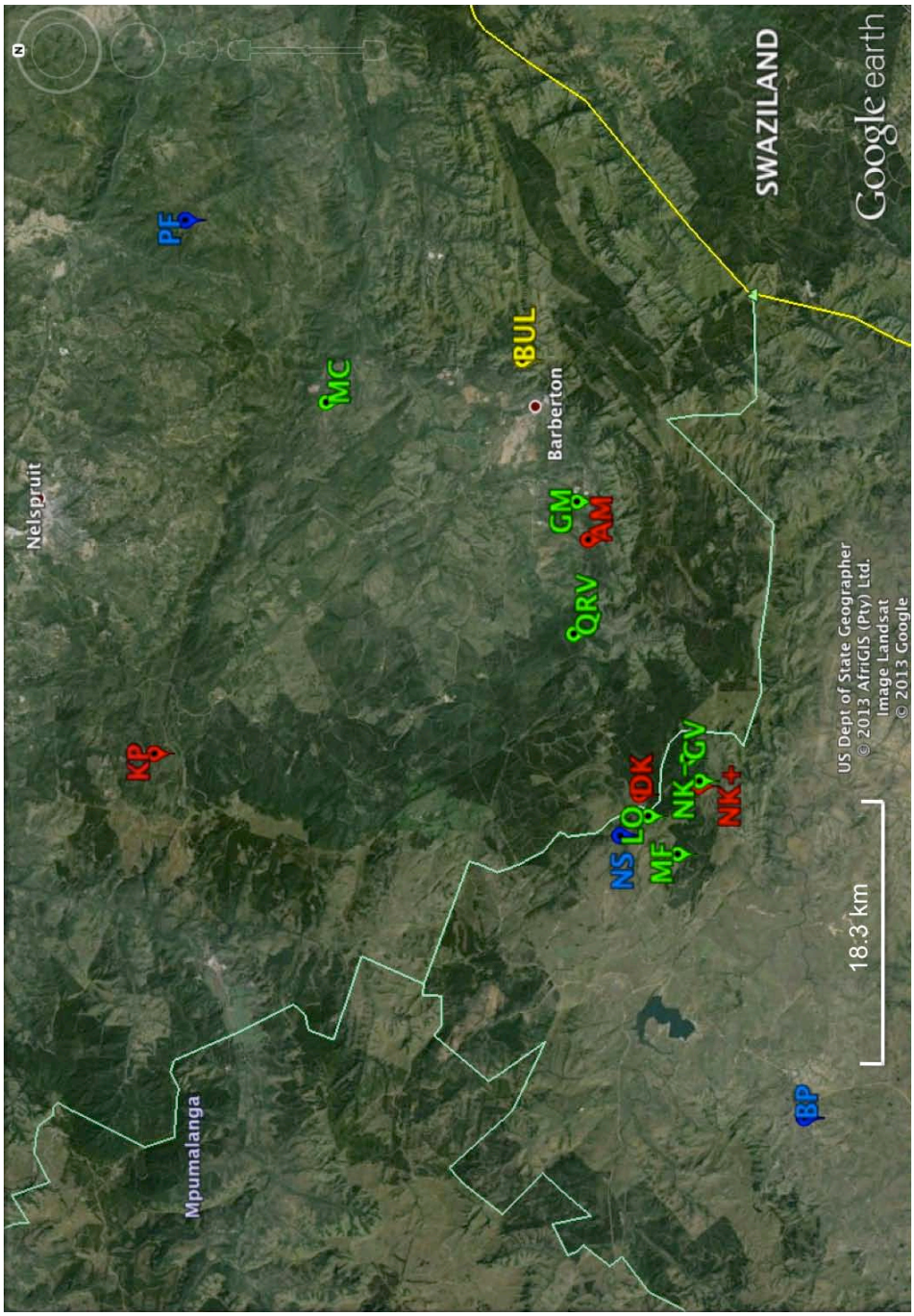

Figure 2.1: Distribution of sample collection sites in the Barberton region. Global location of collection sites is indicated by proximity to the country Swaziland. Three different *S. coronatus* ecotypes were collected on 15 different sites (only 14 sites are shown due to scaling, the Komati site is located approximately 160 km West of Badplaas). *S. coronatus* was sampled to include phenotypes showing Ni hyperaccumulating (**red**), Ni hypertolerant non-accumulating (**green**) and Ni non-accumulating (**blue**) occurrence on normal soil. The **yellow** site name indicates the collection site of sympatric species *S. conrathii*, a non-accumulator species found on normal soil. Sample sites are abbreviated to; Agnus Mine (AM), Badplaas (BP), Bulemba (BUL), Doyershoek (DK), Galaxy Mine (GM), Groen Vallei (GV), Kaapsehoop (KP), Lunar Observatory (LO), Mike's Field (MF), Mund's concession (MC), Nkomazi (NK+/NK-), Non-serpentine (NS), Pullen Farm (PF) and Queen's River Valley (QRV).

Figure 2.2: DMG-indicator paper Ni test. Presence of nickel (Ni^{2+}) within leaf cells was determined by smearing broken leaf tissue directly onto indicator paper (on site) from hyperaccumulator (left) and non-accumulator (right) plants, respectively. Colour development occurred instantly on contact with leaf Ni.

Table 2.1: Co-ordinates of latitude, longitude and altitude are listed for corresponding sample collection sites. Ni accumulation phenotypes hyperaccumulator and hypertolerant non-accumulator have been abbreviated to HA and HTNA, respectively. The presence of high Ni content in sample location soils is indicated as yes (Y) or no (N).

Site name (abbreviation)	Phenotype & Soil Ni	Lattitude	Longitude	Altitude (m)
Agnes Mine (AM)	HA/Y	25 49 48 S	30 57 23 E	1232
Badplaas (BP)	NA/N	25 58 04 S	30 33 06 E	1205
Bulemba (BUL)	NA/N	25 47 16 S	31 04 55 E	1293
Doyershoek (DK)	HA/Y	25 51 44 S	30 46 43 E	1513
Galaxy Mine (GM)	HTNA/Y	25 49 22 S	30 58 59 E	978
Groen Vallei (GV)	HTNA/Y	25 53 34 S	30 48 13 E	1191
Kaapsehoop (KP)	HA/Y	25 33 15 S	30 48 25 E	1243
Komati (KOM)	HTNA/Y	26 06 00 S	29 26 00 E	1548
Lunar Observatory (LO)	HTNA/Y	25 52 04 S	30 45 49 E	1362
Mike's Field (MF)	HTNA/Y	25 53 13 S	30 44 12 E	1355
Mund's Concession (MC)	HTNA/Y	25 39 45 S	31 03 11 E	762
Nkomazi (NK+)	HA/Y	25 54 00 S	30 47 03 E	1139
Nkomazi (NK-)	HTNA/Y	25 54 03 S	30 47 16 E	1147
Non-serpentine (NS)	NA/N	25 51 38 S	30 45 14 E	1440
Pullen Farm (PF)	NA/N	25 34 20 S	31 10 50 E	921
Queen's River Valley (QRV)	HTNA/Y	25 49 15 S	30 53 26 E	912

2.2 Determination of metal ion concentration

Soil and tissue samples (2-5 g) were initially dried overnight at 60°C. The following day samples were homogenized with a Mortar Machine (Agate & General Stonecutters Ltd., London, UK) for 15-20 min or until a fine powder was achieved. The samples were then subjected to an ashing procedure. 1 g of each sample was weighted out and placed into ceramic crucibles. Samples were

further dried at 110°C for 4 h and finally roasted in a kiln at 850-1000°C overnight. Samples were re-weighed to ascertain any moisture loss.

Following ashing, samples were subjected to an acid digestion. 50 mg of each sample was weighted out and Hawaiian Basalt (BHOV-2) was used as a control. 4 mL of concentrated hydrofluoric acid (HF) was added to each sample and placed on a hot plate set at 60-70°C for 48 h. Following digestion, samples were opened and the HF was allowed to evaporate off. Complete evaporation was achieved in approximately 5 h. Samples were prepared for ICP-MS analyses by diluting with an internal standard solution (5% (w/v) HNO_3) containing 10 parts per billion (ppb) of In, Re, Rh and Bi as the internal standards. Standards were prepared in triplicate to produce a calibration curve. Sample analysis was done with the XSeries 2 ICP-MS (Thermo Fisher Scientific Inc., Waltham, MA, USA).

2.3 DNA based methodologies and analysis

2.3.1 Genomic DNA isolation

Genomic DNA was extracted using a modified method based on the protocol published by Dellaporta *et al.,* (1983). Fresh leaf tissue (150 – 250 mg) was homogenized in liquid nitrogen with a pestle and mortar. The homogenate was then transferred to a 2 mL microfuge tube with 100 µL 20% (w/v) SDS and 1.5 mL extraction buffer (100 mM Tris-HCl pH 8, 50 mM EDTA pH 8, 500 mM NaCl and 10 mM β-mercaptoethanol). Silica-desiccated tissue was placed directly into a 2 mL microfuge tube containing 1.5 mL extraction buffer with SDS. Inert ball bearings were added and tubes placed in a gyromixer SO-10m (Fluid Management Europe B.V, IDEX Corporation, UK) for 10 min. Samples were then incubated at 65°C for 10 min. 500 µL of 5 M potassium acetate was then added, vortexed briefly and incubated at 4°C for 20 min. Samples were centrifuged at 10 000 g for 25 min in a bench top centrifuge at 4°C. 1 mL of the resulting supernatant was collected and added to 1 mL isopropanol in a sterile 2 mL microfuge tube. The supernatant and isopropanol were mixed by inversion and incubated at -20°C for a minimum of 1 hour. The DNA was pelleted by

centrifugation at 10 000 g for 5 min at 4°C. The supernatant was discarded and the DNA pellet air dried by inverting tube on a paper towel for 40 min. The pellet was resuspended in 80 μL TE buffer (50 mM Tris-HCl pH 8 and 10 mM EDTA pH 8) and centrifuged at 10 000 g for 6 min to remove insoluble debris. The supernatant was transferred to a sterile eppendorf and 7.5 μL of 3 M sodium acetate (pH 5.2) and 50 μL of isopropanol were added, mixed well by inversion and placed on ice for 25 min. The DNA was pelleted by centrifugation at 10 000 g for 10 min. The pellet was washed with 1 mL 80% (v/v) ethanol, allowed to air dry for 30 min and resuspended in 15 μL TE buffer containing RNase (0.2 μg/μL) and stored at -20°C until needed. DNA concentrations were determined with a NanoDrop ND-100 spectrophotometer (NanoDrop Technologies, Wilmington, USA).

For extraction of gDNA for immediate use in PCR, the rapid technique developed by Bellstedt *et al*., (2010) was employed. 100 mg of plant tissue was placed in a 2 mL microfuge tube and 1.5 mL grinding buffer (15 mM Na_2CO_3, 35 mM $NaHCO_3$, 1% (w/v) $Na_2S_2O_5$, 2% (w/v) PVP40, 0.2% (w/v) BSA and 0.05% (v/v) Tween-20, pH to 9.6 with conc. NaOH) was added. Samples were briefly vortexed, before centrifugation for 15 sec at 10 000 g. Into a sterile PCR tube 4 μL of the resulting supernatant was added to 25 μL GES buffer (0.1 M glycine-NaOH pH 9.0, 50 mM NaCl, 1 mM EDTA pH 8.0 and 0.5% (v/v) Triton-X 100) and placed into a Gene Amp PCR System 2700 (Applied Biosystems, Foster City, USA) set for 10 min at 95°C then 5 min at 4°C. 1 μL of the resulting product was used directly as a template in PCR amplification.

2.3.2 PCR amplification of nuclear and chloroplast gene regions

Two classes of markers were optimized from an initial set of five primer pairs (table 2.2). To amplify the ribosomal internal transcribed spacer (ITS) ITS1 forward and reverse primers, **NNC-18S10:** AGGAGAAGTCGTAACAAG and **C26A:** GTTTCTTTTCCTCCGCT, were used (Wen & Zimmer, 1996). Thermal cycling conditions were modified from Mort *et al*., (2007) as follows; 2 min at 95°C; 35 cycles of 40 sec at 95°C; 40 sec at 52°C; 40 sec at 72°C; and a final extension step

of 10 min at 72°C. The reaction components consisted of 50-250 ng gDNA, 1 x reaction buffer (Fermentas International Inc., Ontario, Canada), 200 µM each dNTP, 1.5 mM $MgCl_2$, 0.7 µM each primer and 1 unit *Taq* DNA polymerase. Samples were equalized to 50 µL with sterile H_2O.

The non-coding chloroplast DNA (cpDNA) region trnfM-trnS was amplified using forward primer **trnfM^{CAU}:** CATAACCTTGAGGTCAGGG and reverse primer **trnS^{UGA}:** GAGAGAGAGGGATTCGAACC (Demesure *et al*., 1995). Thermal cycling conditions were modified from Shaw *et al.,* (2005) as follows; 5 min at 94°C; 35 cycles of 45 sec at 94°C; 45 sec at 60°C; 50 sec at 72°C; and a final extension step of 10 min at 72°C. The reaction components consisted of 100-250 ng gDNA, 1 X reaction buffer (Fermentas International Inc., Ontario, Canada), 200 µM each dNTP, 3 mM $MgCl_2$, 0.75 µM each primer and 1.5 units *Taq* DNA polymerase. Samples were equalized to 50µL with sterile H_2O. All PCR reactions were carried out in a 96 well Gene Amp PCR System 2700 (Applied Biosystems, Foster City, USA) and the size of PCR products was confirmed by agarose gel electrophoresis.

Table 2.2: Gene regions tested for phylogeny reconstruction of *Senecio coronatus*

Marker used	Primer designation and sequence (5' to 3')		Product produced	Source
ITS1	**NNC18s10**	AGGAGAAGTCGTAACAAG	Yes	Wen & Zimmer, 1996
	C26A	GTTTCTTTTCCTCCGCT		
ETS	**1*f***	CTTTTTGTGCATAATGTATATATAGGGGG	No	Linder *et al.,* 2000
	18s-2L	TGACTACTGGCAGGATCAACCAG		
Trn set 1	**trnfM^{cau}**	CATAACCTTGAGGTCACGGG	Yes	Demesure *et al*., 1995
	trnS^{UGA}	GAGAGAGAGGGATTCGAACC		
Trn set 2	**trnL^{UAA}R**	TCTACCGATTTCGCCATATC	No variation	Taberlet *et al*., 1991
	trnT^{UGU}2F	CAAATGCGATGCTCTAACCT		Shaw *et al*., 2005
Trn set 2	**psbA**	GTTATGCATGAACGTAATGCTC	No	Sang *et al.,* 1997
	trnH^{GUG}	CGCGCATGGTGGATTCACAATCC		Tate & Simpson, 2003

2.3.3 Agarose electrophoresis

To validate a single PCR product, a 10 μL aliquot of the product in 1 x loading dye (0.25% (w/v) xylene cyanole FF, 40% (w/v) sucrose and 0.25% (w/v) bromophenol blue) was loaded onto a 1.2% (w/v) agarose gel with ethidium bromide (0.016 μL/mL) added to the gel. The O'Gene Ruler™ 1kb DNA size marker (Fermentas International Inc., Ontario, Canada) was loaded as a standard DNA ladder. Gels were electrophoresed at 120-140 V in 1 x TAE buffer (40 mM Tris, 1 mM EDTA pH 8 and 0.11% (v/v) glacial acetic acid) for 90-120 min. PCR products were visualized with a G:BOX Bioimager (Syngene Bioimaging Private Ltd., USA).

2.3.4 Agarose gel DNA purification

Once a 10 μL aliquot of PCR product was electrophoresed and confirmed to contain a single product, the remaining 40 μL PCR reaction was subjected to agarose gel electrophoresis as described in section 2. 3. 3. PCR products were visualized on a long wavelength (365 nm) UV transilluminator (UVP Inc, San Gabriel, USA) to minimize DNA damage during excision. A sterile razor blade was used to cut out the desired DNA band. DNA extraction from the gel slice was performed using a Wizard® SV Gel and PCR Clean up System (Promega Corporation, Madison, USA) as per manufacturer's instructions with modifications. Modifications include heating the nuclease-free water to approximately 50°C prior to elution and a final elution volume of 30 μL was used. Further all centrifugations took place at 10 000 g for 1.5 min.

2.3.5 Sequencing

PCR products were sequenced in both directions using BigDye® sequencing chemistry (Applied Biosystems, Foster City, USA). The concentrations of purified PCR reactions were first determined using a Nanodrop ND-100 spectrophotometer. Optimum sequencing efficiency occurred at a DNA

concentration of 50 ng/μL and a minimum of 15 μL of each sample was required. DNA sequences were determined with an ABI PRISM® 3700 DNA Analyzer (Applied Biosystems, Foster City, USA) via an automated capillary electrophoresis system using the Macrogen DNA Sequencing Service (Macrogen Inc, Seoul, Korea).

2.4 Sequence data analysis

2.4.1 Sequence editing and alignment

DNA sequences were edited and manually checked for base call errors using eBioX 1.5.1 (Lagercrantz, 2008). Multiple sequence alignments (MSA) were then produced with the ClustalW (Thompson *et al.,* 1994) function in BioEdit (7.0.5.2) (Hall, 1999). Three MSA data sets were produced, including an ITS data set (appendix 1) comprised of 136 sequences (each containing 665 nucleotide base pairs), a TrnfM/S data set (appendix 2) comprised of 37 sequences (each containing 851 nucleotide base pairs), and a combined data set where ITS and corresponding TrnfM/S sequences were spliced together to produce a data set of 35 sequences (each containing 1523 nucleotide base pairs).

2.4.2 Population genetic diversity

Nucleotide (π) and haplotype diversity (Hd) were calculated for each sampling site in Arlequin 3.5.1.3 (Excoffier & Lischer, 2010) and DnaSP v5 (Librado *et al.,* 2009), respectively. DnaSP was further utilized to generate unique haplotype lists for each data set. DnaSP is able to read unphased genotype data files (from diploid individuals) in FASTA format. Haplotype phase reconstruction from unphased data was performed in the sequence analysis package PHASE (Stephens *et al.,* 2001; Stephens & Donelly, 2003). Hd (gene/allele diversity) represents the expected heterozygosity within a population and gives a measure of whether randomly chosen sequences are the same or different from one another.

2.4.3 Phylogenetic relationships and population structure of *Senecio coronatus*

Evolutionary relationships among collected *S. coronatus* populations were explored using distance-based methods in MEGA 5 (Tamura *et al.,* 2011). The Neighbor-joining tree method (Saitou & Nei, 1987) was used to construct phylogenies. Genetic distance matrices were transformed (or corrected) utilizing the Kimura 2-parameter substitution model (Kimura, 1980) for all data sets. The Kimura 2-parameter model (corrected d-distance) takes into account that transition mutations occur at a greater rate than transversion mutations, while assuming that the four-nucleotide frequencies are the same. For all phylogenies, the statistical robustness of the tree was assessed by 10 000 bootstrap replications (Felsenstein, 1985). Phylogenies were created from both edited marker sequence alignment data as well as unique haplotype sequence (identified by DnaSP v5) alignment data.

Using haplotype frequencies an analysis of molecular variance (AMOVA) was used to quantify the degree to which both populations and the different phenotypes were genetically structured. AMOVA was performed in Arlequin 3.5 and calculates the fixation index (Wright, 1949) or ph- (Φ). In this case, for a hierarchically structured data set – this estimates the level of genetic diversity and differentiation between and among defined population groups. Arlequin 3.5 input data files were structured by phenotype for all three data sets, as well as by phylogenetic clusters for the ITS and ITS-TrnfM data sets only.

2.5 Protein based methodologies and analysis

2.5.1 Total protein isolation

Extraction of total protein was adapted from Ingle *et al*. (2005b). 200-400 mg of fresh leaf tissue was homogenized by pestle and mortar in liquid nitrogen. The homogenate was then transferred to a 2 mL microfuge tube containing 1.2 mL of ice-cold extraction buffer (0.5 M Tris-HCl pH 7.5, 10 mM EDTA pH 8, 1% (v/v) Triton X-100, 2% (v/v) β-mercaptoethanol and 1 mM phenylmethylsulfonyl

fluoride (PMSF)) and vortexed for 10 sec. The samples were then centrifuged at 10 000 g for 7 min at 4°C. 500-800 μL of the resulting supernatant was transferred to a sterile 2 mL microfuge tube and the volumes of all samples were equalized with ice-cold extraction buffer. An equal volume of ice-cold Tris-HCl (0.5 M, pH 8)-saturated phenol was added and the samples vortexed for 10 sec before being centrifuged at 10 000 g for 90 sec. Approximately 80% of the upper aqueous phase was removed and discarded, taking care not to disturb the interface. The organic phase was re-extracted by adding an equivalent '80%' volume of ice-cold extraction buffer, vortexing for 10 sec and centrifuged at 10 000 g for 1 min. A volume equal to extraction buffer added (in previous step) was then removed and discarded. Five volumes of 0.1 M ammonium acetate in methanol (MeOH) was added and the sample incubated at -20°C overnight. The following day, the samples were centrifuged at 10 000 g for 8 min at 4°C to obtain the protein pellets. The supernatant was discarded and the pellets washed with 1 mL 0.1 M ammonium acetate in MeOH and then with 80% (v/v) acetone. Pellets were allowed to air dry for 30-60 min in a fume hood.

For protein to be used in 2D-SDS PAGE application (see below), pellets were subsequently resuspended in ULB buffer (6 M urea, 2 M thiourea and 2% (w/v) CHAPS), by adding 20 μL increments to the point just where all protein is in solution. The protein concentration was then determined via an HCL-modified Bradford Assay (adapted from the Bio-Rad Protein Assay Manual), using BSA to produce a standard curve. For 1D-SDS PAGE application, protein pellets were resuspended in 40 μL 1 x sample application buffer (62.5 mM Tris pH 6.8, 10% (v/v) glycerol, 2% (w/v) SDS, 1% (v/v) β-mercaptoethanol and trace bromophenol blue). Protein quantitation was performed via the Bradford Assay (Bradford, 1976). Prior to 1D-SDS PAGE samples were heated to 95°C for 10 min. All protein samples not used were stored at -80°C.

2.5.2 Sodium dodecyl sulphate polyacrylamide gel electrophoresis (SDS-PAGE)

2.5.2.1 1D SDS-PAGE

12% (v/v) polyacrylamide gels were prepared from a 40% (w/v) acrylamide/bis-acrylamide stock solution (Bio-Rad Laboratories, Inc. Hercules, USA) using a Mini-PROTEAN® 3 Multi-Casting Chamber (Bio-Rad Laboratories, Inc. Hercules, USA). The separating gel (12% (v/v) acrylamide/bis-acrylamide, 375 mM Tris pH 8.8, 0.1% (w/v) SDS, 0.1% (w/v) ammonium persulphate (APS) and 0.05% TEMED) was applied to the base of the casting chamber via syringe until all 12 gels were approximately 3/4 from the top of the gel plates and the casting tray was closed with a valve. Gels were immediately covered with 1 mL isopropanol and allowed to set for approximately 30 min at room temperature. Once set, the isopropanol was removed and the gels rinsed with sterile H_2O. The separating gels were then covered with a stacking gel (5% (v/v) acrylamide/bis-acrylamide, 125 mM Tris pH 6.8, 0.1% (w/v) SDS, 0.09% (w/v) APS and 0.1% (v/v) TEMED), and a comb placed into the stacking gel, which set in approximately 45 min at room temperature. Once set, 15-30 μg denatured protein sample and an appropriate molecular marker were loaded onto the stacking gel and electrophoresed at 100-140 V using a Mini-PROTEAN® 3 Dodeca™ Cell (Bio-Rad Laboratories, Inc. Hercules, USA) in 1 x TGS running buffer (25 mM Tris pH 8.3, 192 mM glycine and 0.1% (w/v) SDS) for 2-3 h or until the dye front had just run off the gel.

2.5.2.1.1 Visualization of proteins

Protein resolution and quantity was visualized by staining with 80 mL Coomassie Brilliant Blue R 250 for 1 h with agitation at room temperature. To destain the gels, 100 mL of fixing solution (50% (v/v) MeOH and 10% (v/v) glacial acetic acid) was used initially for 20 min with agitation. This was then discarded and replaced with a destain (Sambrook & Russell, 2001) solution (50% (v/v) MeOH, 10% (v/v) glacial acetic acid and 10% (v/v) glycerol) and left overnight with agitation. The following day, the destain solution was removed

and the gels rinsed twice with sterile H_2O. The gels were stored in sterile H_2O at 4°C.

2.5.2.2 2D gel procedure

2.5.2.2.1 IPG strip rehydration

Protein samples (125 μg) in ULB were allowed to thaw at room temperature. ULB buffer is reconstituted to IPG sample buffer by the addition of 2% (v/v) IPG buffer (BioRad Laboratories, Inc. Hercules, USA), 0.3% (w/v) DTT and trace bromophenol blue. Samples were equalized with ULB to 155 μL and subsequently used to rehydrate ReadyStrip™ IPG strips pH 4-7 (Bio-Rad Laboratories, Inc. Hercules, USA) as per manufacturer's instructions. A disposable rehydration/equilibration tray (Bio-Rad Laboratories, Inc. Hercules, USA) was used to house the IPG strips during rehydration (12-16 h).

2.5.2.2.2 Isoelectric focusing

20 min prior to completion of rehydration a clean focusing tray (Bio-Rad Laboratories, Inc. Hercules, USA) was prepared by covering the wire electrodes with Whatman paper that had been moistened with deionized H_2O. IPG strips were drained of residual mineral oil by blotting the tip of the strips on Whatman/filter paper. The IPG strips were then transferred from the disposable rehydration/equilibration tray to the focusing tray with the gel side facing down, taking note of the IPG strip polarity. 1-2 mL of fresh mineral oil was overlaid on each strip. Focusing the first dimension employed the use of a PROTEAN® IEF Cell (Bio-Rad Laboratories, Inc. Hercules, USA). Isoelectric focusing was performed using a ramp voltage protocol of 250 V for 20 min (ramped), 4000 V for 2 h, 4000 V for 20 000 volt hours and a 500 V hold step (24 h) if required. After completion of focusing, if strips were not to be used immediately the strips were transferred to a clean rehydration/equilibration tray. 1mL of fresh mineral oil was overlaid and the tray covered with cling-film and stored at -80°C. Alternatively, strips used immediately after rehydration were equilibrated in an SDS-containing buffer (see below) prior to running the second dimension.

2.5.2.2.3 2D SDS-PAGE

Stored IPG strips were allowed to thaw at room temperature for 10-15 min. Excess mineral oil was removed by placing IPG strips gel side up onto dry Whatman paper and blotted gently with a wet piece of Whatman paper. Each strip was then equilibrated in 1.5 mL of SDS-PAGE equilibration buffer I (6 M urea, 0.375 M Tris-HCl pH 8.8, 2% (v/v) SDS, 20% (v/v) glycerol and 2% (w/v) DTT) for 10 min with gentle agitation. Strips were then subsequently placed into 1.5 mL of SDS-PAGE equilibration buffer II (6 M urea, 0.375 M Tris-HCl pH 8.8, 2% (v/v) SDS, 20% (v/v) glycerol and 2.5% (w/v) iodoacetamide) for 10 min with gentle agitation.

Twelve 12% (v/v) polyacrylamide separating gels were cast simultaneously with a Mini-PROTEAN® 3 Multi-Casting Chamber as detailed in section 2.5.2.1. The separating gel was filled to approximately 4/5 from the top of the plates, covered with 1 ml isopropanol and allowed to set. Once set, the isopropanol was rinsed off with sterile H_2O. Upon equilibration of the IPG strips, 0.5% (w/v) agarose in 1 x TGS running buffer was pipetted onto the separating gel. Equilibrated IPG strips were rinsed with 1 x TGS running buffer in a 100 mL graduated cylinder and loaded into the agarose overly, ensuring no air bubbles between the strip-separating gel interface occurred before allowing the agarose to set. The second dimension was electrophoresed at 80 V for 1 h, then increased to 140 V for 2-4 h or until the dye front just ran off the gel. After completion of electrophoresis the proteins were fixed in 100 mL fixing solution (50% (v/v) MeOH and 10% (v/v) glacial acetic acid) with gentle agitation for 30 min followed by an overnight incubation in 75 mL fresh fixing solution.

2.5.2.2.4 Visualization of total protein

The following day, the gels were washed in 100 mL sterile deionized H_2O. To visualize total protein, each gel was stained with 100 mL of Colloidal Coomassie G 250 (1% (v/v) coomassie G 250 stock, 3% (v/v) orthophosphoric acid and 6% (w/v) ammonium sulphate) for 6-12 h with gentle agitation at room temperature. The gels were destained using two destains (Sambrook & Russell, 2001). Destain 1 (50% (v/v) MeOH and 10% (v/v) glacial acetic acid) for 45 min

with gentle agitation followed by Destain 2 (5% (v/v) MeOH, 7% (v/v) glacial acetic acid and 3% (v/v) glycerol) 2-3 h with gentle agitation.

Coomassie G 250 stock was made by dissolving 30 g of Coomassie Gerva Blue G in 750 mL 7.5% (v/v) glacial acetic acid at approximately 70°C, whilst slowly adding ammonium sulphate and stirring until the solution became clear. The solution was allowed to cool to room temperature and the supernatant discarded. The resulting precipitate was dissolved in 300 mL 50% (v/v) ethanol and 10% (v/v) acetic acid and stored at room temperature.

2.5.3 Protein gel analysis

Gel images were acquired utilizing a flatbed CanoScan LiDE25 colour scanner (Canon Inc., Lake Success, New York, USA). Scanning parameters within the program SilverFast® 6 (LaserSoft Imaging®) were set to 16-bit grey-scale with a resolution of 300 dots per inch (Dpi).

Protein spot detection, matching and subsequent quantification was carried out using software within the program Melanie 7.0 (Swiss Institute of Bioinformatics). Within Melanie 7.0, default settings were used with the exceptions of smooth(ness), saliency and minimum spot area, which were set to 3, 150 and 50, respectively. In all experiments three biological gel replicates were used for each sample site and are designated as 'gel classes' in this study. Protein spots were compared across gel classes and a statistical analysis (ANOVA) was used to detect spots showing a significant ($P < 0.05$) difference in abundance between gel classes AM, GM, KP and PFX respectively.

2.5.4 Protein identification by nano-LC and Mass Spectrometry (LC-MS/MS)

Protein spots chosen for excision were sent for identification using the Central Analytical Facilities (CAF) at the Proteomics Laboratory, MS Unit, Stellenbosch University, South Africa. Protein identification was achieved utilizing a Thermo Scientific EASY-nLC II connected to a LTQ Orbitrap Velos mass spectrometer,

equipped with a nano-electrospray source (Thermo Scientific, Germany). Thermo Proteome Discoverer 1.3 (Thermo Scientific, Bremen, Germany) was used to identify proteins via automated database searching (Mascot, Matrix Science, London, UK) of all tandem mass spectra against the NCBI green plants database. Data analysis parameters were performed by CAF as follows; carbamidomethyl cysteine was set as fixed modification, and oxidized methionine, N-acetylation and deamidation (NQ) was used as variable modifications. The precursor mass tolerance was set to 20 ppm, and fragment mass tolerance set to 0.8 Da. Two missed tryptic cleavages were allowed. Proteins were considered positively recognized when they were identified with at least 2 tryptic peptides per protein, and a Mascot significance ($P < 0.05$) score as determined by Proteome Discoverer 1.3. Percolator was also used for validation of search results. In Percolator a decoy database was searched with a FDR (strict) of 0.02 and FDR (relaxed) of 0.05 with validation based on the q-value.

Chapter 3

Results and Discussion

3.1 Determination of nickel ion concentration

Nickel hyperaccumulating and hypertolerant non-accumulator taxa are known to display dramatically different phenotypes with respect to the amount of Ni accumulated and subsequent partitioning between root and shoot tissues. While plant HM hyperaccumulation tends be a species-wide or constitutive trait, *S. coronatus* seems to be unique in that some populations found on serpentine outcrops hyperaccumulate Ni, while neighbouring populations on apparently similar serpentine soils do not (table 3.1). A study by Boyd *et al.,* (2008a) has demonstrated this apparent variation in four *S. coronatus* populations distributed within 20 km of one another. Sample collection sites ('Doyershoek', 'Groen Vallei', 'Groen Vallei Mine' and 'Airstrip Serpentine') were shown to contain similar total and soluble Ni content. The study demonstrated Ni content from leaf and root material exhibited total Ni values in the range of 0.012 - 1.2 % Ni on a dry biomass basis (Boyd *et al.,* 2008a). Differences in Ni content between the four populations are thought to be as a consequence of genetics rather than soil Ni content or phytoavailability in this taxon. The 'genetic based' hypothesis is supported by the presence of *B. coddii* at all four sites, which in contrast to *S. coronatus*, accumulated Ni to > 0.8 % on a dry biomass basis (Mesjasz-Przybyłowicz *et al.,* 2007; Boyd *et al.,* 2008a). Furthermore, Ni hyperaccumulating *S. coronatus* individuals removed *in situ*, were shown to maintain their Ni uptake rate when transplanted to serpentine soil collected from sites of hypertolerant non-accumulator occurrence, while the non-accumulator individuals were unable to accumulate Ni when transplanted to serpentine soils from sites of hyperaccumulator occurrence (Mesjasz-Przybyłowicz *et al.,* 2007).

Table 3.1: A summary of Ni concentrations from soil, root and leaf samples of various *Senecio coronatus* populations collected in South Africa. Data shown are means with standard deviation in parenthesis.

Sample site	Sample type	Ni concentration (µg/g)	Sample size	Reference
Agnus Mine	soil	1094.39 (31.45)	n/a	Mesjasz-Przybyłowicz *et al.,* 2007
Songimvelo	soil	2104.92 (363.51)	n/a	Mesjasz-Przybyłowicz *et al.,* 2007
Agnus Mine	root	1760 (18)	10	Mesjasz-Przybyłowicz *et al.,* 2007
Songimvelo	root	34 (1)	10	Mesjasz-Przybyłowicz *et al.,* 2007
Groenvaly	root	2100 (580)	6	Boyd *et al.,* 2008a
Doyershoek	root	1200 (57)	2	Boyd *et al.,* 2008a
Groenvaly Mine	root	25 (8.9)	6	Boyd *et al.,* 2008a
Airstrip	root	50 (12)	6	Boyd *et al.,* 2008a
Groenvaly	leaf	12000 (1800)	11	Boyd *et al.,* 2008a
Doyershoek	leaf	8800 (2000)	6	Boyd *et al.,* 2008a
Groenvaly Mine	leaf	130 (36)	6	Boyd *et al.,* 2008a
Airstrip	leaf	120 (29)	16	Boyd *et al.,* 2008a
Groenvaly	leaf	9200 (670)	10	Boyd *et al.,* 2008b
Doyershoek	leaf	15000 (610)	10	Boyd *et al.,* 2008b
Groenvaly Mine	leaf	130 (13)	10	Boyd *et al.,* 2008b
Airstrip	leaf	16 (2.6)	10	Boyd *et al.,* 2008b
East of Badplaas	leaf	12100 (1790)	3	Boyd *et al.,* 2002
East of Badplaas	leaf	684 (64.3)	3	Boyd *et al.,* 2002

Considering that samples collected for this study come from the same Mpumalanga region as those collected by Boyd *et al.,* (2008a), we expected that some populations of *S. coronatus* collected from serpentine sites would hyperaccumulate Ni, while others would instead display a hypertolerant non-accumulator phenotype. As detailed in section 2.1, plant samples were preliminarily screened for the ability to hyperaccumulate Ni by use of DMG-indicator paper. Subsequently, all sites chosen for Ni ion content analysis were in close proximity. Specifically, the serpentine site Nkomazi was sampled for hyper- and non-accumulator populations (namely, NK+ and NK-) within a 500 m range. Similarly, serpentine sites Agnus Mine (AM) and Galaxy Mine (GM), which are 3 km apart were sampled for hyperaccumulator and hypertolerant non-

accumulator populations, respectively. Further, sampling from Pullen Farm (PF) represents a non-serpentine site.

To assess whether *S. coronatus* populations collected do indeed exhibit different and distinct Ni tolerance phenotypes, Ni quantitation of soil samples (collected directly around roots) and corresponding leaf material was achieved by sample homogenization, ashing and subsequent Ni determination by ICP-MS.

As is evident in figure 3.1, the Ni content of soils collected from sites AM, GM, NK+ (Nkomazi soil around hyperaccumulator *S. coronatus* occurrence), NK- (Nkomazi soil around non-accumulator *S. coronatus* occurrence) and KP (Kaapsehoop) all show average values over 1000 parts per million (ppm) Ni, characteristic of serpentine outcrops. In particular soil from the KP site showed the greatest amount of Ni content, with an average of ~ 3500 ppm Ni. Soil collected from the non-serpentine site PF displayed an average Ni content of only ~ 60 ppm Ni (appendix 3).

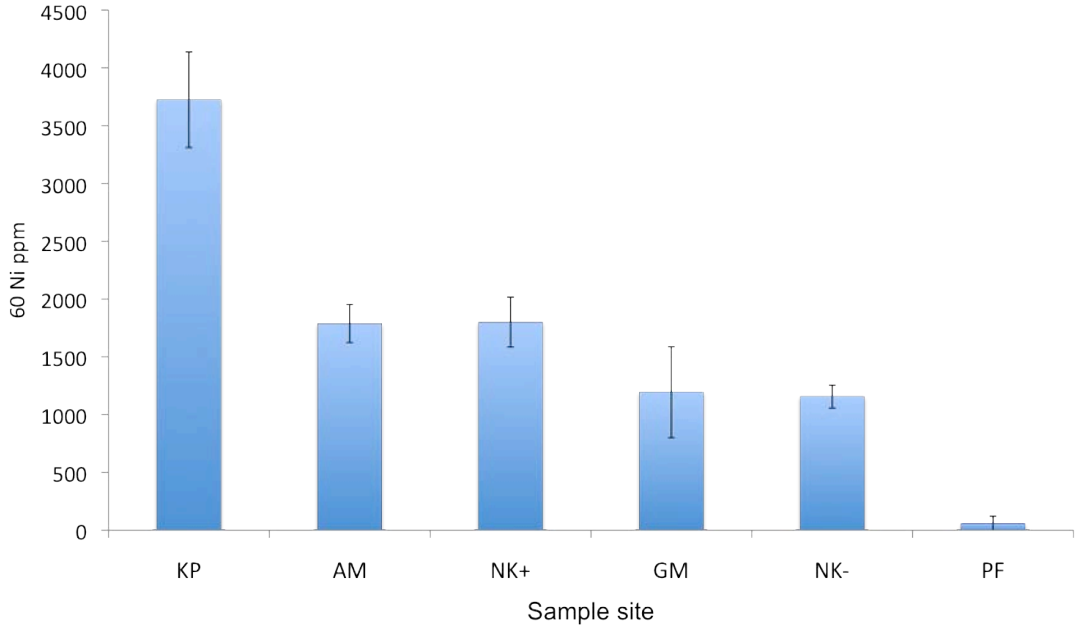

Figure 3.1: Mean total Ni content ± SD in soil samples (n = 3) collected from Kaapsehoop (KP), Agnus Mine (AM), Nkomazi soil around hyperaccumulator occurrence (NK+), Galaxy Mine (GM), Nkomazi soil around non-accumulator occurrence (NK-) and Pullen Farm (PF).

Following soil analysis, corresponding leaf samples were analyzed (figure 3.2). Of the five serpentine sites, the three populations AM, KP and NK+ all contained an average Ni content > 4000 ppm Ni (0.4 % on a dry biomass basis), which is equivalent to four times the threshold criterion set for Ni hyperaccumulation (Reeves & Baker, 2000; Verbruggen *et al.,* 2009). In stark contrast however, Ni content of leaf samples collected from GM and NK-, display average Ni content of ~ 106 ppm and ~ 130 ppm respectively (appendix 4), which is approximately 10-fold below the internal Ni hyperaccumulation threshold (0.1 % on a dry biomass) and are therefore likely hypertolerant non-accumulators. These results are in agreement with *in situ* DMG testing of leaf materials.

A direct comparison of Ni content in leaf and corresponding soil samples highlights the large degree of Ni enrichment that occurs in hyperaccumulator populations compared to nearby non-accumulator populations. Figure 3.3 shows hyperaccumulators AM, KP and NK+ actively move Ni into the plant against the soil-plant concentration gradient, resulting in leaf Ni content greater than the surrounding soils. In contrast, populations GM and NK- did not show any Ni enrichment as soil Ni content was seen to be greater than the leaf content. Further, as soil samples from PF contained relatively negligible Ni content, corresponding plant specimens sampled did not show any noticeable Ni accumulation.

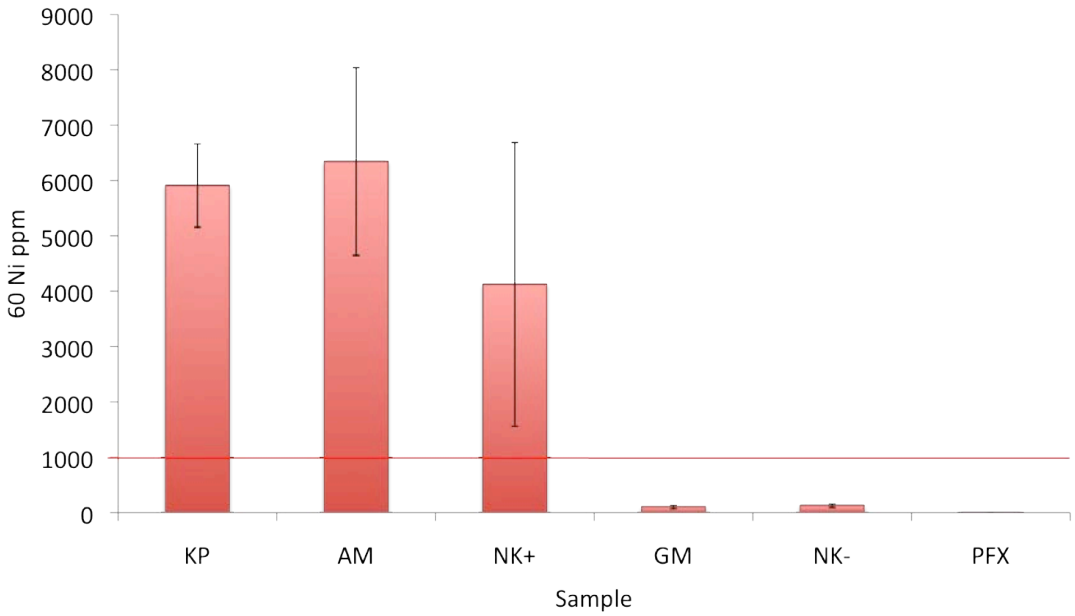

Figure 3.2: Mean total Ni ion content ± SD in ashed leaf samples (n = 3) collected from Kaapsehoop (KP), Agnus Mine (AM), Nkomazi serpentine (NK+), Galaxy Mine (GM), Nkomazi non-serpentine (NK-), and Pullen Farm (site; PF, sample; PFX). The horizontal red line indicates the internal Ni threshold for defining Ni hyperaccumulating plant taxa.

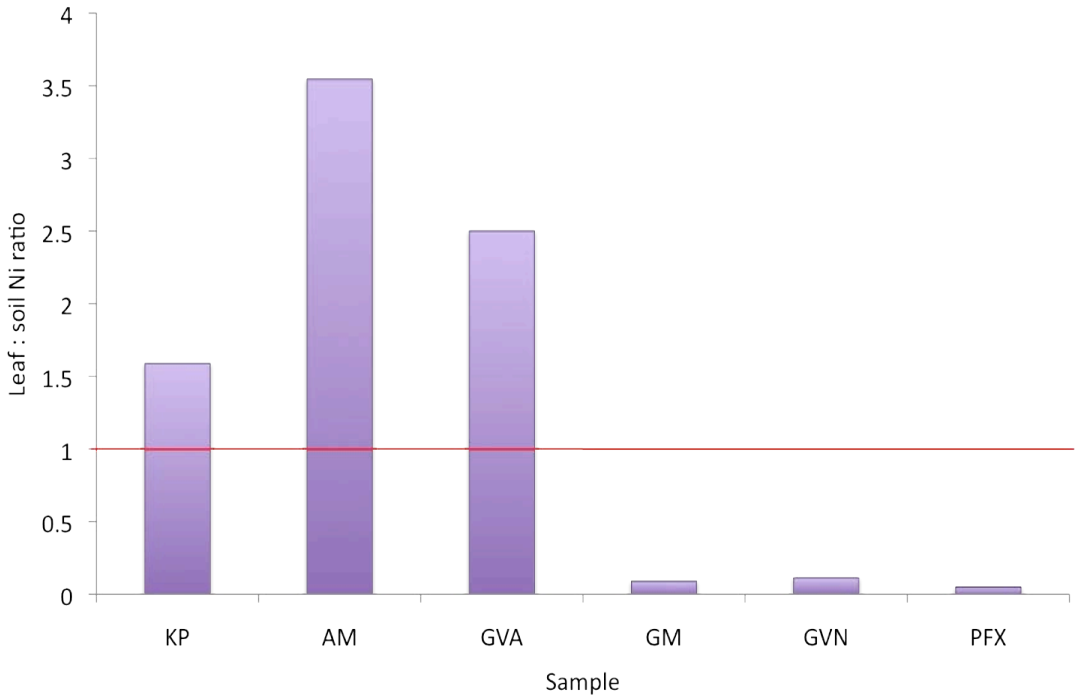

Figure 3.3: Leaf Ni enrichment. Leaf Ni content was divided by corresponding soil Ni content so as to infer enrichment of samples (n = 3) collected from Kaapsehoop (KP), Agnus Mine (AM), Nkomazi serpentine (NK+), Galaxy Mine (GM), Nkomazi non-serpentine (NK-), and Pullen Farm (site; PF, sample; PFX). A ratio ≥ 1 as indicated by the horizontal red line, highlights samples displaying active Ni enrichment.

The data confirms that populations of *S. coronatus* found on similar serpentine outcrops display two distinct Ni tolerance phenotypes, namely, Ni hyperaccumulator and Ni hypertolerant non-accumulator. Populations from the PF site did not accumulate any Ni, however as the soil Ni content at this site is negligible, it is not possible to determine from this data which Ni accumulation phenotype PF samples would express under elevated soil Ni levels.

Soil Ni content does not seem to be a major selective pressure for evolution towards Ni hyperaccumulation, as populations that inhabit similar soil types with respect to Ni content, display two distinct adaptive mechanisms. This is most prominent in the Nkomazi area, where populations NK+ and NK- are situated within 500 m of each other, and yet display two very different Ni accumulation phenotypes. Hence, a hypothesis of genetic differentiation along phenotypic expression with respect to Ni tolerance and not Ni phytoavailability is supported by these data.

Occurrence of different Ni accumulation phenotypes informs on different physiological adaptive mechanisms used to cope with elevated soil Ni content, yet phenotypic plasticity does not infer much on the evolutionary relationships between the aforementioned populations. Hence, to ascertain whether the phenotypically diverse populations of *S. coronatus* collected display a similar degree of genotypic variation, we undertook an initial genomic characterization by examination of non-coding nuclear and plastid gene regions.

3.2 Genetic diversity in populations of *Senecio coronatus*

Serpentine outcrops essentially occur as discontinuities across the landscape and have been described as 'ecological or edaphic islands' (Lefèbvre & Vernet, 1990). As these islands are colonized, newly established populations may experience significant physiological stress and, as a result, exhibit founder effects as plants adapt to the local conditions (Lefèbvre & Vernet, 1990); this would likely influence patterns of genetic variation across a landscape and may influence local population genetic differentiation with respect to phenotype.

To explore this process at a fine scale, a number of population genetic parameters were estimated for *S. coronatus* populations in the study area. Estimates of haplotype and nucleotide distance and diversity were calculated across data sets and used to infer phylogenetic relationships and population genetic structure across populations. Diversity estimates provide insight about the history of populations (Staton *et al.,* 2001). For example, populations that contain low nucleotide (π) and haplotype (Hd) diversities may have experienced an acute bottleneck event relatively recently. While populations that contain high haplotype diversity and moderate to low nucleotide diversity could suggest fast population growth and recent colonization from a relatively small founder population.

Diversity estimates of ITS and TrnfM *S. coronatus* data sets reveal relatively high Hd and π values (table 3.2). Both data sets show a similar pattern of moderate π diversity and high Hd diversity with values over 0.001 and 0.8, respectively. Analysis of the ITS data set for hyper- versus non-accumulators, reveals a higher diversity in the hyperaccumulator group with a diversity of approximately $\sim$ 0.8, compared to non-accumulator diversity calculated to approximately $\sim$ 0.7. These results are unexpected given the hypothesis that plant populations on metal-rich outcrops may experience strong founder effects and hence a reduction in diversity (Lefèbvre & Vernet, 1990). The TrnfM data on the other hand demonstrates a significantly lower diversity within the hyperaccumulator group, specifically π diversity which gave values of approximately $\sim$ 0.001 and $\sim$ 0.003 for hyper- and non-accumulator populations, respectively (table 3.2). This is accordance with a 'hyperaccumulator founder effect' hypothesis. Overall high Hd and moderately high nucleotide diversities may further represent populations that are historically divergent, and have recently gained access to one another.

Table 3.2: Diversity estimates for ITS and TrnfM sequences in *Senecio coronatus*. In addition, data was further arranged to contain only hyperaccumulator (HA) and non-accumulator population (NA) sequences. To ensure accuracy of *S. coronatus* population diversity, all *S. conrathii* (BUL) sequences were removed before diversity estimates were made.

Data set	Number of sequences	Number of polymorphic sites	Number of haplotypes	Nucleotide diversity	Haplotype diversity
ITS	132	37	20	0.014 ± 0.00073	0.82 ± 0.014
ITS (HA)	53	18	9	0.011 ± 0.00040	0.81 ± 0.020
ITS (NA)	79	28	13	0.011 ± 0.00120	0.70 ± 0.032
TrnfM	36	11	14	0.003 ± 0.00017	0.82 ± 0.023
TrnfM (HA)	13	5	5	0.001 ± 0.00025	0.55 ± 0.100
TrnfM (NA)	23	10	10	0.003 ± 0.00023	0.68 ± 0.047

The ITS data haplotype structure reveals that in general haplotypes are shared between sampling sites where *S. coronatus* individuals display the same Ni accumulation phenotype (table 3.3 and figure 3.4). For example, hyperaccumulator populations DK and NK+ share haplotypes 9, 10 and 11 while non-accumulator populations GM, GV, MF and QRV share haplotype 12. Plants collected from the non-serpentine PF site, which do not exhibit Ni accumulation, share haplotypes with hypertolerant populations GM, GV, KOM and QRV for example. Interestingly however, hyperaccumulator samples collected from KP are seen to share haplotypes 14 and 18 with numerous hypertolerant non-accumulators such as GM, GV, LO, MC, MF and QRV which advocates some degree of gene flow between these sample occurrences.

Table 3.3: List of unique haplotype sequences with respect to sample locality and generated from ITS data (see appendix 5 for list of unique TrnfM haplotype sequences).

Site name (abbreviation)	Haplotype number(s)
Agnes Mine (AM)	5, 6, 7, 8
Doyershoek (DK)	9, 10, 11
Kaapsehoop (KP)	14, 18
Nkomazi (NK+)	9, 10, 11
Galaxy Mine (GM)	12, 13, 14, 15, 16, 18
Groen Vallei (GV)	12, 13, 14, 18
Komati (KOM)	14, 19, 20
Lunar Observatory (LO)	14
Mike's Field (MF)	12, 14, 18
Mund's Concession (MC)	14, 18
Nkomazi (NK-)	14, 17, 18
Queen's River Valley (QRV)	12, 14
Badplaas (BP)	1, 2, 3
Pullen Farm (PF)	2, 12, 13, 14, 18
Non-serpentine (NS)	1, 2, 4
Bulemba (BUL)	21, 22, 23, 24

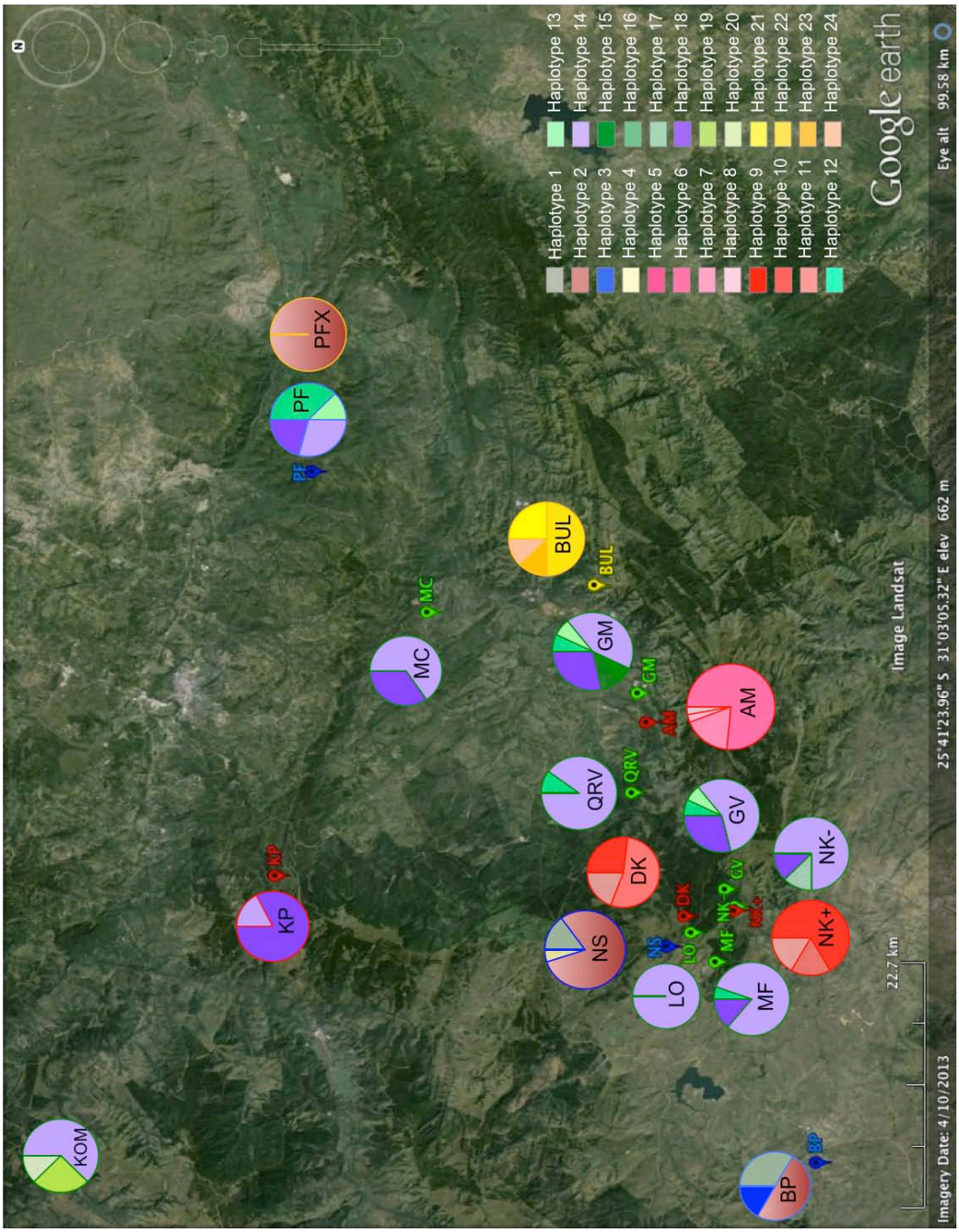

Figure 3.4: The distribution of ITS haplotypes across *Senecio coronatus* ecotypes collected in the Mpumalanga province, South Africa. Pie charts represent the presence (by colour) and frequency (%) of a specific haplotype within that population. Site names are coloured by soil type and plant phenotype. Site name colours of red, green and blue indicate Ni hyperaccumulator, non-accumulator and non-accumulator occurrence on non-serpentine soils, respectively. The yellow site name indicates the collection site of the sympatric species *S. conrathii*, a non-accumulator species on non-serpentine soil (see appendix 6 for TrnfM haplotype frequency figure).

A population genetics study on *T. caerulescens* samples collected across western Switzerland, examined whether natural variation in soil metal content has an effect on genetic structure (Besnard *et al.,* 2009). The study employed nuclear and plastid markers (such as TrnS-TrnG). In line with our results on diversity of collected *S. coronatus* populations, nuclear gene diversity and genetic differentiation between *T. caerulescens* populations were relatively high (Hd = 0.535 and Φst = 0.591, respectively). The authors suggested that a combination of events such as frequent population inbreeding coupled within limited gene flow between locations might contribute to the relatively high genetic differentiation observed (Dubois *et al.,* 2003; Besnard *et al.,* 2009). Plastid (CpDNA) gene diversity between populations was also very high (Hd = 0.65) and three separate genetic lineages were identified by CpDNA haplotype distribution (Besnard *et al.,* 2009). A study by Quintela-Sabarís *et al.,* (2010) which utilized chloroplast microsatellite sequences from 33 natural populations of *Cistus ladanifer* L, (distributed across Morocco, Portugal and Spain), also reports significantly high haplotype diversity (0. 91), yet no significant differences in diversity within and/or between metalliferous and non-metalliferous populations of the metal hypertolerant shrub were seen. The study further demonstrates that hypertolerant metalliferous populations might have evolved through multiple independent events, with no evidence of a genetic bottleneck event occurring due to elevated metal soil content (Quintela-Sabarís *et al.,* 2010).

Our results (table 3.2, 3.3 & figure 3.4) together suggest that populations of *S. coronatus* support similar levels of diversity and may be significantly differentiated with respect to phenotype, however a notable degree of gene flow is suggested as hyperaccumulator population KP is seen to share haplotypes with several hypertolerant non-accumulator populations. Similar results were see for populations of *T. caerulescens* growing on both Zn contaminated and noncontamined soils across southern France (Jiménez-Ambriz *et al.,* 2007), and within several metallophyte species, significant genetic differentiation is observed even in the presence of limited gene flow (Linhart & Grant, 1996; Vekemans & Lefèbvre, 1997). Therefore, to explore the evolutionary

relationships across the sampled populations a distance-based phylogenetic reconstruction was performed.

3.3 Phylogenetic relationships and fine-scale population structure in *Senecio coronatus*

The metal hyperaccumulation trait is present throughout many different plant lineages. Specifically, Ni hyperaccumulation has been shown by phylogenetic reconstruction, to have evolved independently at least six times within the Brassicaceae family alone. Similarly, within the Alysseae tribe, multiple evolution towards Ni hyperaccumulation is observed with at least two independent events characterized (Cecchi *et al.,* 2010). In addition, a noticeable degree of phylogenetic divergence has been shown between closely related species of the *Alyssum* genus, and further, within *Alyssum bertolonii* genetic differentiation correlates with geographic isolation on metalliferous soils (Mengoni *et al.,* 2003; Galardi *et al.,* 2007). Nonetheless, constitutive metal hyperaccumulation is well documented, with species of a genus or family displaying distinct metal tolerance phenotypes. For example, populations of *Berkheya coddii* collected across serpentine sites in South Africa (Mesjasz-Przybyłowicz *et al.,* 2007; Boyd *et al.,* 2008a) have been shown to constitutively hyperaccumulate Ni (Morrey *et al.,* 1992; Robinson *et al.,* 2003). The Ni hyperaccumulator *Alyssum lesbiacum* and the tree species *Sebertia acuminata* both endemic to Ni serpentine outcrops also exhibit constitutive Ni hyperaccumulation (Sagner *et al.,* 1998; Kazakou *et al.,* 2010).

Uniquely amongst Ni hypertolerant taxa, *S. coronatus* is characterized by a large degree of phenotypic variation, forming distinct hyperaccumulator and non-accumulator populations with identical morphology. To assess if *S. coronatus* exhibits any degree of intraspecific structure with respect to Ni tolerance, phylogenetic reconstruction was used to infer evolutionary relatedness among the sites sampled in this study. Analysis was based on two independent non-coding markers, the ribosomal ITS and the chloroplast TrnfM regions (table 2.2). Together with nuclear markers, non-coding chloroplast (Cp) DNA markers are used extensively in both plant systematic and population genetic studies, and

have been shown to provide sufficient information to resolve both species relationships and population genetic history and structure (Shaw *et al.,* 2005; Mort *et al.,* 2007). Furthermore, assuming hyperaccumulating and hypertolerant non-accumulating *S. coronatus* populations are distinct from one another, genetic drift within populations may result in distinct haplotypes between said populations (as seen in figure 3.4). Additionally, gene flow between populations with identical Ni accumulation phenotype (and assumed genetics) could affect haplotype sharing where populations display little hierarchical sequence structure.

To assess the genetic structure of *S. coronatus* populations, for nucleotide and haplotype data sets (all three data sets), various genetic parameters were estimated utilizing the programs DnaSP v5 and MEGA 5 (as described in sections 2.4.2 and 2.4.3, respectively).

3.3.1 Phylogenetic reconstruction

Variations at the genomic level within a given taxon recently derived are expected to be minimal; it was therefore desirable to attain sequence data from multiple rapidly evolving loci. The use of chloroplast loci for reconstructing evolutionary relationships has been shown to provide sufficient information to resolve species relationships, but may not always provide the same stringency at the population level. Consequently, multiple plastid (Trn) and nuclear non-coding markers were employed for PCR (see table 2.2), before ITS and TrnfM marker sets were optimized for adequate sequence generation. Within produced phylogenies, interior branches that showed low statistical support in resolving individual terminals, a condensed (or multifurcating) tree was produced (as in figures 3.5 and 3.6) for ease of viewing.

Our analysis of ITS and chloroplast TrnfM marker data, clearly identifies three *S. coronatus* lineages in the Barberton region, designated A, B and C (figures 3.5 to 3.7). Individuals collected from serpentine soils form two sister clades (A and B), while non-accumulator individuals collected from non-serpentine soils form a third sister lineage (C). Lineage A is dominated by hypertolerant non-

accumulator individuals (from GM, GV, KOM, LO, MC, MF, NK- and QRV) but does include Ni hyperaccumulator individuals (KP) embedded in the clade. Lineage B is comprised solely of Ni hyperaccumulators (from AM, DK and NK+) while non-accumulator non-serpentine individuals (such as BP, PF and NS) make-up the third clade. This general pattern is recovered in both single marker and the combined analysis. Hyperaccumulator individuals from the population KP are embedded in a clade of non-accumulator populations, suggesting that an independent evolutionary event promoting Ni hyperaccumulation may have occurred within the clade, possibly from a non-accumulator ancestor. The TrnfM data set alone (appendices 7 and 8) did not determine any obvious pattern with respect to geographic location or Ni tolerance phenotype.

An alternate interpretation could be that only two lineages are resolved where one lineage is composed of two sister clades (A and B) and the second grouping C making up the second lineage. This implies that all serpentine populations are contained within a single lineage and Ni hyperaccumulation may have evolved once from a common ancestor to (the A/B lineage), but has consequently been lost in all populations in clade A, except for hyperaccumulator population KP.

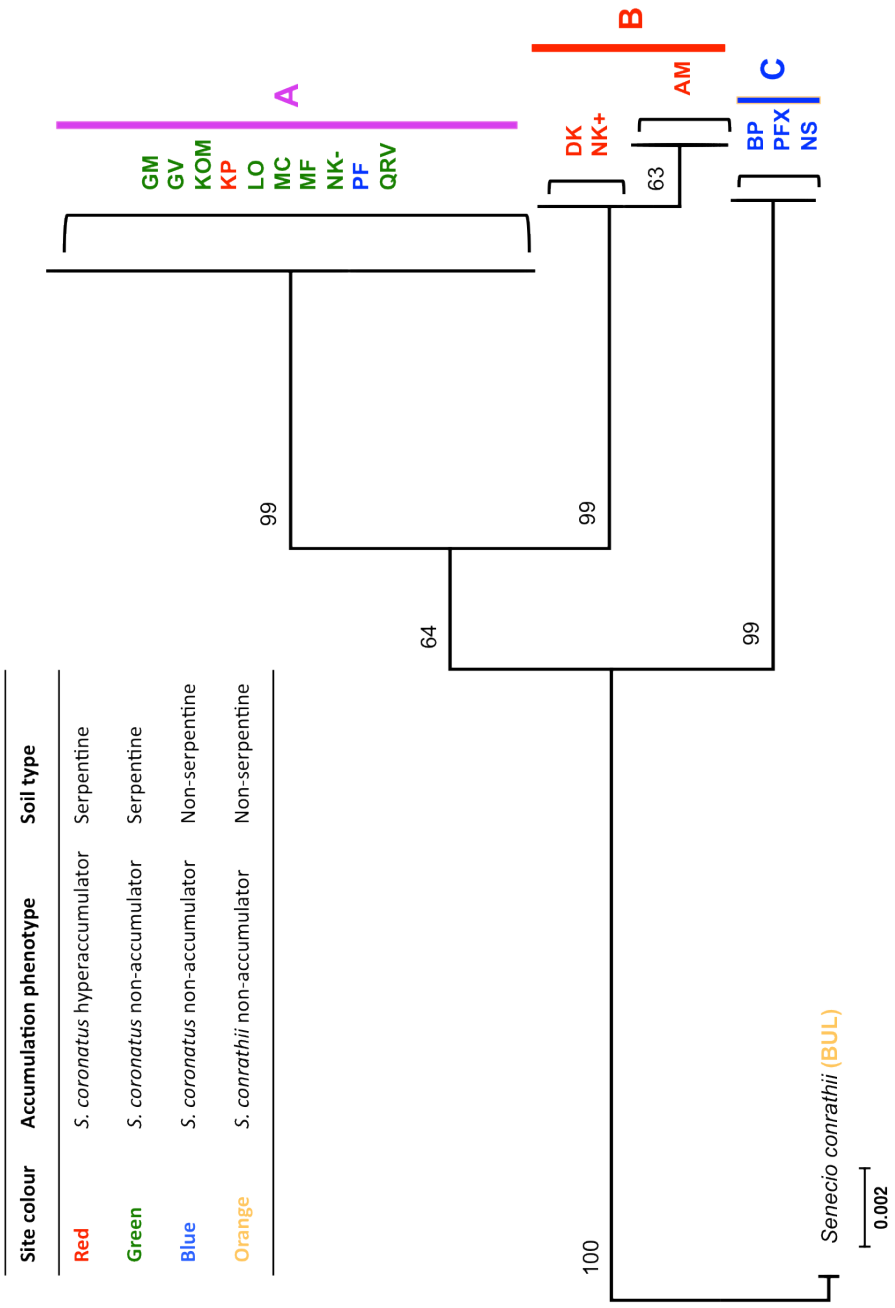

Figure 3.5: Neighbor-joining phylogram of ITS sequences based on Kimura 2-parameter (corrected d-distance). All positions containing gaps or missing data were deleted, resulting in a final data set of 639 positions. The tree is to scale, where branch length is in the same units as those of the evolutionary distances used to infer the phylogenetic tree. The accuracy of the tree generated was evaluated by a bootstrap test (10 000 replicates), where the percentage of replicate trees associated with a given clade is shown at branch nodes. Only bootstrap values over 50% are shown. The tree is rooted with *S. conrathii*. Sample name indicate Ni hyperaccumulating (red), Ni non-accumulating on serpentine soil (green) and non-accumulating plants on non-serpentine soil (blue), respectively.

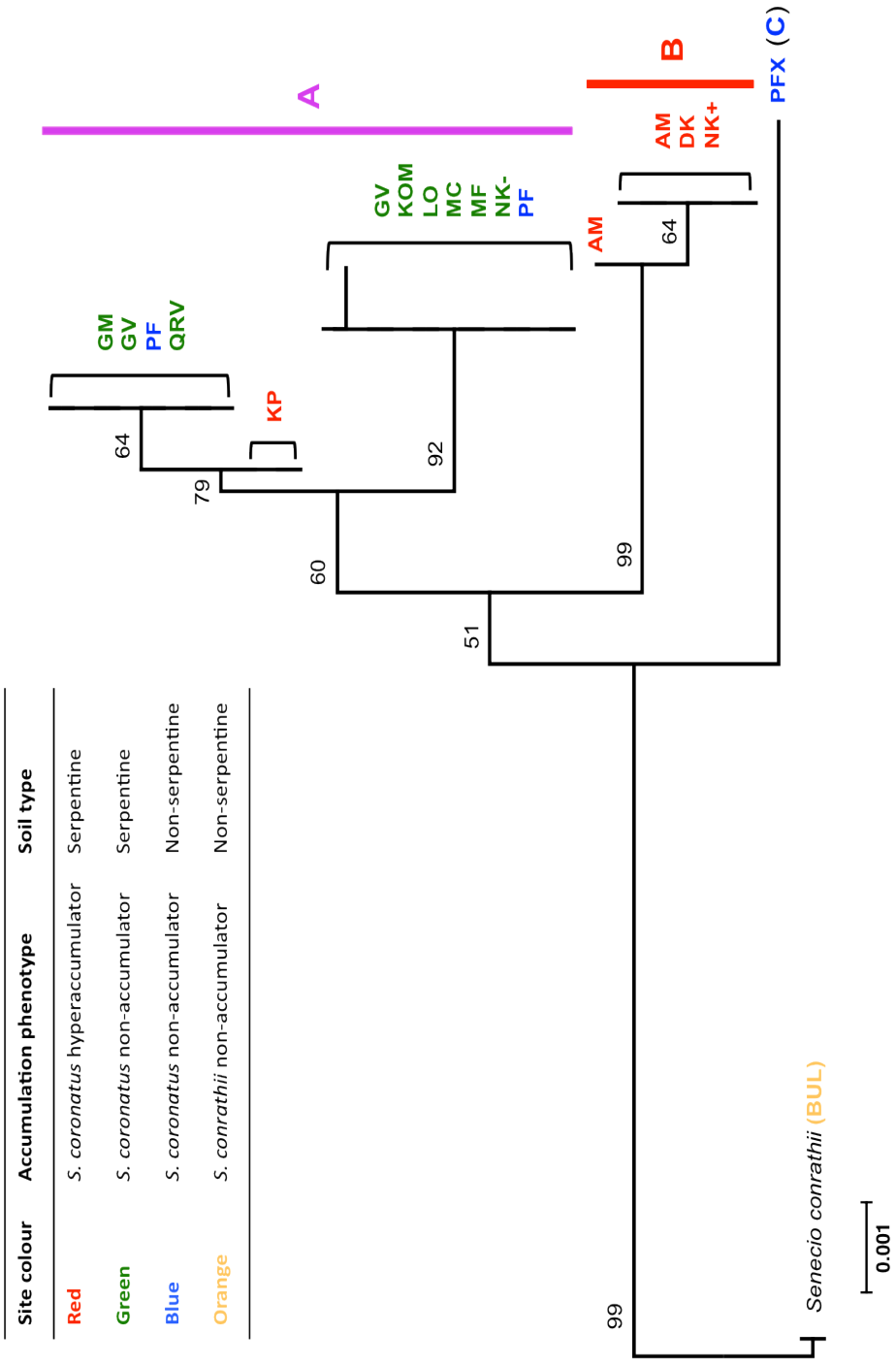

Figure 3.6: Neighbor-joining phylogram of combined ITS-TrnfM sequence data. All positions containing gaps or missing data were deleted, resulting in a final data set of 1474 positions. As before the tree was rooted with *S. conrathii* collected on non-serpentine soils. Sample name colours of red, green and blue indicate Ni tolerance phenotypes of Ni hyperaccumulating, Ni non-accumulating and Ni non-accumulating occurrence on non-serpentine soil, respectively.

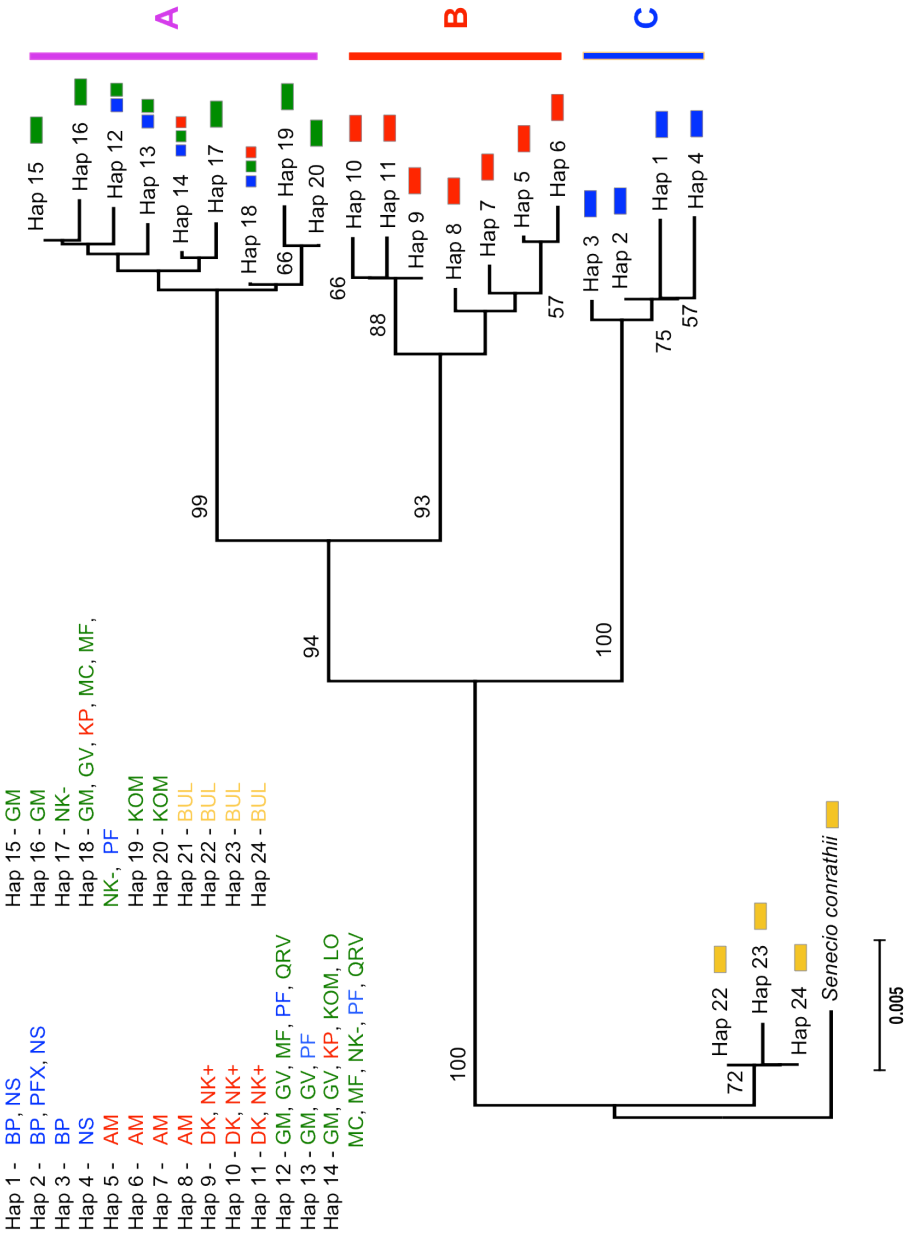

Figure 3.7: Neighbor-joining phylogram of unique ITS haplotypes. All positions containing gaps or missing data were deleted, resulting in a final data set of 661 positions. The tree is to scale, where branch length is in the same units as those of the evolutionary distances used to infer the phylogenetic tree. The accuracy of the tree generated was evaluated by a bootstrap test (10 000 replicates), where the percentage of replicate trees associated with a given clade is shown at branch nodes. Only bootstrap values over 50% are shown. The tree was rooted with *S. conrathii*.

A study into intraspecific variation in the taxa *Erigeron thunbergii* (Kawase *et al.,* 2007) by phylogenetic reconstruction, utilized the same ITS nuclear ribosomal and plastid gene regions (TrnL-F and psbA-TrnH) as those optimized in this study (table 2.2). Populations of *E. thunbergii spp.* (and closely related species *E. miyabeanus*) were collected across disjunctive ultramafic rock sites from northern, central and southern Japan (Mizuno & Nosaka, 1992). Phylogenetic analysis used both Maximum Parsimony (MP) and Neighbor-joining (NJ) tree building methods, and found a strict consensus of the two most parsimonious trees based on the ITS region. The NJ reconstruction showed a similar topology to the generated MP tree. Analysis of the plastid gene regions corroborates the observed inadequacy of plastid loci in resolving species and subspecies-level relationships. However, ITS phylogeny (both MP and NJ) showed two major clades (designated 1 and 2), each containing ultramafic and non-ultramafic populations. Notably, the phylogeny shows serpentine plant occurrences (across Japan) demonstrate a closer phylogenetic relationship to one another than to geographically closer non-serpentine populations (Kawase *et al.,* 2007).

These results are consistent with phylogenetic studies on the tribe Alysseae (Brassicaceae), which showed that within the *Alyssum* sect. *Odontarrhena*, Ni accumulation is not a monophyletic trait and provides evidence of multiple evolutionary events towards Ni hyperaccumulation (Cecchi *et al.,* 2010). Our results suggest that evolution towards Ni hyperaccumulation in the *S. coronatus* complex follows a similar precedent, as we identify two independent lineages that contain hyperaccumulator populations.

3.3.2 Fine-scale population structure

Population differentiation can occur via a number of micro-evolutionary processes including selection and genetic drift, and particularly in small 'island' populations, such as newly colonized and now isolated patches on serpentine soils (Wild & Bradshaw, 1977; Lefèbvre & Vernet, 1990). As genetic drift and/or selection acts on these subpopulations, changes in allele and haplotype frequencies will occur. These changes can be quantified by Wright's *F*-statistic or

fixation index (Wright, 1949, 1965). Wright's *F*-statistic ($\mathbf{F_{ST}}$) and its analogues (developed for bi-allelic markers) measure the degree to which sub-populations have diverged via drift in their allele and haplotype frequencies relative to the total sample. Values ranges from zero to a theoretical 1, where 0 indicates no genetic differentiation and 1 represents sub-populations fixed for unshared diversity (Yang, 1998).

Fixation indices are calculated based on haplotype frequencies among defined groups. Molecular data however provides additional information on the degree of mutational differences between DNA sequences. Using a hierarchical framework, analysis of molecular variance (AMOVA) can therefore be used to quantify the degree to which populations have differentiated. Differences in the distribution of the variance between populations are used to calculate statistics analogous to Wright's *F*-statistic, and are designated here as phi (Φ). Phi-statistics measure the degree to which sub-populations have diverged via drift in their allele and haplotype frequencies relative to the total sample. In this study AMOVA was used to determine the degree to which Ni tolerance phenotype and evolutionary relatedness (as inferred by phylogenetic reconstruction) have influenced population genetic structure in *S. coronatus* across non-serpentine and serpentine soils in the Barberton area. In this study, Φst (Hartl & Clark, 1997) was used to describe the degree to which variance in haplotype diversity is distributed within and among a number of defined groups i.e. all sampling sites, phylogenetic clusters (ITS and ITS-TrnfM data sets only) and phenotype.

AMOVA analysis on all data sets revealed exceptionally high Φst values (table 3.4) suggesting significant and strong genetic differentiation between both *S. coronatus* ecotypes displaying contrasting Ni tolerance phenotypes as well as between the two evolutionary lineages (A and B) identified in the tree-based analysis.

Table 3.4: Summary statistics of AMOVA on ITS, TrnfM and ITS-TrnfM data sets structured by phenotype and by phylogenetic relatedness.

Data set	Percentage of variance (AMOVA)			Fixation index
	Among Groups	Among populations within Groups	Within populations	ΦST
ITS phenotype	48.81	43.88	7.31	0.9269
TrnfM phenotype	19.85	42.02	38.12	0.6188
ITS-TrnfM phenotype	38.23	44.90	16.88	0.8312
ITS phylogeny	91.12	3.58	5.31	0.9469
ITS-TrnfM phylogeny	67.25	19.92	12.83	0.8717

A comparison of the AMOVA percentage variance between the ITS data set structured by phenotype and by phylogenetic inference (table 3.4), shows that when the hyperaccumulator population at KP is grouped by phylogeny (in lineage A), as opposed to by phenotype, we notice a percentage variance increase among groups from ~ 50% to ~ 90%. This suggests that a substantial degree of genetic differentiation characterizes the *S. coronatus* lineages (A and B), and suggests that limited shared gene flow might characterize these populations today. Further, as populations from KP display greatest shared variance with non-accumulator populations, this might suggest the Ni hyperaccumulation trait is gained or lost through relatively few genetic changes.

Plant population genetic studies on *A. halleri* (Pauwels *et al.,* 2008) and *C. ladanifer* (Quintela-Sabarís *et al.,* 2010), both taxa which exhibit a high degree of phenotypic plasticity across a wide range of soil types, show strong population structure along metal tolerance phenotype. Analysis of molecular variance in both cases indicates significant differentiation among populations with Φst values of 0.727 (Pauwels *et al.,* 2008) and 0.690 (Quintela-Sabarís *et al.,* 2010), which is of a similar gradation to the mean value found for angiosperms (Petit *et al.,* 2005). Population differentiation in the *A. halleri* study did not correlate significantly with phylogeography, but a clear distinction across the Alps suggests differentiation through vicariance. A strict phylogeographic relationship

however, is not evident in *C. ladanifer* populations, as metalliferous and non-metalliferous populations are found within most observed lineages as inferred by phylogeny, and genetic estimates of diversity and differentiation suggested 'metallicolous' populations have arisen through multiple independent evolutionary events.

The Ni tolerance phenotype of *S. coronatus* populations sampled in the Barberton area, not only seems to indicate strict physiological differentiation, but also significant genetic structure along said phenotypes. These results confirm that two distinct Ni tolerance phenotypes exist in genetically differentiated *S. coronatus* lineages. Furthermore, the Ni hyperaccumulation trait in *S. coronatus* may have evolved more than once (Mesjasz-Przybyłowicz *et al*., 1997; Comes & Abbott, 2001).

3.4 Proteomic analysis of total shoot proteins from *Senecio coronatus*

Although Ni hyperaccumulators are by far the most common group of metal hyperaccumulating plants, the molecular basis of nickel hyperaccumulation remains unclear. The high degree of intraspecific variation in Ni accumulation observed within *S. coronatus*, (coupled with the possibility that Ni hyperaccumulation has evolved twice in this species) represents a potential model system to identify the genes underpinning the Ni hyperaccumulation phenotype. As a first step towards this, total protein from shoot tissue was extracted from plants collected from four sites, and profiled using two-dimensional SDS-polyacrylamide gel electrophoresis (2D SDS-PAGE). The choice of sites was informed by the population genetic studies undertaken above. The two hyperaccumulator populations chosen were Agnes Mine (representative of lineage B which contains only hyperaccumulators) and Kaapsehoop (the sole Ni hyperaccumulator in lineage A). The hypertolerant non-accumulator was sampled from Galaxy Mine (only 3 km from Agnes Mine), and *S. coronatus* plants collected from Pullen Farm, PF (PFX variety) were used as a representative of the non-serpentine plants.

Given that a number of previous studies have suggested that changes in gene expression, specifically high constitutive expression of genes involved in metal hyperaccumulation such as transport proteins, chelators and anti-oxidants, rather than the evolution of novel genes underpins the hyperaccumulation phenotype (Kerkeb & Krämer, 2003; Ingle *et al.,* 2005a; Hanikenne *et al.,* 2008; Krämer, 2010), the aim of this study was to identify proteins showing increased expression in both hyperaccumulator lineages, relative to non-accumulator hypertolerant and non-serpentine plants.

Comparative shoot proteome analysis was achieved by 2D SDS-PAGE separation of total protein isolate, followed by gel image protein spot detection, matching and manual editing. Statistical evaluation of gel images was performed using software within Melanie 7.0 (as described in section 2.5.3).

After initial manual editing of gel classes, 27 protein spots (out of a total 237 spots matched across all gels) were seen to display a significant difference in expression ($P < 0.05$) between plants collected from all four sites as determined by ANOVA, with 14 of these displaying elevated expression in AM and KP plants relative to GM and PFX plants (figures 3.8, 3.9 and table 3.5).

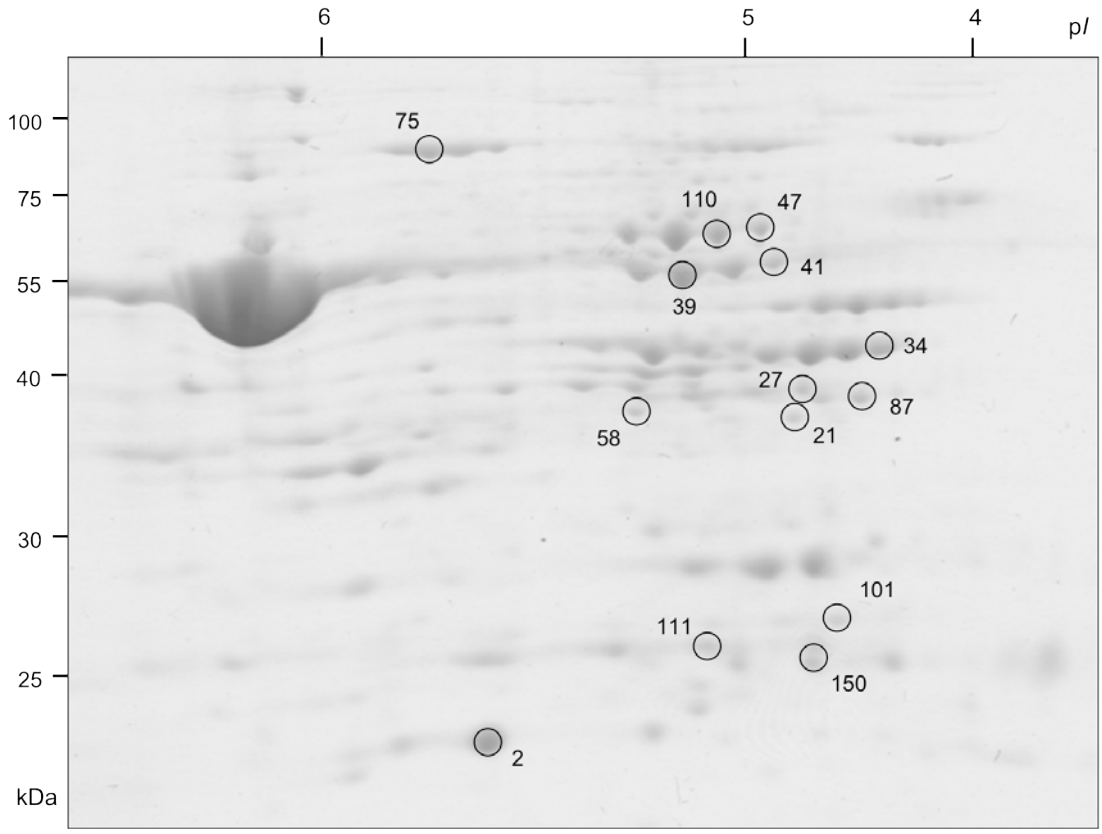

Figure 3.8: Changes in protein abundance in leaf tissue between four different *Senecio coronatus* populations. Circled are 14 spots showing greater abundance in hyperaccumulator gel classes AM and KP relative to non-accumulator gel classes GM and PFX.

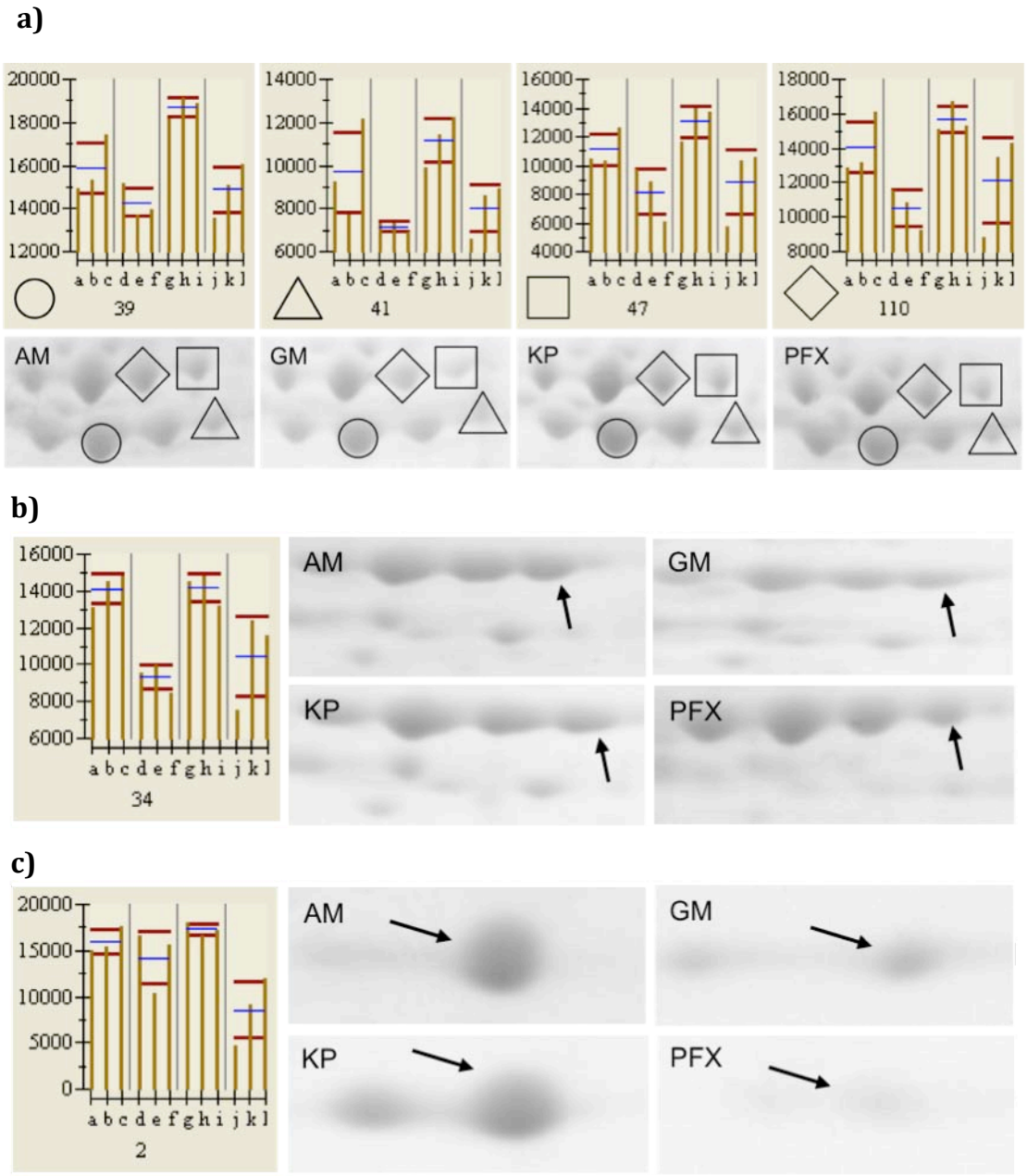

Figure 3.9: Enlarged 2D-PAGE photo exerts show changes in protein abundance in *Senecio coronatus* leaf tissue. Accompanying photo exerts are spot intensity histograms, as generated by Melanie 7.0. Histograms show relative protein intensity of three biological gel repeats of **AM** (a, b, c) **GM** (d, e, f) **KP** (g, h, i) and **PFX** (j, k, l) gels. The blue and red bars on histograms represent the mean spot intensity and ± SD, respectively. Protein spots 2, 34, 39, 41, 47 and 110 were selected to illustrate potential overexpression of proteins in hyperaccumulator gel classes AM and KP compared to non-accumulator gel classes GM and PFX. **a)** Four protein spots in close proximity (39, 41, 47 and 110) showing greater abundance in hyperaccumulator gel classes. **b)** Protein spot 34. **c)** Protein spot 2.

Subsequently, the fourteen protein spots showing increased expression in AM and KP plants relative to GM and PFX plants (table 3.5) were chosen for gel excision and identification by mass spectrometry (LC-MS/MS). For nine of these, a positive identification was obtained (table 3.6).

Table 3.5: A list of 14 protein spots showing greater abundance in accumulator classes Agnus Mine (AM) and Kaapsehoop (KP) compared to non-accumulator classes Galaxy Mine (GM) and Pullen Farm variety PFX. Values shown in columns 2 to 5 are protein spot intensities in arbitrary units. The significance ($P < 0.05$) of relative spot intensities between gel classes AM, KP, GM and PFX (n = 3) was determined by ANOVA statistics within Melanie 7.0.

Protein spot	Kaapsehoop	Agnus Mine	Galaxy Mine	Pullen Farm	*P*-value
2	17280.70	15932.70	14182.70	8538.33	0.0147709
21	7141.67	6455	5193.33	3821	0.0204963
27	10557.70	8304.33	6448.33	2644.67	0.0129058
34	14156.30	14125	9303.33	10485.70	0.0073158
39	18723.30	15890	14275.30	14880.30	0.0032566
41	11188.30	9690.33	7156.67	8030.67	0.0351156
47	13071	11131.70	8180.33	8856	0.0462156
58	8271.67	7953.33	4625.67	6898.67	0.0023617
75	12132.70	12778	8238	7084	0.0176164
87	10570	9780.67	6823.33	5020.33	0.0361238
101	6995.33	6140	3653.33	3486.33	7.23E-04
110	15660.70	14058	10530.70	12161.70	0.0458132
111	5618.33	6629.33	3923.67	3268.67	0.0020901
150	10222.30	8862.33	7024.33	8389.67	0.0210495

As is evident from table 3.6, this proof of concept proteomic analysis shows greater abundance of multiple proteins involved in photosynthesis including Photosystem II proteins, chloroplast ATP synthase subunits and enzymes of the Calvin cycle within *S. coronatus* hyperaccumulators, compared to non-

accumulator plants. In fact, all proteins successfully identified were chloroplastic proteins.

Table 3.6: Nine protein spots identified by LC-MS/MS which show greater abundance in hyperaccumulator classes (AM and KP) compared to non-accumulator classes (GM and PFX). A Mascot score > 24 is considered significant, and % sequence coverage > 5% of the protein as detected by the MS is considered robust (see section 2.5.4 for details).

Spot number	Description	Score	Coverage (%)	Number of unique peptides	Accession
2	• Oxygen-evolving enhancer protein 2, chloroplastic	742.10	18.63	2	302595736
21	• Photosystem II stability/assembly factor HCF136, chloroplastic	971.51	20.19	2	75252730
	• Photosystem II stability/assembly factor HCF136 chloroplast - precursor, putative (*Ricinus communis*)	646.25	18.64	2	255559812
	• Photosystem II stability/assembly factor HCF136 (*Arabidopsis thaliana*)	271.28	14.39	2	15237225
27	• Chloroplast ribulose 1,5-bisphosphate carboxylase/oxygenase activase (*Flaveria bidentis*)	361.59	23.97	3	158726716
34	• Chloroplast ribulose 1,5-bisphosphate carboxylase/oxygenase activase (*Flaveria bidentis*)	1775.43	36.53	3	158726716
	• Rubisco activase (Glycine max)	502.48	29.80	2	290766485
39	• ATP synthase CF1 beta subunit (*Jacobaea vulgaris*)	4737.46	49.80	6	334702331
	• ATP synthase beta subunit (*Echiochilon pauciflorum*)	3791.93	33.82	2	24940264
41	• ATP synthase CF1 beta subunit (*Jacobaea vulgaris*)	3711.17	51.41	20	334702331
47	• ATP synthase CF1 alpha subunit (*Jacobaea vulgaris*)	1981.04	38.78	7	334702318
	• ATP synthase CF1 beta subunit (*Jacobaea vulgaris*)	1060.59	56.22	5	334702331
87	• Sedoheptulose-1,7-bisphosphatase, chloroplastic	414.46	16.54	2	3914940
111	• Triosephosphate isomerase, chloroplastic	232.50	17.52	2	13431949

The combination of considerable active Ni^{2+} leaf enrichment observed within hyperaccumulator populations such as those found at Kaapsehoop (section 3.1) and the extreme phytotoxic potential of study sites (with respect to Ni content), implies Ni hyperaccumulation may affect increased energy expenditure, so as to translocate, chelate and detoxify excessive cellular Ni^{2+} ions.

Ni hyperaccumulators have indeed been shown to require ATP in order to drive Ni^{2+}/H^{+} antiport activity (Ingle *et al.,* 2008). Further, as described in sections

1.9.4.1 and 1.9.4.2, effective metal hyperaccumulation requires synthesis of specific antioxidants and chelators to detoxify and assist in long-distance translocation of metals to the plants aerial parts. Enhanced metal-transporter expression coupled with increased chelator synthesis may contribute to an elevated energy demand within hyperaccumulator plants, compared to non-accumulator plants. What's more, across a number of unrelated plant taxa, heavy metal hyperaccumulation indeed appears to be associated with proteins involved in energy metabolism, as well as the oxidative stress response and abiotic and biotic stress (Visioli & Marmiroli, 2013).

In order to assess whether hyperaccumulator populations exhibit a greater capacity for energy production (as inferred by Photosystem II efficiency) compared to non-accumulator populations, a measure of chlorophyll fluorescence was carried out with a Portable Chlorophyll Fluorometer PAM-2100 (Heinz Walz GmbH, Germany). The maximal quantum yield of Photosystem (PS) II was measured (FvM) after 12 and 24 hour dark adaptation times (table 3.7), as was the effective PS II quantum yield in the illuminated state (table 3.8).

Samples utilized were from population sites AM, GM, KP and PF (as those used in the proteomic analysis). The results do not support a hypothesis of increased photosynthetic rates in Ni hyperaccumulators versus non-accumulators.

Table 3.7: Maximal quantum yield of Photosystem II was measured after 12 and 24 hour dark adaptation times. FvM is calculated from the ratio between Fo (minimal fluorescence yield of PS II) and Fm (maximal fluorescence yield of PS II). FvM gives information on the photochemical quantum yield of PS II. A healthy dark-adapted leaf once illuminated typically shows an FvM value of ~ 0.8.

Sample	FvM (12 h)	Average	FvM (24 h)	Average
KP	0.838	0.837	0.849	0.798
	0.839		0.700	
	0.834		0.846	
AM	0.845	0.839	0.804	0.789
	0.837		0.779	
	0.834		0.783	
GM	0.844	0.838	0.818	0.793
	0.824		0.728	
	0.845		0.833	
PF	0.816	0.844	0.828	0.842
	0.858		0.850	
	0.857		0.848	

Data represented in both table 3.6 and 3.7 do not show any variation in PS II efficiency, as values between hyperaccumulator populations KP and AM do not differ significantly from hypertolerant non-accumulator and non-serpentine populations GM and PF, respectively.

Table 3.8: An averaging measurement or yield of leaf tissues in the illuminated state. Yield calculations measure the essence of fluorescence quenching by saturation pulse method giving the overall photochemical quantum yield and is used as an indicator of photosynthetic efficiency. To illustrate field condition (steady illumination) readings, nine pulse values were taken (column 2) and an average yield value was calculated (column 3).

Sample	Yield	Average (n = 9)
KP	0.785, 0.737, 0.473 0.781, 0.594, 0.661 0.721, 0.763, 0.678	0.688
AM	0.743, 0.785, 0.755 0.702, 0.706, 0.700 0.690, 0.736, 0.776	0.733
GM	0.775, 0.740, 0.784 0.694, 0.743, 0.774 0.772, 0.780, 0.759	0.758
PF	0.798, 0.758, 0.559 0.770, 0.802, 0.814 0.769, 0.791, 0.789	0.761

Chapter 4

General syntheses

4.1. Research conclusions

Our combined results of *in situ* DMG-indicator nickel (Ni) testing and ICP-MS Ni concentration analysis, confirm that populations of *Senecio coronatus* found on comparable serpentine outcrops demonstrate two distinct Ni tolerance phenotypes. These findings suggest two different adaptive mechanisms are employed. Despite being a necessary prerequisite, soil Ni content does not seem to be the major selective pressure for evolution towards Ni hyperaccumulation, as the occurrence of both hyper- and non-accumulator *S. coronatus* plants have been confirmed on the same serpentine outcrops (specifically on the Nkomazi site). Hence, to determine if the distinct phenotypic variation in *S. coronatus* populations reflects a significant degree of intraspecific variation, different genetic parameters based on nuclear non-coding and plastid sequences were tested.

Phylogenetic analyses on *S. coronatus* are in line with other studies demonstrating a polyphyletic nature of the Ni hyperaccumulation trait in certain genera and/or species. For example, Mengoni *et al.,* (2003) revealed by phylogeny reconstruction that within *Alyssum*, all resolved tree clades contain both Ni hyper- and non-accumulator species, and *A. peltarioides* has been shown to contain Ni hyperaccumulator, hypertolerant non-accumulator and non-serpentine non-accumulator populations. Our phylogenetic reconstructions of *S. coronatus* serpentine populations, suggests that Ni hyperaccumulation may have evolved twice in this species complex, as emphasized by the hyperaccumulating population Kaapsehoop, which show greater sequence similarity to the non-accumulator clade ('lineage A') than to the other hyperaccumulator populations ('lineage B'). However as noted, a second scenario is possible in that 'lineage A

and B' constitutes a single lineage where all populations in sister 'clade A' excluding KP have lost the hyperaccumulation trait. Nonetheless, these data support the hypothesis that the Ni hyperaccumulation trait is rapidly gained or lost by few genetic changes affecting gene expression (Cecchi *et al.,* 2010).

Further, this study represents the first analysis of phenotypically distinct *S. coronatus* plants within a population genetics context. An AMOVA structured by Ni accumulation phenotype and by evolutionary relatedness (as inferred by phylogeny), revealed a large genetic differentiation exists between Ni hyperaccumulator and hypertolerant non-accumulator populations. However, a comparison between AMOVA phenotype versus phylogeny confirms the genetic similarity (seen in phylogenetic reconstructions) between hyperaccumulator population Kaapsehoop (KP) and other hypertolerant non-accumulator populations. As phylogenies show KP nested within a predominantly hypertolerant non-accumulator clade, genetic segregation does not show a perfect correspondence with observed phenotypic differentiation.

Interestingly, as most population genetic studies sample large population distributions, our focused sampling area (approximately 1400 km^2) therefore emphasizes the degree and significance of genetic structure observed in *S. coronatus*. Ni tolerance phenotype of *S. coronatus* populations sampled in the Barberton area, not only seems to indicate strict physiological differentiation, but also significant genetic structure along said phenotypes. These results confirm that two distinct Ni tolerance phenotypes exist in genetically differentiated *S. coronatus* lineages and hence suggest that *S. coronatus* could provide a suitable model system to dissect Ni hyperaccumulation.

4.2 Problem identification and future work

To more effectively examine local genomic adaptation in naturally occurring *S. coronatus* populations, historical effects should be identified to better test for possible relationships between the environment and intraspecific variation. Sampling of *S. coronatus* consisted of 15 naturally occurring populations within a

50 km (approximate distance between two furthest sites, Badplaas and Pullen Farm) range, and one hypertolerant non-accumulator population (Komati) 160 km away from the main collection area (see figure 2.1). The relatively narrow sampling range may support a hypothesis that Ni hyperaccumulation is regulated by genetics and not Ni ion availability, however historical effects such as vicariance would be difficult to resolve with such a small sample distribution (Beerli, 2004). As it were, most recent metalliferous-plant population structure studies utilize samples distributed across a number of countries and significant geographical entities. For example, as mentioned a study on *A. halleri* populations across Western Europe (Pauwels *et al.,* 2008) showed evidence of genetic divergence across the Alps mountain range. Therefore, to further investigate any potential historical effects on *S. coronatus* genetic structure, ideally the complete geographic distribution of *S. coronatus* should be sampled. This would also aid in resolving the evolution towards Ni hyperaccumulation in *S. coronatus*, such as the genetic relationship of samples from the KP site with the majority collected hypertolerant non-accumulators. Distribution of *S. coronatus* has been observed predominately in South Africa and moving North towards Tanzania, Zambia and Angola (Hilliard, 1977; Boyd *et al.,* 2008a).

The combination of different molecular markers increases the amount of informative sequence data available for phylogenetic reconstruction and therefore augments confidence in any subsequent phylogeny produced. Sequence acquisition employed an initial five markers, two of which failed to produce significant sequence signal and one (TrnLR marker), which produced sequence data, but contained no variation (as confirmed by DNA sequencing described in section 2.3.5). Phylogenetic reconstruction of *S. coronatus* populations consequently utilized the final two markers after optimization, namely non-coding nuclear 'ITS' and plastid marker 'TrnfM' (see section 2.3.2 and table 2.2 for details on PCR optimization). TrnfM data alone did not resolve any clear phylogenetic relationship between populations with respect to phenotype or geographic distribution. The lack of plastid marker resolution may be attributed to the ITS data set (136 sequences) being almost four times larger than the TrnfM data set (37 sequences). Hence, a larger plastid marker data set is

essential to better corroborate the ITS phylogenetic reconstruction. Genetic divergence of KP from other hyperaccumulator populations (lineage B) implies genetic segregation is possible even in the presence of gene flow. Our data however, demonstrate significant genetic differentiation along Ni accumulation phenotype, suggesting a limited amount of gene flow between hyper- and non-accumulator populations. Nonetheless, observed differentiation along Ni accumulation phenotype coupled with findings that unique haplotype sequences are predominately shared between *S. coronatus* populations with the same Ni accumulation phenotype, could support the taxonomic subdivision of hyper- and non-accumulator populations. Species delimitation based on morphology of *S. coronatus* populations should ideally be corroborated with mating experiments to establish whether hyperaccumulator and hypertolerant non-accumulator populations can interbreed and subsequently, how the Ni hyperaccumulation trait might segregate in potential progeny. As such, no clear genetic or molecular regulation function linked to Ni hyperaccumulation has been identified.

Nevertheless, the observed phenotypic variation observed in some metal hypertolerant taxa (such as *S. coronatus*) presumably mirrors at least some interaction between gene action and protein function. As described earlier, various proteins, specifically metal-transporters, have been identified as integral components of hyperaccumulator physiology (section 1.9 and sub-sections therein and section 3.4). Hence, a more thorough inspection of the respective proteomes of hyper- and non-accumulator *S. coronatus* individuals may identify numerous additional proteins involved in the Ni hyperaccumulation mechanism. In the past few decades 2D-gel electrophoresis has been the technique used most often prior to MS-based identification techniques. 2D-gel electrophoresis has many advantages and is capable of separating complex polypeptide mixtures. However, a prominent problem with 2D-gel electrophoresis is the inability to separate out hydrophobic proteins (as they precipitate out at their isoelectric point), which suggests the resolution of membranous metal-transporter proteins, is highly unlikely. Further, with our leaf proteome analysis on *S. coronatus*, the large signal generated from the abundant protein RuBisCO (1,5

bisphosphate carboxylase/oxygenase), may have masked the signal from lower abundance proteins of similar isoelectric properties (Rose *et al.,* 2004; Fröhlich *et al.,* 2012). Nonetheless, our proof of concept leaf proteome analysis identified nine proteins involved in energy metabolism, representing a potential starting point for study of Ni hyperaccumulation physiology in *S. coronatus*.

References

Anderson CWN, Brooks RR, Chiarucci A, LaCoste CJ, Leblanc M, Robinson BH, Simcock R, Stewart RB (1999). Phytomining for nickel, thallium and gold. *Journal of Geochemical Exploration* 67: 407-415.

Appenroth KJ (2010). What are "heavy metals" in plant sciences? *Acta Physiologiae Plantarum* 32: 615-619.

Assunção AGL, Da Costa Martins P, De Folter S, Vooijs R, Schat H, Aarts MGM (2001). Elevated expression of metal transporter genes in three accessions of the metal hyperaccumulator *Thlaspi caerulescens*. *Plant, Cell & Environment* 24: 217–226.

Assunção AGL, Bleeker P, ten Bookum WM, Vooijis R, Schat H (2008). Intraspecific variation of metal preference patterns for hyperaccumulation in *Thlaspi caerulescens*: evidence from binary metal exposures. *Plant Soil* 303: 289-299.

Baker AJM, Brooks RR (1989). Terrestrial higher plants which hyperaccumulate metallic elements: a review of their distribution, ecology and phytochemistry. *Biorecovery* 1: 81-126.

Baker AJM, Walker PL (1990). Ecophysiology of metal uptake by tolerant plants. In: Shaw AJ, ed. *Heavy metal tolerance plants: evolutionary aspects.* Boca Raton, FL, USA: CRC Press, 155-177.

Baldwin BG, Sanderson MJ, Porter JM, Wojciechowski MF, Campbell CS, Donoghue MJ (1995). The ITS region of nuclear ribosomal DNA: a valuable source of evidence on Angiosperm phylogeny. *Annals of the Missouri Botanical Garden* 82: 247-277.

Baumann A (1885). Das Verhalten von Zinksalzen gegen Pflanzen und in Böden. *Die landwirtsch* 31: 1-53.

Becher M, Talke IN, Krall L, Krämer U (2004). Cross-species microarray transcript profiling reveals high constitutive expression of metal homeostasis genes in shoots of the zinc hyperaccumulator *Arabidopsis halleri*. *The Plant Journal* 37: 251-268.

Beerli P (2004). Effects of unsampled populations on the estimation of population sizes and migration rates between sampled populations. *Molecular Ecology* 13: 827-836.

Behmer ST, Lloyd CM, Raubenheimer D, Stewart-Clark J, Knight J, Leighton RS, Harper FA, Smith JAC (2005). Metal hyperaccumulation in plants: mechanisms of defence against insect herbivores. *Functional Ecology* 19: 55-66.

Bellstedt DU, Pirie MD, Visser JC, de Villiers MJ, Gehrke B (2010). A rapid and inexpensive method for the direct PCR amplification of DNA from plants. *American Journal of Botany* 97: e1-e4.

Bernard C, Roosens N, Czernic P, Lebrun M, Verbruggen N (2004). A novel CPx-ATPase from the cadmium hyperaccumulator *Thlaspi caerulescens*. *FEBS Letters* 569: 140–148.

Bert V, Bonnin I, Saumitou-Laprade P, de Laguérie P, Petit D (2002). Do *Arabidopsis halleri* from nonmetallicolous populations accumulate zinc and cadmium more effectively than those from metallicolous populations? *New Phytologist* 155: 47-57.

Besnard G, Basic N, Christin P-A, Savova-Bianchi D, Galland N (2009). *Thlaspi caerulescens* (Brassicaceae) population genetics in western Switzerland: is the genetic structure affected by natural variation of soil heavy metal concentrations? *New Phytologist* 181: 974-984.

Boyd RS, Martens SN (1998). The significance of metal hyperaccumulation for biotic interactions. *Chemoecology* 8: 1-7.

Boyd RS, Jaffré T (2001). Phytoenrichment of soil Ni content by *Sebertia acuminata* in New Caledonia and the concept of elemental allelopathy. *South African Journal of Science* 97: 535-538.

Boyd RS, Davis MA, Wall MA, Balkwill K (2002). Nickel defends the South African hyperaccumulator *Senecio coronatus* (Asteraceae) against *Helix aspersa* (Mollusca: Pulmonidae). *Chemoecology* 12: 91-97.

Boyd RS, Davis MA, Wall MA, Balkwill K (2006). Metal concentrations of insects associated with the South African Ni hyperaccumulator *Berkheya coddii* (Asteraceae). *Insect Science* 13: 85-102.

Boyd RS, Davis MA, Balkwill K (2008a). Elemental patterns in Ni hyperaccumulating and non-hyperaccumulating ultramafic soil populations of *Senecio coronatus*. *South African Journal of Botany* 74: 158-162.

Boyd RS, Davis MA, Balkwill K (2008b). Does hyperaccumulated nickel affect leaf decomposition? A field test using *Senecio coronatus* (Asteraceae) in South Africa. *Chemoecology* 18: 1-9.

Bradford MM (1976). A rapid and sensitive method for the quantitation of microgram quantities of protein utilizing the principal of protein-dye binding. *Analytical Biochemistry* 72: 248-254.

Brooks RR, Lee J, Jaffré T (1974). Some New Zealand and New Caledonian plant accumulators of nickel. *Journal of Ecology* 62: 493-499.

Brooks RR, Lee J, Reeves RD, Jaffré T (1977). Detection of nickeliferous rocks by analysis of herbarium specimens of indicator plants. *Journal of Geochemical Exploration* 7: 49-57.

Brooks RR (1983). *Biological Methods of Prospecting for Minerals*, Wiley, New York.

Cecchi L, Gabbrielli R, Arnetoli M, Gonnelli C, Hasko A, Selvi F (2010). Evolutionary lineages of nickel hyperaccumulation and systematics in European Alysseae (Brassicaceae): evidence from nrDNA sequence data. *Annals of Botany* 106: 751-767.

Chaney R, Malik M, Li Y M, Brown SL, Brewer EP, Angle JS, Baker AJM (1997). Phytoremediation of soil metals. *Current Opinion in Biotechnology* 8: 279-284.

Chiarucci A, Baker AJM (2007). Advances in the ecology of serpentine soils. *Plant Soil* 293: 1-2.

Cho U, Seo N (2005). Oxidative stress in *Arabidopsis thaliana* exposed to cadmium is due to hydrogen peroxide accumulation. *Plant Science* 168: 113-120.

Clauss MJ, Koch MA (2006). Poorly known relatives of *Arabidopsis thaliana*. *TRENDS in Plant Science* 11: 449-459.

Clemens S, Palmgren MG, Krämer U (2002). A long way ahead: understanding and engineering plant metal accumulation. *TRENDS in Plant Science* 7: 309-315.

Clemens S (2006). Toxic metal accumulation, responses to exposure and mechanisms of tolerance in plants. *Biochimie* 88: 1707-1719.

Comes HP, Abbott RJ (2001). Molecular phylogeography, reticulation and lineage sorting in Mediterranean *Senecio* Sect. *Senecio* (Asteraceae). *Evolution* 55: 1943-1962.

Cramer GR, Urano K, Delrot S, Pezzotti M, Shinozaki K (2011). Effects of abiotic stress on plants: a systems biology perspective. *BMC Plant Biology* 11: 163.

Curie C, Panaviene Z, Loulergue C, Dellaporta SL, Briat JF, Walker EL (2001). Maize yellow stripe1 encodes a membrane protein directly involved in Fe(III) uptake. *Nature* 409: 346-349.

Curie C, Cassin G, Couch D, Divol F, Higuchi K, Le Jean M, Misson J, Schikora A, Czernic P, Mari S (2009). Metal movement within the plant: contribution of nicotianamine and yellow stripe 1-like transporters. *Annals of Botany* 103: 1-11.

Dellaporta SL, Wood J, Hicks JB (1983). A plant DNA minipreparation: Version 2. *Molecular Biology Reporter* 1: 19-22.

Demesure B, Sodzi N, Petit RJ (1995). A set of universal primers for amplification of polymorphic non-coding regions of mitochondrial and chloroplast DNA in plants. *Molecular Ecology* 4: 129-131.

Deniau AX, Pieper B, Ten Bookum WM, Lindhout P, Aarts MGM, Schat H (2006). QLT analysis of cadmium and zinc accumulation in the heavy metal hyperaccumulator *Thlaspi caerulescens*. *Theoretical and Applied Genetics* 113: 907-920.

Dubois S, Cheptou PO, Petit C, Meerts P, Poncelet M, Vekemans X, Lefèbvre C, Escarré J (2003). Genetic structure and mating systems of metallicolous and nonmetallicolous populations of *Thlaspi caerulescens*. *New Phytologist* 157: 633-641.

Duffus JH (2002). "Heavy metals" – a meaningless term? *Pure and Applied Chemistry* 74: 793-807.

Duruibe JO, Ogwuegbu MOC, Egwurugwu JN (2007). Heavy metal pollution and human biotoxic effects. *International Journal of Physical Sciences* 2: 112-118.

Excoffier L, Lischer HEL (2010). Arlequin suite ver 3.5: a new series of programs to perform population genetics analyses under Linux and Windows. *Molecular Ecology Resources* 10: 564-567.

Felsenstein J (1985). Confidence limits on phylogenies: an approach using the bootstrap. *Evolution* 39: 783-791.

Filatov V, Dowdle J, Smirnoff N, Ford-Lloyd B, Newbury HJ, Macnair MM (2006). Comparison of gene expression in segregating families identifies genes and genomic regions involved in a novel adaptation, zinc hyperaccumulation. *Molecular Ecology* 15: 3045-3059.

Fones H, Davis CAR, Rico A, Fang F, Smith JAC (2010). Metal hyperaccumulation armors plants against disease. *PloS Pathogens* 6: e1001093.

Fröhlich A, Gaupels F, Sarioglu H, Holzmeister C, Spannagl M, Durner J (2012). Looking deep inside: detection of low-abundance proteins in leaf extracts of *Arabidopsis* and phloem exudates of pumpkin. *Plant Physiology* 159: 902-914.

Galardi F, Mengoni A, Pucci S, Barletti L, Massi L, Barzanti R, Gabbrielli R, Gonnelli C (2007). Intra-specific differences in mineral element composition in the Ni-hyperaccumulator *Alyssum bertolonii*: a survey of populations in nature. *Environmental and Experimental Botany* 60: 50-56.

Garbisu C, Alkorta I (2001). Phytoextraction: a cost-effective plant-based technology for the removal of metals from the environment. *Bioresource Technology* 77: 229-236.

Garrett RH, Grisham CM (2005). *Biochemistry*. Thomson Learning™ Inc. pp. 512-522.

Gygi SP, Rochon Y, Franza BR, Aebersold R (1999). Correlation between protein and mRNA abundance in yeast. *Molecular and Cellular Biology* 19: 1720-1730.

Hall TA (1999). BioEdit: a user-friendly biological sequence alignment editor and analysis program for Windows 95/98/NT. *Nucleic Acids Symposium Series* 41: 95-98.

Hammond JP, Bowen HC, White PJ, Mills V, Pyke KA, Baker AJ, Whiting SN, May ST, Broadley MR (2006). A comparison of the *Thlaspi caerulescens* and *Thlaspi arvense* shoot transcriptomes. *New Phytologist* 170: 239-260.

Hanikenne M, Talke IN, Haydon MJ, Lanz C, Nolte A, Motte P, Kroymann J, Weigel D, Krämer U (2008). Evolution of metal hyperaccumulation required *cis*-regulatory changes and triplication of *HMA4*. *Nature* 453: 391-396.

Harford JB, Morris DR (1997). *mRNA Metabolism & Post-transcriptional gene regulation*. Wiley-Liss, Inc. New York, N.Y.

Hartl DL, Clark AG (1997). *Principles of Population Genetics*. 3rd Edition. Sinauer Associates, Inc. Publishers, Sunderland, Massachusetts, USA.

Haydon MJ, Cobbett CS (2007). Transporters of ligands for essential metal ions in plants. *New Phytologist* 174: 499-506.

Hilliard OM (1977). Compositae in Natal. University of Natal Press. Pietermaritzburg.

Hussain D, Haydon MJ, Wang Y, Wong E, Sherson SM, Young J, Camakaris J, Harper JF, Cobbetta CS (2004). P-Type ATPase heavy metal transporters with roles in essential zinc homeostasis in *Arabidopsis*. *The Plant Cell* 16: 1327–1339.

Hutton M, Symon C (1986). The quantities of cadmium, lead, mercury and arsenic entering the U.K. environment from human activities. *Science of the Total Environment* 57: 129-150.

Ideker T, Thorsson V, Ranish JA, Christmas R, Buhler J, Eng JK, Bumgarner R, Goodlett DR, Aebersold R, Hood L (2001). Integrated genomic and proteomic analyses of a systematically perturbed metabolic network. *Science* 292: 929-934.

Ingle RA, Mugford ST, Rees JD, Campbell MM, Smith JAC (2005a). Constitutively high expression of the histidine biosynthetic pathway contributes to nickel tolerance in hyperaccumulator plants. *The Plant Cell* 17: 2089-2106.

Ingle RA, Smith JAC, Sweetlove LJ (2005b). Responses to nickel in the proteome of the hyperaccumulator plant *Alyssum lesbiacum*. *BioMetals* 18: 627-641.

Ingle RA, Fricker MD, Smith JAC (2008). Evidence for nickel/proton antiport activity at the tonoplast of the hyperaccumulator plant *Alyssum lesbiacum*. *Plant Biology* 10: 746-753.

Jaffré T, Brooks RR, Lee J, Reeves RD (1976). *Sebertia acuminata*: a hyperaccumulator of nickel from New Caledonia. *Science* 193: 579-580.

Jhee EM, Boyd RS, Eubanks MD (2005). Nickel hyperaccumulation as an elemental defence of *Streptanthus polygaloides* (Brassicaceae): influence of herbivore feeding mode. *New Phytologist* 168: 331-344.

Jiménez-Ambriz G, Petit C, Bourrié I, Dubois S, Olivieri I, Ronce O (2007). Life history variation in the heavy metal tolerant plant *Thlaspi caerulescens* growing in a network of contaminated and noncontaminated sites in southern France: role of gene flow, selection and phenotypic plasticity. *New Phytologist* 173: 199-215.

Kawase D, Yumoto T, Hayashi K, Sato K (2007). Molecular phylogenetic analysis of the intraspecific taxa of *Erigeron thunbergii* A. Gray distribution in ultramafic rock sites. *Plant Species Biology* 22: 107-115.

Kazakou E, Adamidis GC, Baker AJM, Reeves RD, Godino M, Dimitrakopoulos PG (2010). Species adaptation in serpentine soils in Lesbos Island (Greece): metal hyperaccumulation and tolerance. *Plant Soil* 332: 369-385.

Kerkeb L, Krämer U (2003). The role of free histidine in xylem loading of nickel in *Alyssum lesbiacum* and *Brassica juncea*. *Plant Physiology* 131: 716-724.

Kim D, Gustin JL, Lahner B, Persans MW, Baek D, Yun DJ, Salt DE (2004). The plant CDF family member TgMTP1 from the Ni/Zn hyperaccumulator *Thlaspi goesingense* acts to enhance efflux of Zn at the plasma membrane when expressed in *Saccharomyces cerevisiae*. *The Plant Journal* 39: 237-251.

Kimura M (1980). A simple method for estimating evolutionary rate of base substitutions through comparative studies of nucleotide sequences. *Journal of Molecular Evolution* 16: 111-120.

Klein MA, Sekimoto H, Milner MJ, Kochian LV (2008). Investigation of heavy metal hyperaccumulation at the cellular level: development and characterization of *Thlaspi caerulescens* suspension cell lines. *Plant Physiology* 147: 2006-2016.

Kobae Y, Uemura T, Sato MH, Ohnishi M, Mimura T, Nakagawa T, Maeshima M (2004). Zinc transporter of *Arabidopsis thaliana* AtMTP1 is localized to vacuolar membranes and implicated in zinc homeostasis. *Plant & Cell Physiology* 45: 1749-1758.

Koch M, Al-Shehbaz IA (2004). Taxonomic and phylogenetic evaluation of the American "*Thlaspi*" species: identity and relationship to the Eurasian genus *Noccaea* (Brassicaceae). *Systematic Botany* 29: 375-384.

Krämer U, Cotter-Howells JD, Charnock JM, Baker AJM, Smith JAC (1996). Free histidine as a metal chelator in plants that accumulate nickel. *Nature* 397: 635-638.

Krämer U (2005). MTP1 mops up excess zinc in *Arabidopsis* cells. *TRENDS in Plant Science* 10: 313-315.

Krämer U, Talke IN, Hanikenne M (2007). Transition metal transport. *FEBS Letters* 581: 2263-2272.

Krämer U (2010). Metal hyperaccumulation in plants. *The Annual Review of Plant Biology* 61: 28.1-28.18.

Küpper H, Kochian LV (2010). Transcriptional regulation of metal transport genes and mineral nutrition during acclimatization to cadmium and zinc in the Cd/Zn hyperaccumulator, *Thlaspi caerulescens* (Ganges population). *New Phytologist* 185: 114-129.

Lagercrantz E (2008). eBioX version 1.5.1 (25). Software available at http://www.ebioinformatics.org.

Lasat MM, Baker AJM, Kochian LV (1996). Physiological characterization of root Zn^{2+} absorption and translocation to shoots in Zn hyperaccumulator and nonaccumulator species of *Thlaspi*. *Plant Physiology* 112: 1715-1722.

Lasat MM, Baker AJM, Kochian LV (1998). Altered Zn compartmentation in the root symplasm and stimulated Zn absorption into the leaf as mechanisms involved in Zn hyperaccumulation in *Thlaspi caerulescens*. *Plant Physiology* 118: 875-883.

Lasat MM, Pence NS, Garvin DF, Ebbs SD, Kochian LV (2000). Molecular physiology of zinc transport in the Zn hyper accumulator *Thlaspi caerulescens*. *Journal of Experimental Botany* 51: 71-79.

Lefèbvre C, Vernet P (1990). Microevolutionary processes on contaminated deposits. In: Shaw AJ, ed. *Heavy Metal Tolerance in Plants: Evolutionary Aspects*. Boca Raton, FL, USA: CRC Press, 286-297.

Librado P, Rozas J (2009). DnaSP v5: a software for comprehensive analysis of DNA polymorphism data. *Bioinformatics* 25: 1451-1452.

Linder CR, Goertzen LR, Heuvel BV, Francisco-Ortega J, Jansen RK (2000). The complete external transcribed spacer of 18S-26S rDNA: amplification and phylogenetic utility at low taxonomic levels in Asteraceae and closely allied families. *Molecular Phylogenetics and Evolution* 14: 285-303.

Linhart YB, Grant MC (1996). Evolutionary significance of local genetic differentiation in plants. *Annual Review of Ecology, Evolution, and Systematics* 27: 237-277.

Lozet J, Mathieu C (1991). *Dictionary of Soil Science*, 2nd ed., A. A. Balkema Rotterdam.

Macnair MR, Bert V, Huitson SB, Saumitou-Laprade P, Petit D (1999). Zinc tolerance and hyperaccumulation are genetically independent characters. *Proceedings of the Royal Society of London Series B* 266: 2175-2179.

Maestri E, Marmiroli M, Visioli G, Marmiroli N (2010). Metal tolerance and hyperaccumulation: Costs and trade-offs between traits and environment. *Environmental and Experimental Botany* 68: 1-13.

Mari S, Gendre D, Pianelli K, Ouerdane L, Lobinski R, Brita J-F, Lebrun M, Czernic P (2006). Root-to-shoot long-distance circulation of nicotianamine and nicotianamine–nickel chelates in the metal hyperaccumulator *Thlaspi caerulescens*. *Journal of Experimental Botany* 57: 4111-4122.

Martínez M, Bernal P, Almela C, Vélez D, García-Agustín P, Serrano R, Navarro-Aviñó J (2006). An engineered plant that accumulates higher levels of heavy metals than *Thlaspi caerulescens*, with yields of 100 times more biomass in mine soils. *Chemosphere* 64: 478-485.

Mengoni A, Baker AJM, Bazzicalupo M, Reeves RD, Adigüzel N, Chianni E, Galardi F, Gabbrielli R, Gonnelli C (2003). Evolutionary dynamics of nickel hyperaccumulation in *Alyssum* revealed by ITS nrDNA analysis. *New Phytologist* 159: 691-699.

Mesjasz-Przybyłowicz J, Balkwill K, Przybyłowicz WJ, Annegarn HJ (1994). Proton microprobe and X-ray fluorescence investigations of nickel distribution in serpentine flora from South Africa. *Nuclear Instruments and Methods in Physics Research Section B* 89: 208-212.

Mesjasz-Przybyłowicz J, Przybyłowicz WJ, Prozesky VM, Pineda CA (1997). Quantitative micro-PIXE comparison of elemental distribution in Ni-hyperaccumulating and non-accumulating genotypes of *Senecio coronatus*. *Nuclear Instruments and Methods in Physics Research Section B* 140: 368-373.

Mesjasz-Przybyłowicz J, Przybyłowicz WJ, Pineda CA (2001). Nuclear microprobe studies of elemental distribution in apical leaves of the Ni hyperaccumulator *Berkheya coddii*. *South African Journal of Science* 97: 591-593.

Mesjasz-Przybyłowicz J, Barnabas A, Przybyłowicz WJ (2007). Comparison of cytology and distribution of nickel in roots of Ni-hyperaccumulating and non-hyperaccumulating genotypes of *Senecio coronatus. Plant Soil* 293: 61-78.

Mills RF, Krijger GC, Baccarini PJ, Hall JL, Williams LE (2003). Functional expression of AtHMA4, a P1B-type ATPase of the Zn/Co/Cd/Pb subclass. *Plant Journal* 35: 164–176.

Milner MJ, Kochian LV (2008). Investigating heavy-metal hyperaccumulation using *Thlaspi caerulescens* as a model system. *Annals of Botany* 102: 3–13.

Minguzzi C, Vergnano O (1948). Il contenuto del nichel nelle ceneri di *Alyssum bertolonii* Desv. *Atti Soc. Tosc. Sci. Nat. Ser. A* 55: 49-77.

Mithöfer A, Schulze B, Boland W (2004). Biotic and heavy metal stress response in plants: evidence for common signals. *FEBS Letters* 566: 1-5.

Mizuno N, Nosaka S (1992). The distribution and extent of serpentinized areas in Japan. In: Roberts B. A. & Proctor J. (eds). *The Ecology of Areas with Serpentinized Rocks. A World View*. Kluwer Academic Publishers, Dordrecht, pp. 271-311.

Morrey DR, Balkwill K, Balkwill M-J, Williamson S (1992). A review of some studies of the serpentine flora of southern Africa. In: Baker AJM, Proctor J, Reeves RD. eds. *The Vegetation of Ultramafic (Serpentine) Soils*. Intercept, Andover, pp. 147-157.

Mort ME, Archibald JK, Randle CP, Levsen ND, O'Leary RT, Topalov K, Wiegand CM, Crawford DJ (2007). Inferring phylogeny at low taxonomic levels: utility of rapidly evolving cpDNA and nuclear ITS loci. *American Journal of Botany* 94: 173-183.

van de Mortel JE, Schat H, Moerland PD, Ver Loren van Themaat E, van der Ent S, Blankestijn H, Ghandilyan A, Tsiatsiani S, Aarts MG (2008). Expression differences for genes involved in lignin, glutathione and sulphate metabolism in response to cadmium in *Arabidopsis thaliana* and the related Zn/Cd-hyperaccumulator *Thlaspi caerulescens*. *Plant, Cell & Environment* 31: 301-324.

Murphy RC (2002). *Coral Reefs: Cities Under The Seas.* The Darwin Press, Inc.

Noret N, Meerts P, Tolrà R, Poschenrieder C, Barceló J, Escarré J (2005). Palatability of *Thlaspi caerulescens* for snails: influence of zinc and glucosinolates. *New Phytologist* 165: 763-772.

Noret N, Meerts P, Vanhaelen M, Dos Santos A, Escarré J (2007). Do metal-rich plants deter herbivores? A field test of the defence hypothesis. *Oecologia* 152: 92-100.

Nriagu JO (1989). A global assessment of natural sources of atmospheric trace metals. *Nature* 338: 47-49.

Palomino M, Kennedy PG, Simms EL (2007). Nickel hyperaccumulation as an anti-herbivore trait: considering the role of tolerance to damage. *Plant Soil* 293: 189-195.

Papoyan A, Piñeros M, Kochin LV (2007). Plant Cd^{2+} and Zn^{2+} status effects on root and shoot heavy metal accumulation in *Thlaspi caerulescens. New Phytologist* 175: 51–58.

Parker SP (1989). *McGraw-Hill Dictionary of Scientific and Technical Terms*, 4th ed., McGraw-Hill, New York.

Pauwels M, Saumitou-Laprade P, Holl A-C, Petit D, Bonnin I (2005). Multiple origin of metallicolous populations of the pseudometallophyte *Arabidopsis halleri* (Brassicaceae) in Central Europe: the cpDNA testimony. *Molecular Ecology* 14: 4403-4414.

Pauwels M, Frérot H, Bonnin I, Saumitou-Laprade P (2006). A broad-scale analysis of population differentiation for Zn tolerance in an emerging model species for tolerance study: *Arabidopsis halleri* (Brassicaceae). *Journal of Evolutionary Biology* 19: 1838-1850.

Pauwels M, Willems G, Roosens N, Frérot H, Saumitou-Laprade P (2008). Merging methods in molecular and ecological genetics to study the adaptation of plants to anthropogenic metal-polluted sites: implications for phytoremediation. *Molecular Ecology* 17: 108-119.

Pawlowska TE, Błaszkowski J, Rühling Å (1996). The mycorrhizal status of plants colonizing a calamine spoil mound in southern Poland. *Mycorrhiza* 6: 499-505.

Peer WA, Mamoudian M, Lahner B, Reeves RD, Murphy AS, Salt DE (2003). Identifying model metal hyperaccumulating plants: germplasm analysis of 20 Brassicaceae accessions from a wide geographical area. *New Phytologist* 159: 421-430.

Peiter E, Montanini B, Gobert A, Pedas P, Husted S, Maathuis FJM, Blaudez D, Chalot M, Sanders D (2007). A secretory pathway-localized cation diffusion facilitator confers plant manganese tolerance. *Proceedings of the National Academy of Sciences, USA* 104: 8532-8537.

Pence NS, Larsen PB, Ebbs SD, Letham DLD, Lasat MM, Garvin DF, Eide D, Kochian LV (2000). The molecular physiology of heavy metal transport in the Zn/Cd hyperaccumulator *Thlaspi caerulescens. Proceedings of the National Academy of Science, USA* 97: 4956-4960.

Pepper AE, Norwood LE (2001). Evolution of *Caulanthus amplexicaulis* var. *barbarae* (Brassicaceae), a rare serpentine endemic plant: a molecular phylogenetic perspective. *American Journal of Botany* 88: 1479-1489.

Persans MW, Yan X, Patnoe J-M, Krämer U, Salt DE (1999). Molecular dissection of the role of histidine in nickel hyperaccumulation in *Thlaspi goesingense* (Hálácsy). *Plant Physiology* 121: 1117-1126.

Persans MW, Nieman K, Salt DE (2001). Functional activity and role of cation-efflux family members in Ni hyperaccumulation in *Thlaspi goesingense. Proceedings of the National Academy of Science USA* 98: 9995-10000.

Petit RJ, Duminil J, Fineschi S, Hampe A, Salvini D, Vendramin GG (2005). Comparative organization of chloroplast, mitochondrial and nuclear diversity in plant populations. *Molecular Ecology* 14: 689-701.

Pianelli K, Mari S, Marquez L, Lebrun M, Czernic P (2005). Nicotianamine over-accumulation confers resistance to nickel in *Arabidopsis thaliana*. *Transgenic Research* 14: 739-748.

Pollard AJ, Powell KD, Harper FA, Smith JAC (2002). The genetic basis of metal hyperaccumulation in plants. *Critical Reviews in Plant Sciences* 21: 539-566.

Purugganan M, Gibson G (2003). Merging ecology, molecular evolution, and functional genetics. *Molecular Ecology* 12: 1109-1112.

Quintela-Sabarís C, Vendramin GG, Castro-Fernández D, Fraga MI (2010). Chloroplast microsatellites reveal that metallicolous populations of the Mediterranean shrub *Cistus ladanifer* L have multiple origins. *Plant Soil* 334: 161-174.

Rascio N, Navari-Izzo F (2011). Heavy metal hyperaccumulating plants: how and why do they do it? And what makes them so interesting? *Plant Science* 180: 169-181.

Reeves RD, Macfarlane RM, Brooks, RR (1983). Accumulation of nickel and zinc by western North American genera containing serpentine-tolerant species. *American Journal of Botany* 70: 1297-1303.

Reeves RD, Baker AJM (2000). Metal-accumulating plants. *Phytoremediation of Toxic Metals – Using Plants to Clean Up the Environment*, ed. Raskin I, Ensley BD, pp. 193-229. New York: Wiley.

Reeves RD, Schwartz C, Morel JL, Edmondson J (2001). Distribution and metal-accumulating behavior of *Thlaspi caerulescens* and associated metallophytes in France. *International Journal of Phytoremediation* 3: 145-172.

Rigola D, Fiers M, Vurro E, Aarts MGM (2006). The heavy metal hyperaccumulator *Thlaspi caerulescens* expresses many species-specific genes, as identified by comparative expressed sequence tag analysis. *New Phytologist* 170: 753-766.

Robinson BH, Brooks RR, Howes AW, Kirkman JH, Gregg PEH (1997). The potential of the high-biomass nickel hyperaccumulator *Berkheya coddii* for phytoremediation and phytomining. *Journal of Geochemical Exploration* 60: 115-126.

Robinson BH, Lombi E, Zhao FJ, McGrath SP (2003). Uptake and distribution of nickel and other metals in the hyperaccumulator *Berkheya coddii*. *New Phytologist* 158: 279-285.

Roosens NHCJ, Willems G, Saumitou-Laprade P (2008). Using *Arabidopsis* to explore zinc tolerance and hyperaccumulation. *TRENDS in Plant Science* 13: 208-215.

Rose JKC, Bashir S, Giovannoni JJ, Jahn MM, Saravanan RS (2004). Tackling the plant proteome: practical approaches, hurdles and experimental tools. *Plant Journal* 39: 715-733.

Sachs J (1865). Handbuch der Experimentalphysiologie der Pflanzen. *Handbuch der Physiologischen Botanik*, ed. W Hofmeister, pp. 153-154. Leipzig: Engelmann.

Sagner S, Kneer R, Wanner G, Cosson J-P, Deus-Neumann B, Zenk MH (1998). Hyperaccumulation, complexation and distribution of nickel in *Sebertia acuminata*. *Phytochemistry* 47: 339-347.

Saitou N, Nei M (1987). The neighbor-joining method: a new method for reconstructing phylogenetic trees. *Molecular Biology and Evolution* 4: 406-425.

Sambrook J, Russell DW (2001). *Molecular Cloning: A laboratory Manual* 3rd Ed. Cold Spring Harbor Laboratory Press, Cold Spring Harbor, NY.

Sang T, Crawford DJ, Stuessy TF (1997). Chloroplast DNA phylogeny, reticulate evolution, and biogeography of *Paeonia* (Paeoniaceae). *American Journal of Botany* 84: 1120-1136.

Shaw J, Lickey EB, Beck JT, Farmer SB, Liu W, Miller J, Siripun KC, Winder CT, Schilling EE, Small RL (2005). The tortoise and the hare II: relatively utility of 21 noncoding chloroplast DNA sequences for phylogenetic analysis. *American Journal of Botany* 92: 142-166.

Staton JL, Schizas NV, Chandler GT, Coull BC, Quattro JM (2001). Ecotoxicology and population genetics: the emergence of "phylogeographic and evolutionary ecotoxicology". *Ecotoxicology* 10: 217-222.

Stephens M, Smith N, Donelly P (2001). A new statistical method for haplotype reconstruction from population data. *American Journal of Human Genetics* 68: 978-989.

Stephens M, Donelly P (2003). A comparison of bayesian methods for haplotype reconstruction from population genotype data. *American Journal of Human Genetics* 73: 1162-1169.

Taberlet PL, Gielly P, Patou G, Bouvet J (1991). Universal primers for the amplification of three non-coding regions of chloroplast DNA. *Plant Molecular Biology* 17: 1105-1109.

Talke IN, Hanikenne M, Krämer U (2006). Zinc-dependent global transcriptional control, transcriptional deregulation and higher gene copy number for genes in metal homeostasis of the hyperaccumulator *Arabidopsis halleri*. *Plant Physiology* 142: 148-167.

Tamura K, Peterson D, Peterson N, Stecher G, Nei M, Kumar S (2011). MEGA5: molecular evolutionary genetics analysis using maximum likelihood, evolutionary distance, and maximum parsimony methods. *Molecular Biology and Evolution* 28: 2731-2739.

Tate JA, Simpson BB (2003). Paraphyly of *Tarasa* (Malvaceae) and diverse origins of the polyploid species. *Systematic Botany* 28: 723-737.

Thompson JD, Higgins DG, Gibson TJ (1994). CLUSTAL W: improving the sensitivity of progressive multiple sequence alignment through sequence weighting, position-specific gap penalties and weight matrix choice. *Nucleic Acids Research* 22: 4673-4680.

Tschugaeff L (1905). Ueber ein neues, empfindliches Reagens auf Nickel. *Berichte der deutschen chemischen Gesellschaft* 38: 2520-2522.

Ueno D, Milner MJ, Yamaji N, Yokosho K, Koyama E, Zambrano MC, Kaskie M, Ebbs S, Kochian LV, Feng MA J (2011). Elevated expression of *TcHMA3* plays a key role in the extreme Cd tolerance in a Cd-hyperaccumulating ecotype of *Thlaspi caerulescens*. *The Plant Journal* 66: 852-862.

Urlinger S, Kuchler K, Meyer TH, Uebel S, Tampé R (1997). Intracellular location, complex formation, and function of the transporter associated with antigen processing in yeast. *European Journal of Biochemistry* 245: 266-272.

Vacchina V, Mari S, Czernic P, Marquez L, Pianelli K, Schaumlöffel D, Lebrun M, Lobinski R (2003). Speciation of nickel in a hyperaccumulating plant by high-performance liquid chromatography-inductively coupled plasma mass spectrometry and electrospray MS/MS assisted by cloning using yeast complementation. *Analytical Chemistry* 75: 2740-2745.

Van der Zaal BJ, Neuteboom LW, Pinas JE, Chardonnens AN, Schat H, Verkleij JAC, Hooykaas PJJ (1999). Overexpression of a novel *Arabidopsis* gene related to putative zinc-transporter genes from animals can lead to enhanced zinc resistance and accumulation. *American Society of Plant Physiologists* 119: 1047-1055.

Varshavsky A (1996). The N-end rule: functions, mysteries, uses. *Proceedings of the National Academy of Sciences of the United States of America* 93: 12142-12149.

Vekemans X, Lefèbvre C (1997). On the evolution of heavy-metal tolerant populations in *Armeria maritima*: evidence from allozyme variation and reproduction barriers. *Journal of Evolutionary Biology* 10: 175-191.

Velculescu VE, Zhang L, Zhou W, Vogelstein J, Basrai MA, Bassett DE Jr, Hieter P, Vogelstein B, Kinzler KW (1997). Characterization of the yeast transcriptome. *Cell* 88: 243-251.

Verbruggen N, Hermans C, Schat H (2009). Molecular mechanisms of metal hyperaccumulation in plants. *New Phytologist* 181: 759-776.

Verret F, Gravot A, Auroy P, Leonhardt N, David P, Nussaume L, Vavasseur A, Richaud P (2004). Overexpression of AtHMA4 enhances root-to-shoot translocation of zinc and cadmium and plant metal tolerance. *FEBS Letters* 576: 306–312.

Visioli G, Marmiroli N (2013). The proteomics of heavy metal hyperaccumulation by plants. *Journal of Proteomics* 79: 133-145.

Weber M, Harada E, Vess C, von Roepenack-Lahaye E, Clemens S (2004). Comparative microarray analysis of *Arabidopsis thaliana* and *Arabidopsis halleri* roots identifies nicotianamine synthase, a ZIP transporter and other genes as potential metal hyperaccumulation factors. *The Plant Journal* 37: 269–281.

Weber M, Trampczynska A, Clemens S (2006). Comparative transcriptome analysis of toxic metal responses in *Arabidopsis thaliana* and the Cd^{2+}-hypertolerant facultative metallophyte *Arabidopsis halleri*. *Plant, Cell & Environment* 29: 950-963.

Wen J, Zimmer EA (1996). Phylogeny and biogeography of *Panax* L. (the ginseng genus, Araliaceae): inference from ITS sequences of nuclear ribosomal DNA. *Molecular Phylogenetics and Evolution* 6: 167-177.

Whiting SN, Reeves RD, Richards D, Johnson MS, Cooke JA, Malaisse F, Paton A, Smith JAC, Angle JS, Chaney RL, Ginocchio R, Jaffré T, Johns R, McIntyre T, Purvis OW, Salt DE, Schat H, Zhao FJ, Baker AJM (2004). Research priorities for conservation of metallophyte biodiversity and their potential for restoration and site remediation. *Restoration Ecology* 12: 106-116.

Wild H, Bradshaw AD (1977). The evolutionary effects of metalliferous and other anomalous soils in south central Africa. *Evolution* 31: 282-293.

Wright S (1949). The genetical structure of populations. *Annals of Eugenics* 15: 323-354.

Wright S (1965). The interpretation of population structure by *F*-statistics with special regard to systems of mating. *Evolution* 19: 395-420.

Yang R-C (1998). Estimating hierarchical *F*-statistics. *Evolution* 52: 950-956.

Zhang Z-C, Qiu B-S (2007). Reactive oxygen species metabolism during cadmium hyperaccumulation of a new hyperaccumulator *Sedum alfredii* (Crassulaceae). *Journal of Environmental Sciences* 19: 1311-1317.

Appendices

Appendix 1: Nucleotide sequence alignment of 136 ITS sequences.

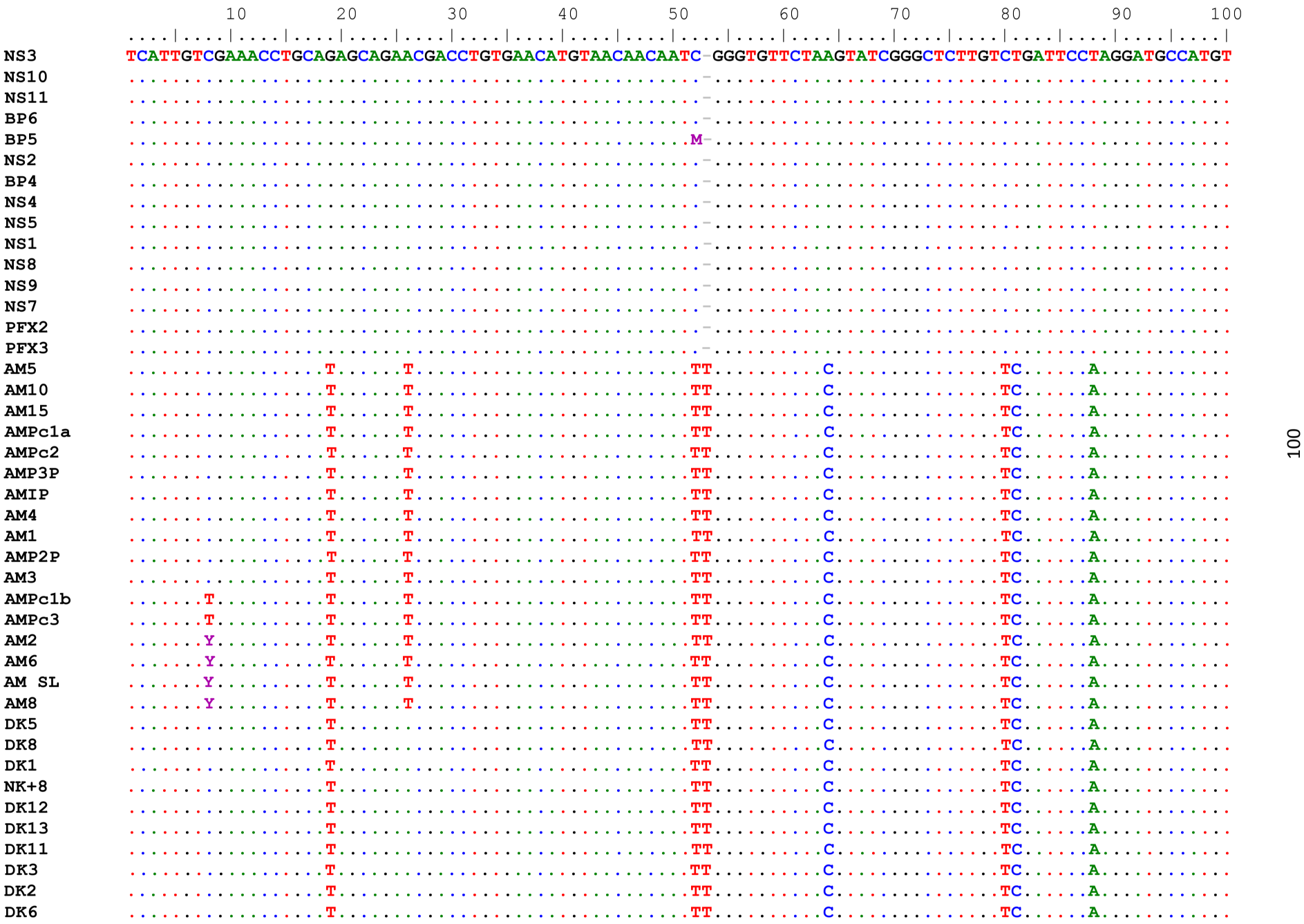

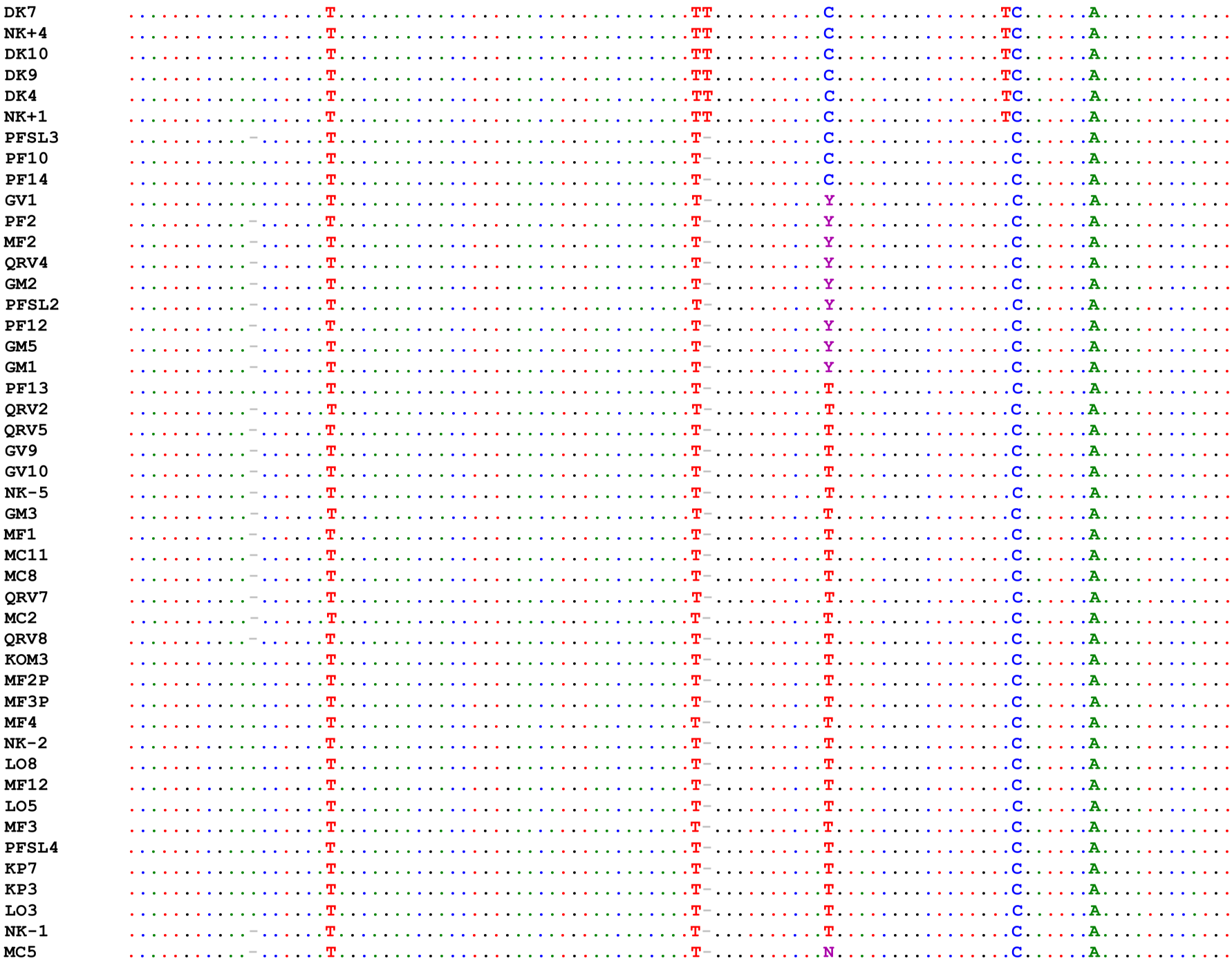
DK7
NK+4
DK10
DK9
DK4
NK+1
PFSL3
PF10
PF14
GV1
PF2
MF2
QRV4
GM2
PFSL2
PF12
GM5
GM1
PF13
QRV2
QRV5
GV9
GV10
NK-5
GM3
MF1
MC11
MC8
QRV7
MC2
QRV8
KOM3
MF2P
MF3P
MF4
NK-2
LO8
MF12
LO5
MF3
PFSL4
KP7
KP3
LO3
NK-1
MC5

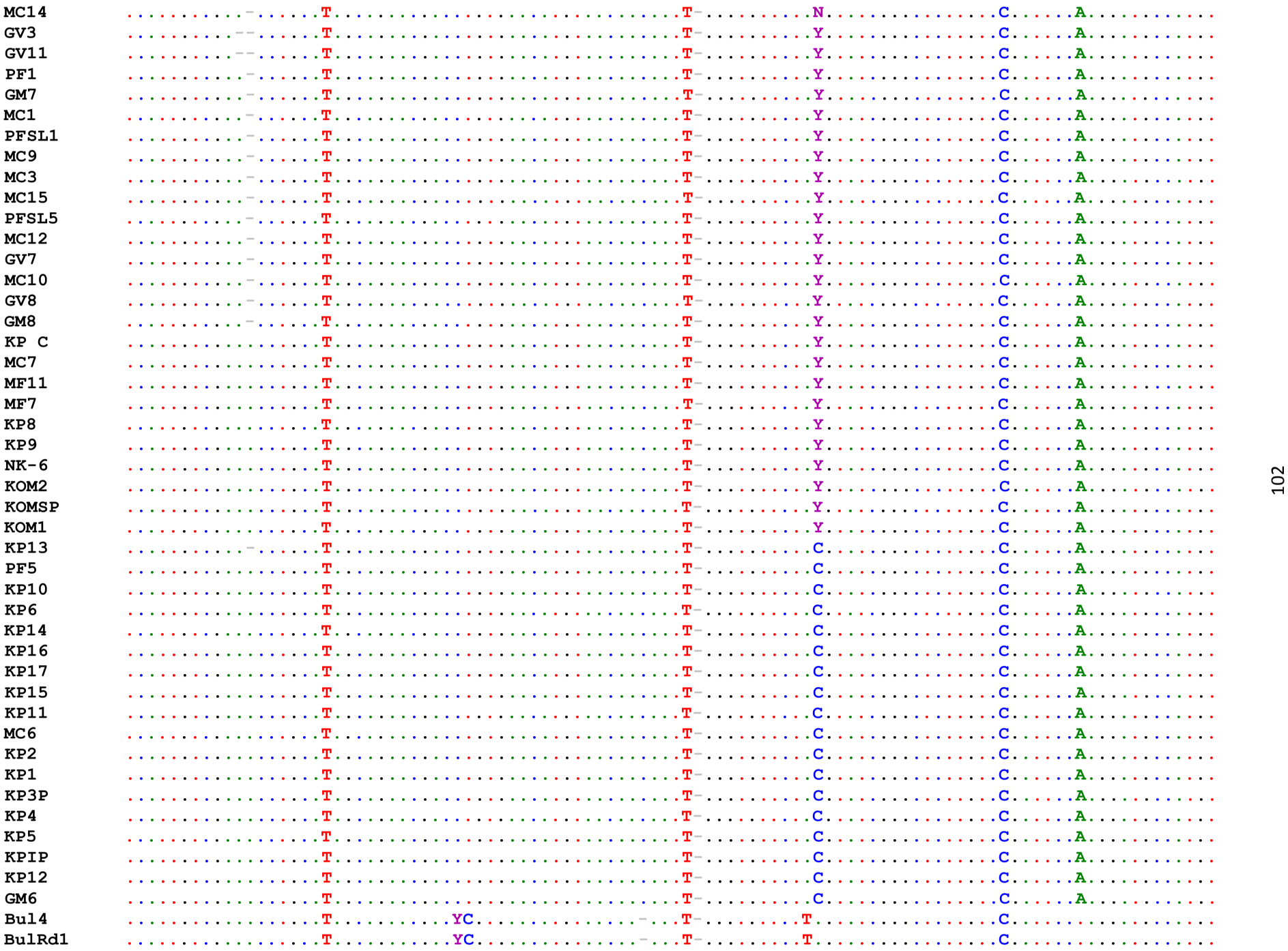
MC14
GV3
GV11
PF1
GM7
MC1
PFSL1
MC9
MC3
MC15
PFSL5
MC12
GV7
MC10
GV8
GM8
KP C
MC7
MF11
MF7
KP8
KP9
NK-6
KOM2
KOMSP
KOM1
KP13
PF5
KP10
KP6
KP14
KP16
KP17
KP15
KP11
MC6
KP2
KP1
KP3P
KP4
KP5
KPIP
KP12
GM6
Bul4
BulRd1

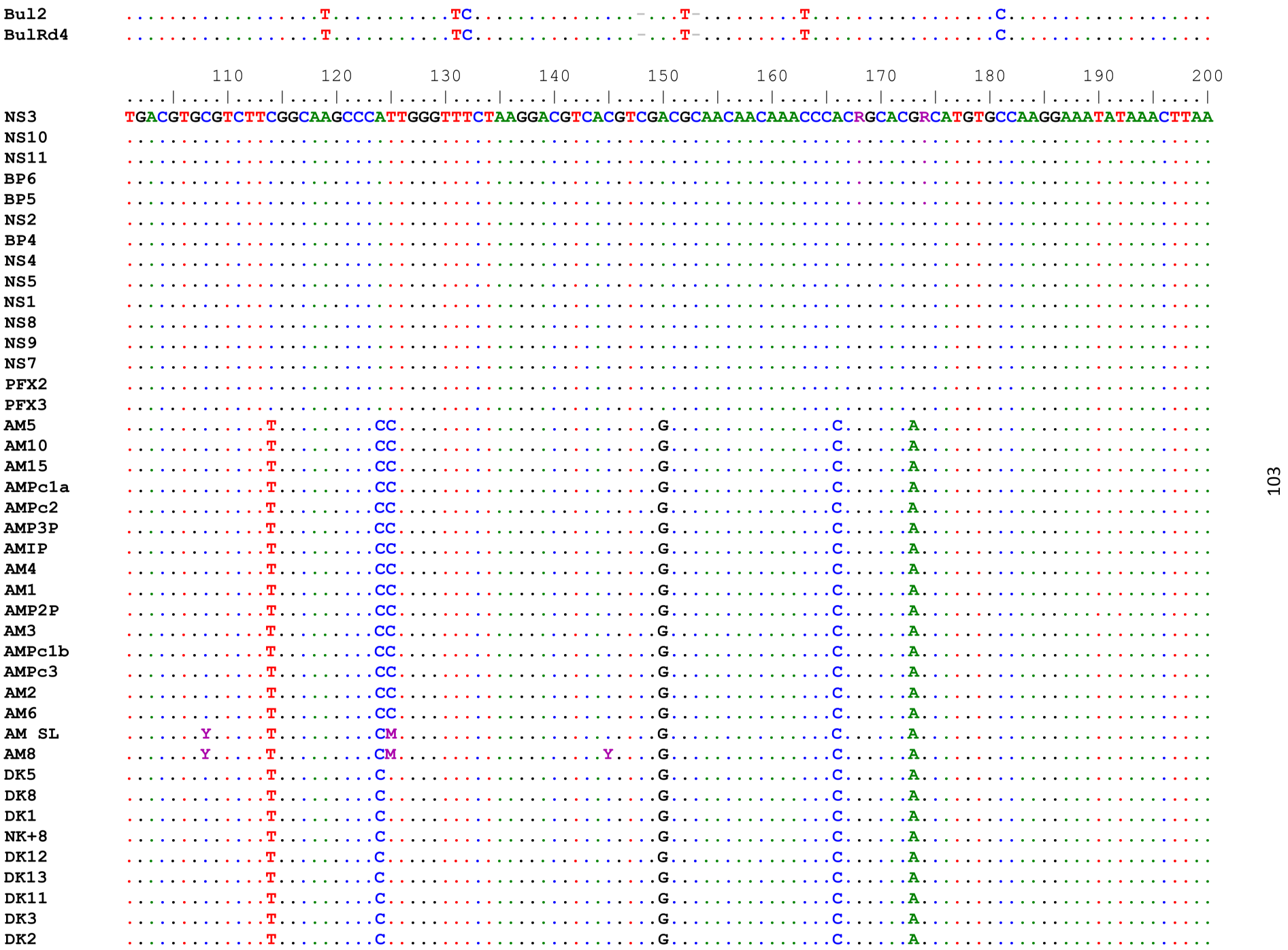
Bul2
BulRd4
110
120
130
140
150
160
170
180
190
200
NS3 TGACGTGCGTCTTCGGCAAGCCCATTGGGTTTCTAAGGACGTCACGTCGACGCAACAACAAACCCACRGCACGRCATGTGCCAAGGAAATATAAACTTAA
NS10
NS11
BP6
BP5
NS2
BP4
NS4
NS5
NS1
NS8
NS9
NS7
PFX2
PFX3
AM5
AM10
AM15
AMPc1a
AMPc2
AMP3P
AMIP
AM4
AM1
AMP2P
AM3
AMPc1b
AMPc3
AM2
AM6
AM SL
AM8
DK5
DK8
DK1
NK+8
DK12
DK13
DK11
DK3
DK2

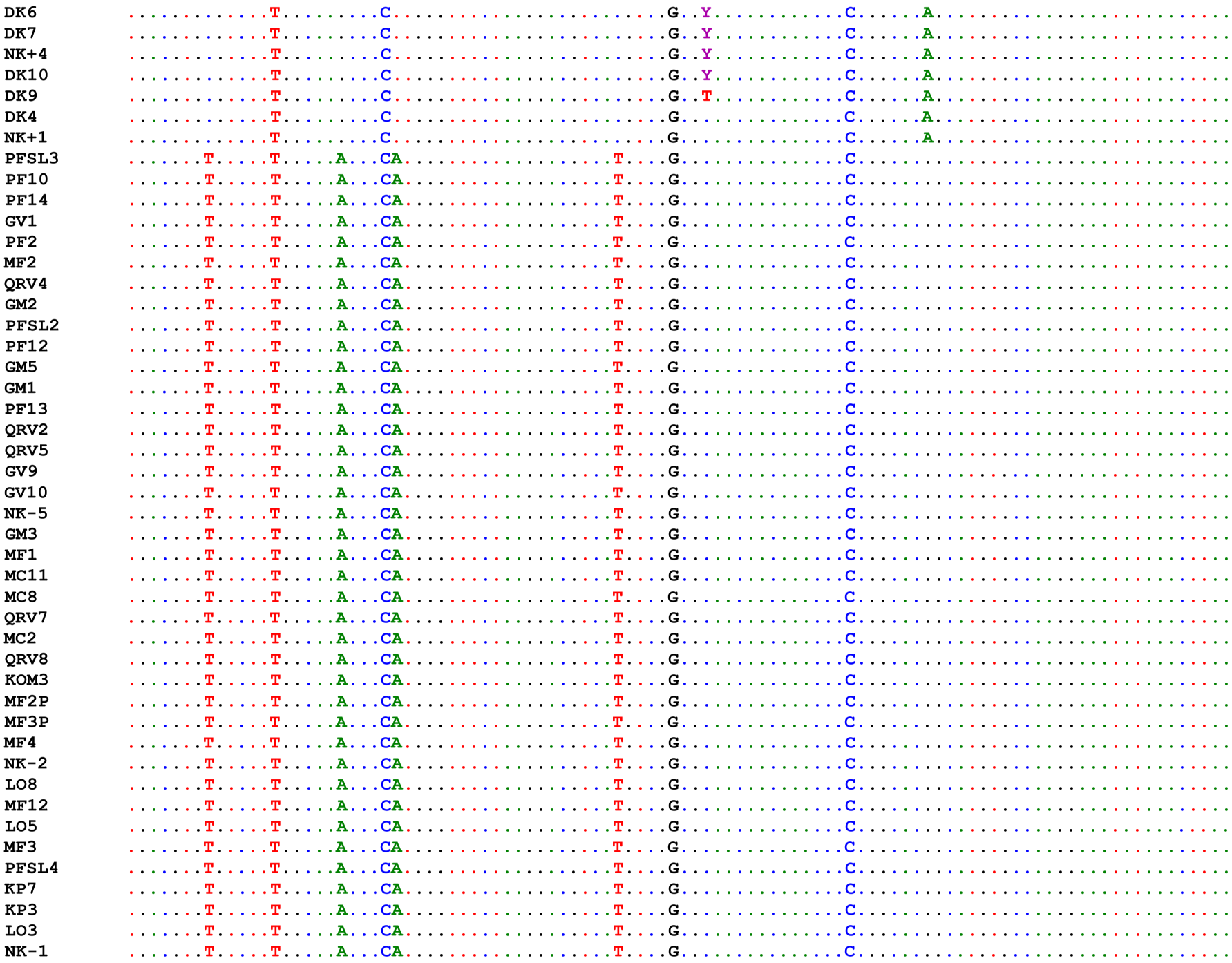
DK6
DK7
NK+4
DK10
DK9
DK4
NK+1
PFSL3
PF10
PF14
GV1
PF2
MF2
QRV4
GM2
PFSL2
PF12
GM5
GM1
PF13
QRV2
QRV5
GV9
GV10
NK-5
GM3
MF1
MC11
MC8
QRV7
MC2
QRV8
KOM3
MF2P
MF3P
MF4
NK-2
LO8
MF12
LO5
MF3
PFSL4
KP7
KP3
LO3
NK-1

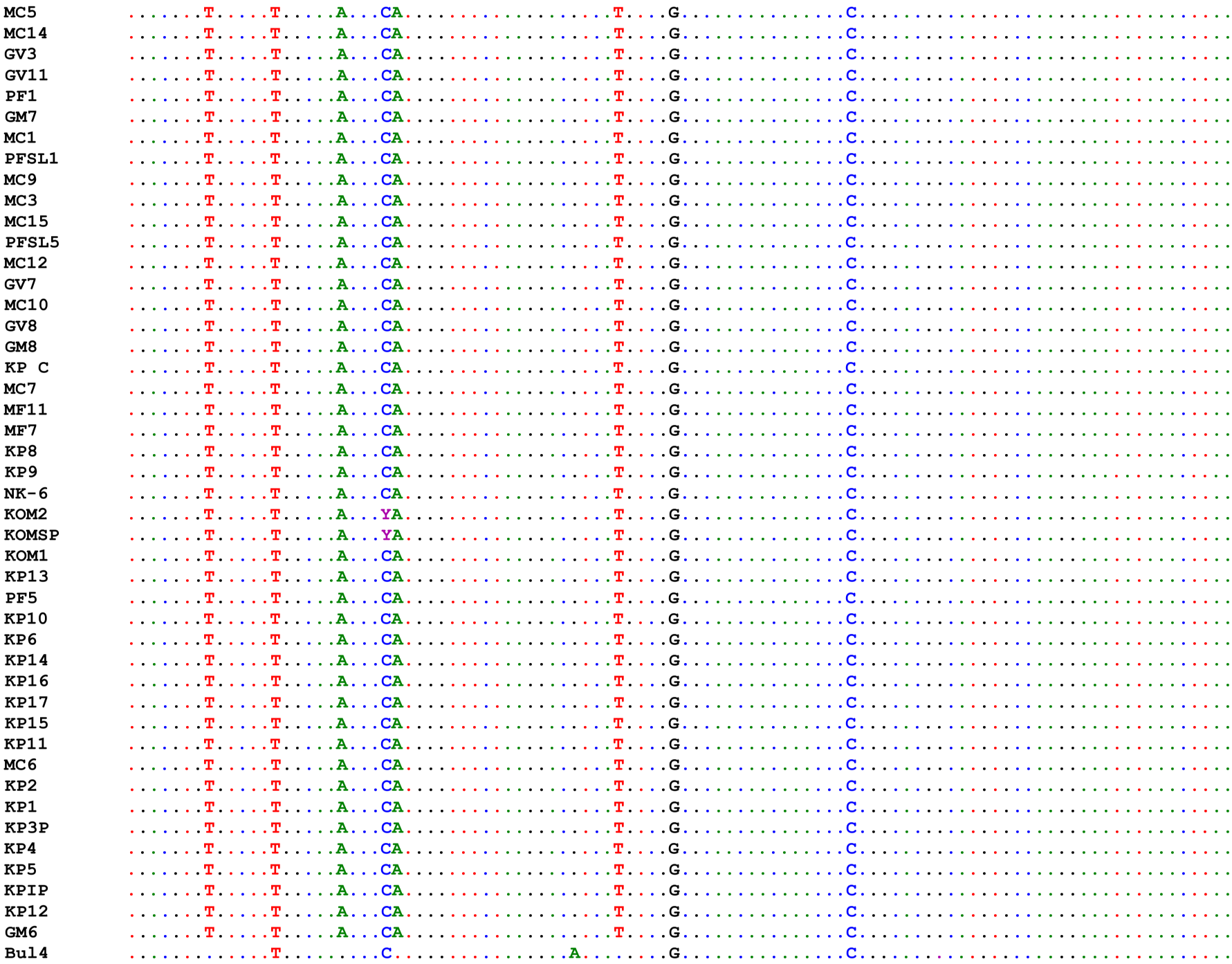
MC5
MC14
GV3
GV11
PF1
GM7
MC1
PFSL1
MC9
MC3
MC15
PFSL5
MC12
GV7
MC10
GV8
GM8
KP C
MC7
MF11
MF7
KP8
KP9
NK-6
KOM2
KOMSP
KOM1
KP13
PF5
KP10
KP6
KP14
KP16
KP17
KP15
KP11
MC6
KP2
KP1
KP3P
KP4
KP5
KPIP
KP12
GM6
Bul4

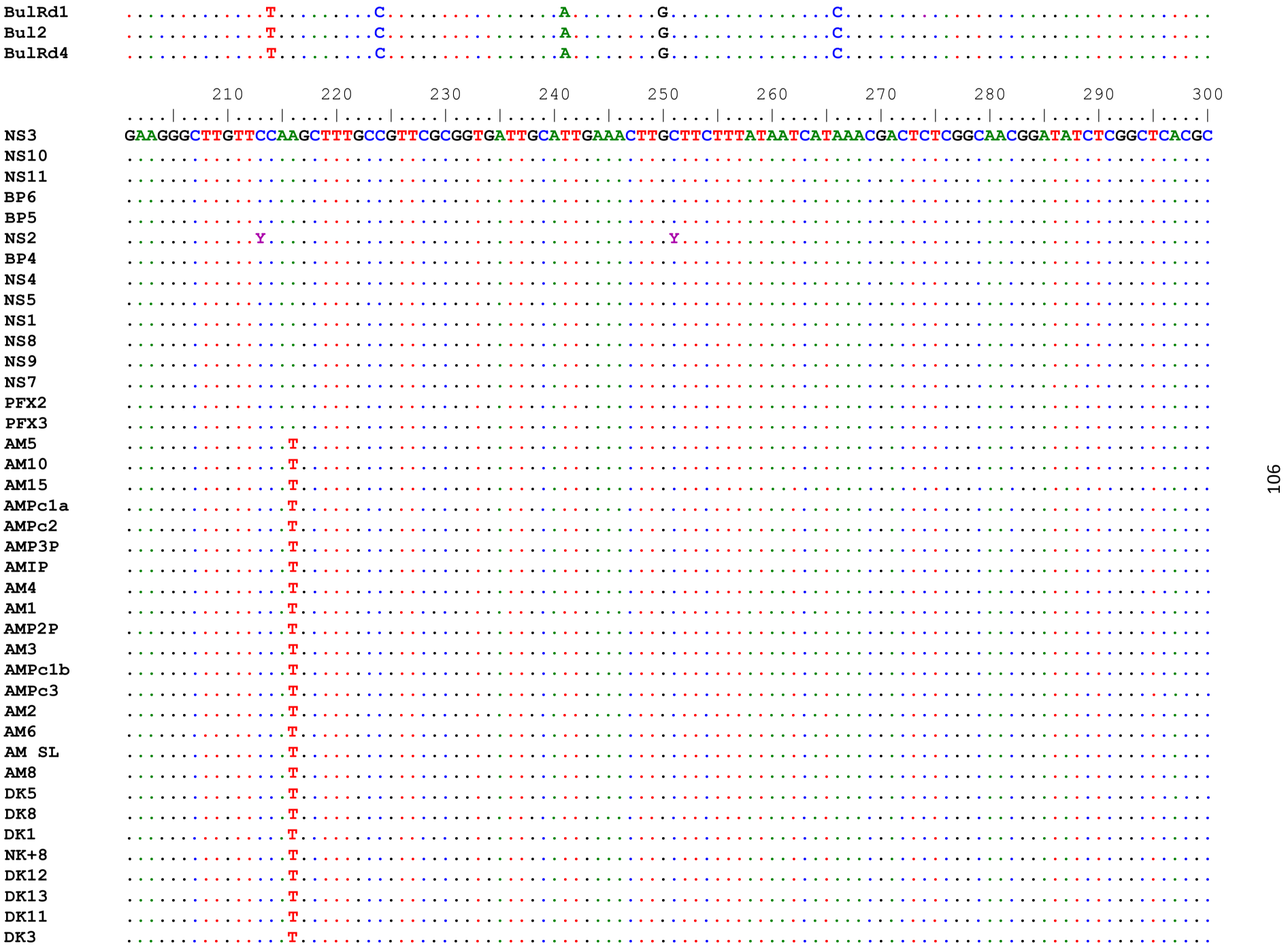
BulRd1
Bul2
BulRd4
210
220
230
240
250
260
270
280
290
300
NS3 GAAGGGCTTGTTCCAAGCTTTGCCGTTCGCGGTGATTGCATTGAAACTTGCTTCTTTATAATCATAAACGACTCTCGGCAACGGATATCTCGGCTCACGC
NS10
NS11
BP6
BP5
NS2
BP4
NS4
NS5
NS1
NS8
NS9
NS7
PFX2
PFX3
AM5
AM10
AM15
AMPc1a
AMPc2
AMP3P
AMIP
AM4
AM1
AMP2P
AM3
AMPc1b
AMPc3
AM2
AM6
AM SL
AM8
DK5
DK8
DK1
NK+8
DK12
DK13
DK11
DK3

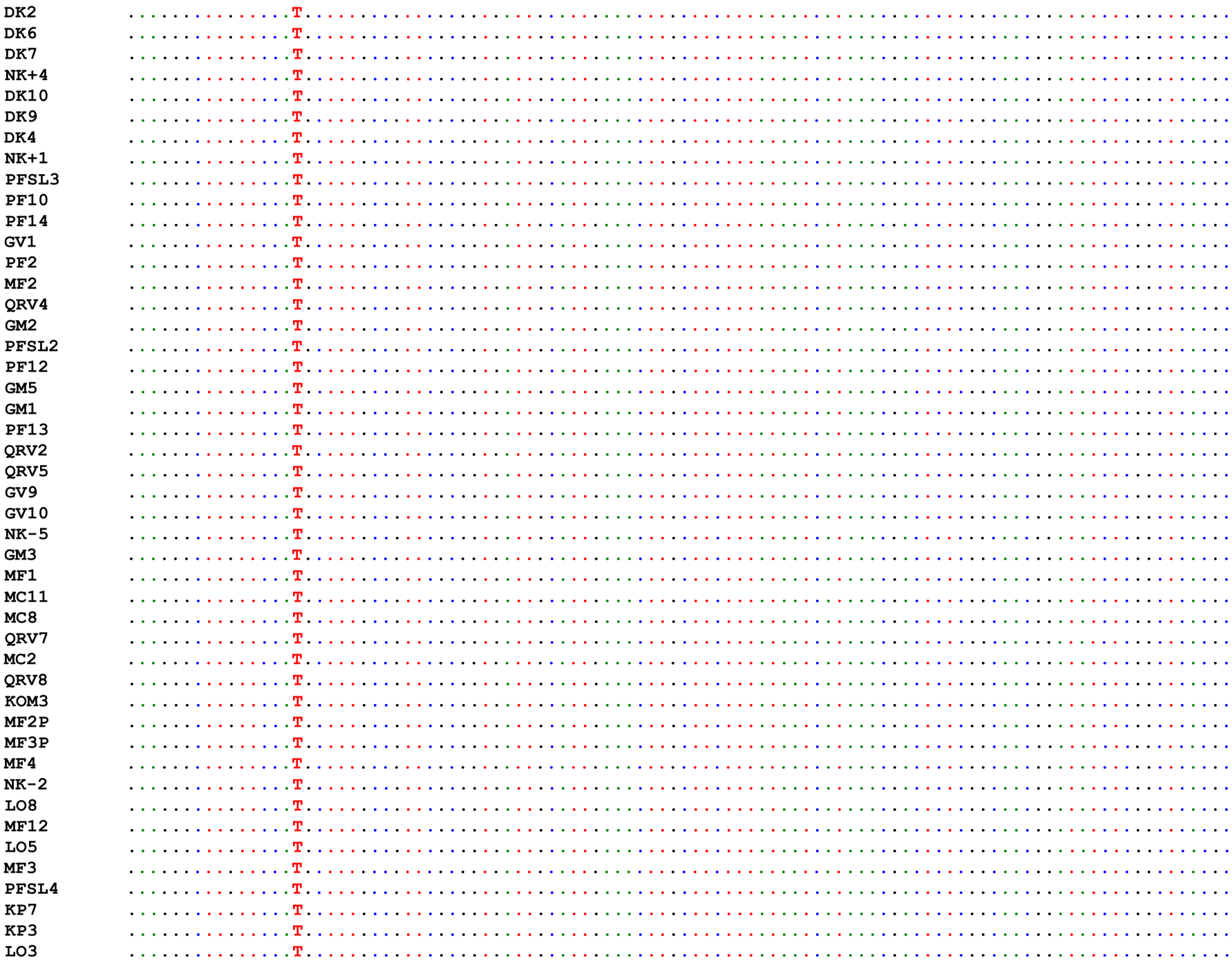
DK2
DK6
DK7
NK+4
DK10
DK9
DK4
NK+1
PFSL3
PF10
PF14
GV1
PF2
MF2
QRV4
GM2
PFSL2
PF12
GM5
GM1
PF13
QRV2
QRV5
GV9
GV10
NK-5
GM3
MF1
MC11
MC8
QRV7
MC2
QRV8
KOM3
MF2P
MF3P
MF4
NK-2
LO8
MF12
LO5
MF3
PFSL4
KP7
KP3
LO3

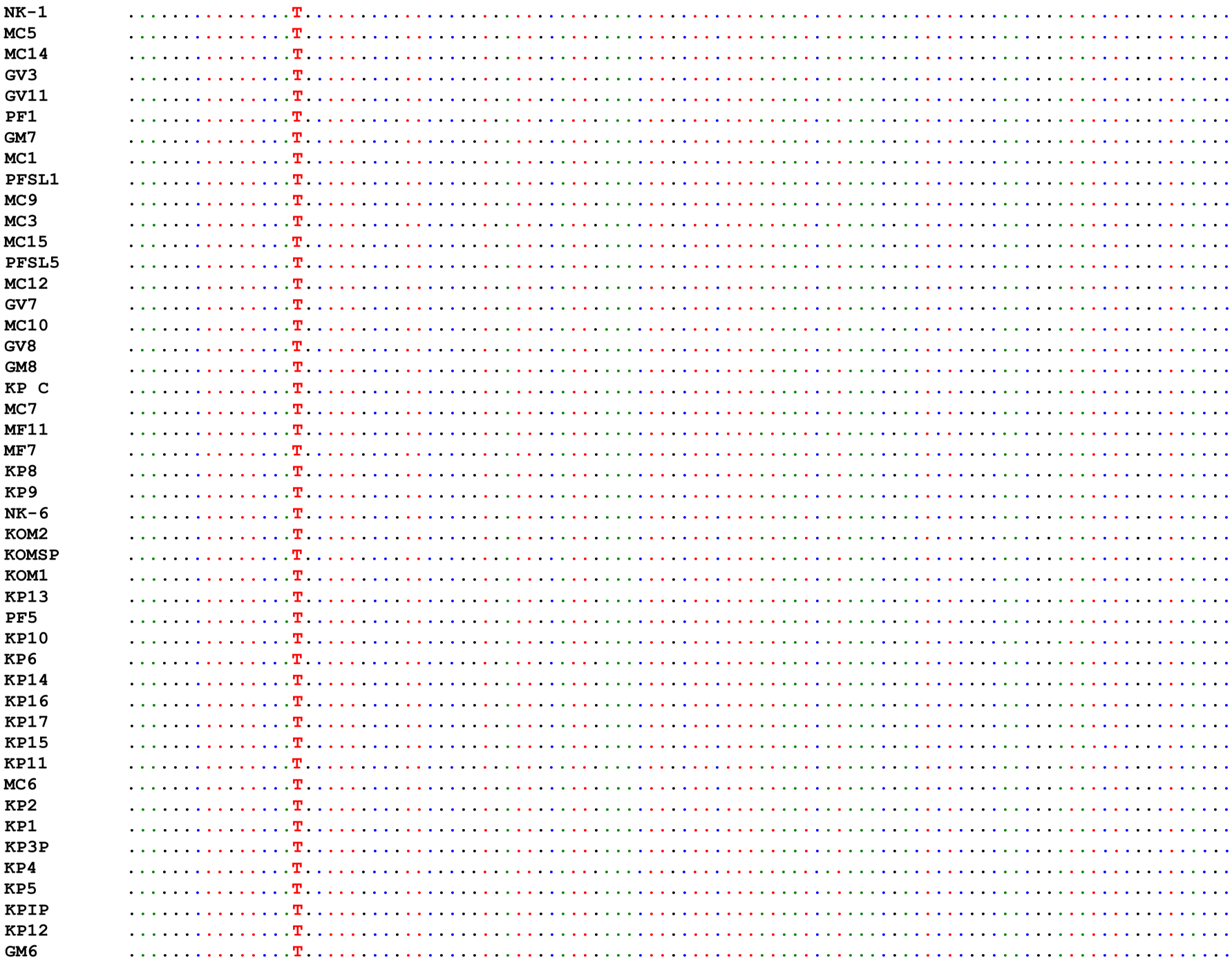
NK-1
MC5
MC14
GV3
GV11
PF1
GM7
MC1
PFSL1
MC9
MC3
MC15
PFSL5
MC12
GV7
MC10
GV8
GM8
KP C
MC7
MF11
MF7
KP8
KP9
NK-6
KOM2
KOMSP
KOM1
KP13
PF5
KP10
KP6
KP14
KP16
KP17
KP15
KP11
MC6
KP2
KP1
KP3P
KP4
KP5
KPIP
KP12
GM6

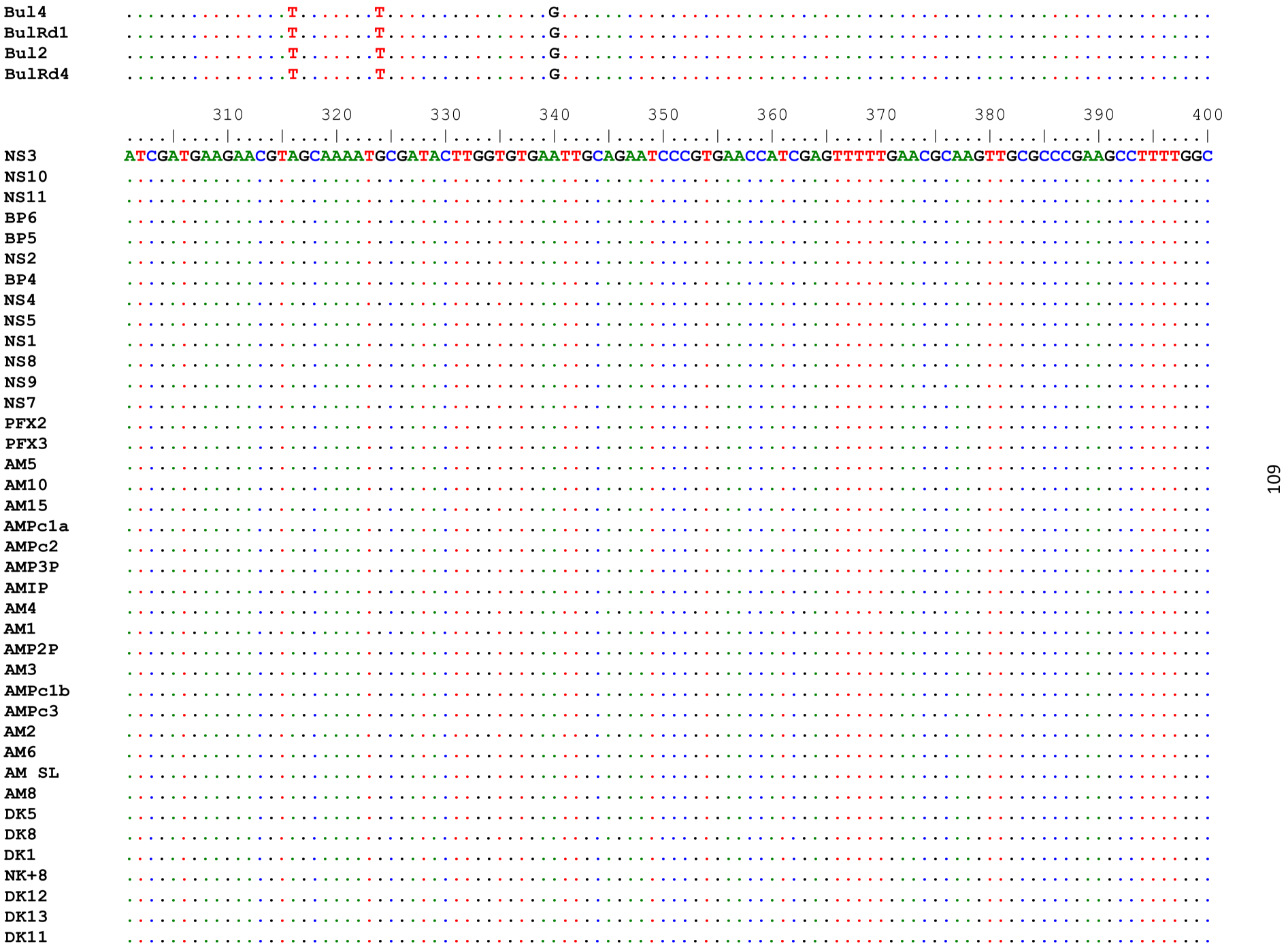
Bul4
BulRd1
Bul2
BulRd4
310
320
330
340
350
360
370
380
390
400
NS3
NS10
NS11
BP6
BP5
NS2
BP4
NS4
NS5
NS1
NS8
NS9
NS7
PFX2
PFX3
AM5
AM10
AM15
AMPc1a
AMPc2
AMP3P
AMIP
AM4
AM1
AMP2P
AM3
AMPc1b
AMPc3
AM2
AM6
AM SL
AM8
DK5
DK8
DK1
NK+8
DK12
DK13
DK11

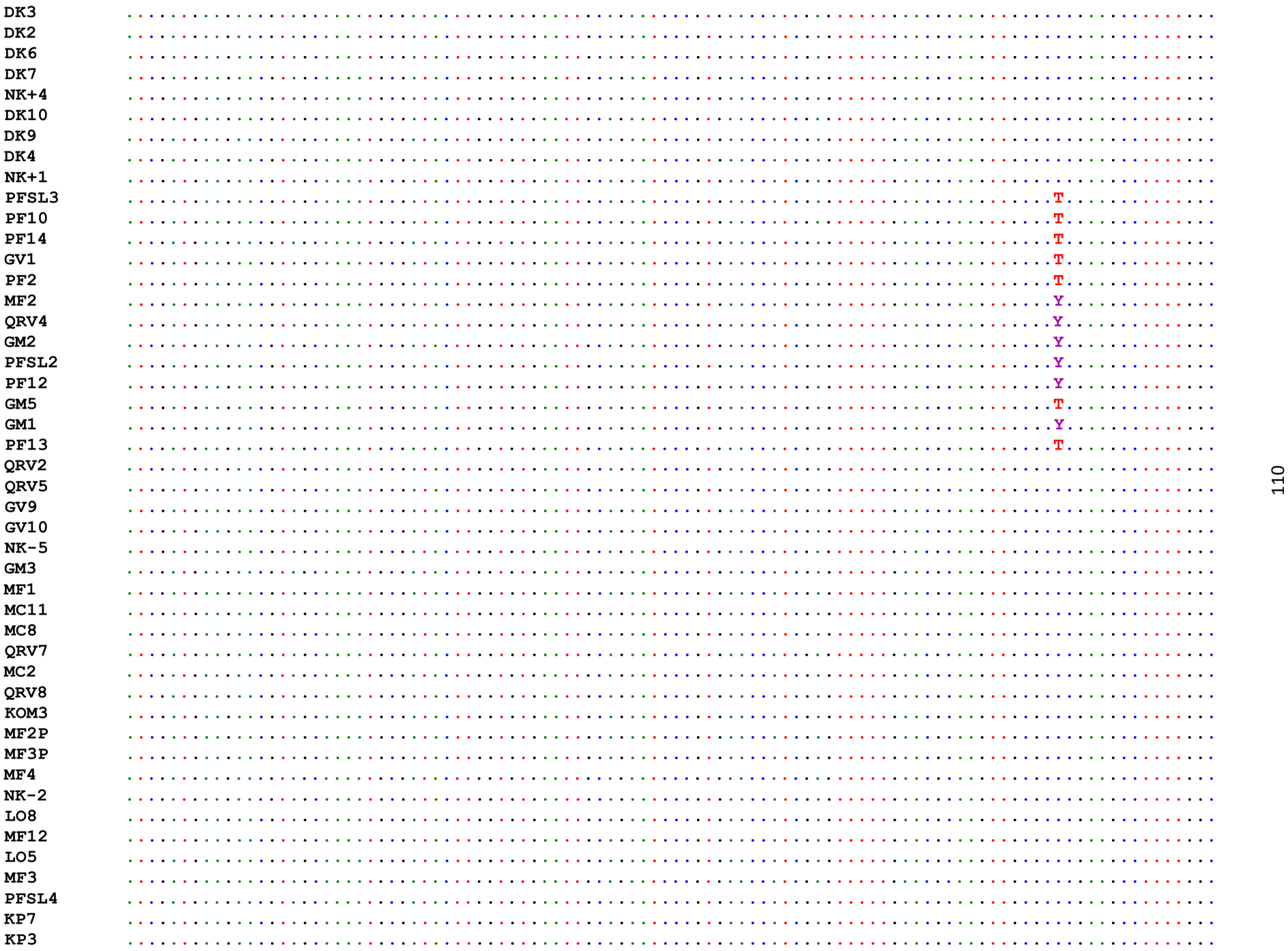
DK3
DK2
DK6
DK7
NK+4
DK10
DK9
DK4
NK+1
PFSL3
PF10
PF14
GV1
PF2
MF2
QRV4
GM2
PFSL2
PF12
GM5
GM1
PF13
QRV2
QRV5
GV9
GV10
NK-5
GM3
MF1
MC11
MC8
QRV7
MC2
QRV8
KOM3
MF2P
MF3P
MF4
NK-2
LO8
MF12
LO5
MF3
PFSL4
KP7
KP3
110

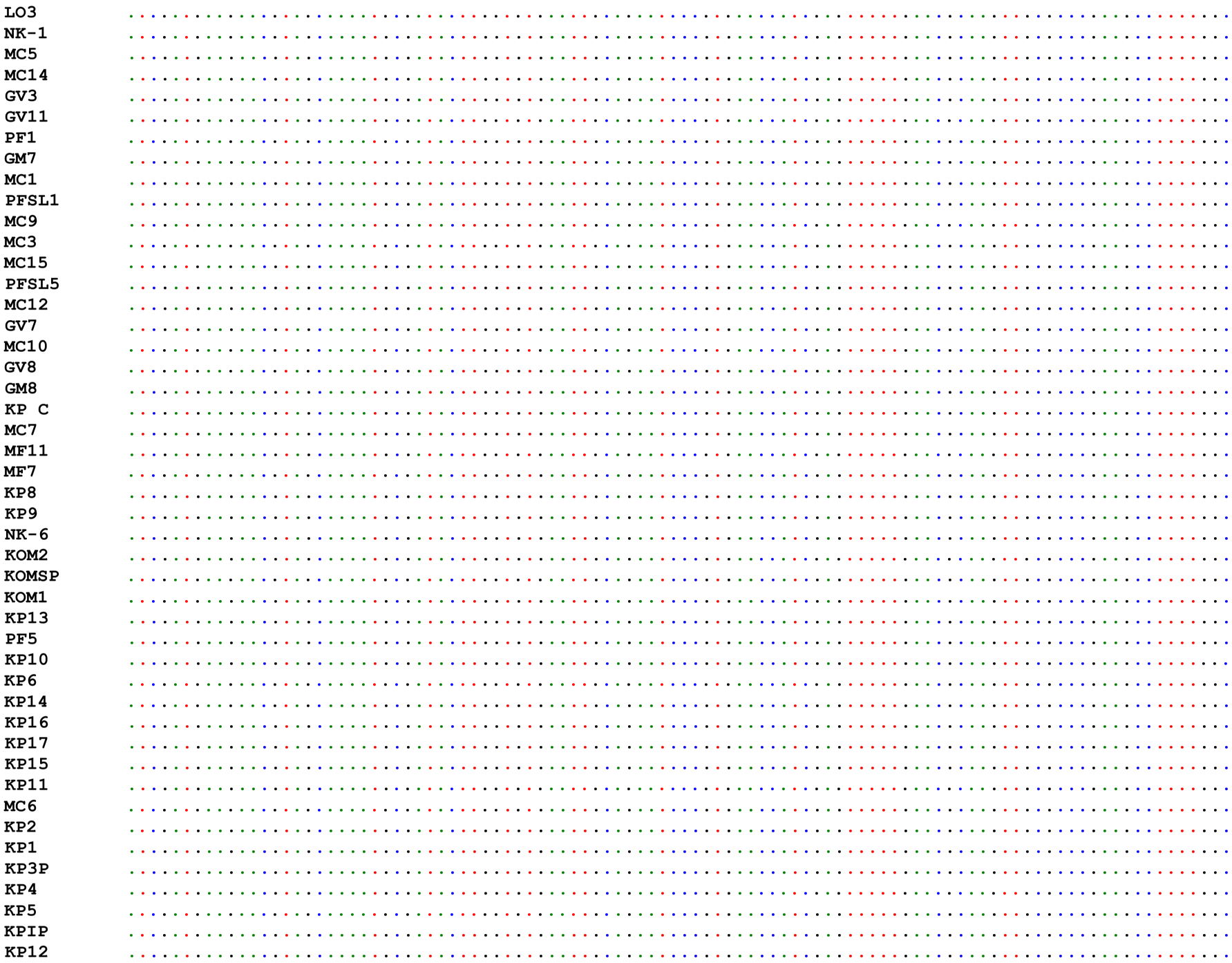
LO3
NK-1
MC5
MC14
GV3
GV11
PF1
GM7
MC1
PFSL1
MC9
MC3
MC15
PFSL5
MC12
GV7
MC10
GV8
GM8
KP C
MC7
MF11
MF7
KP8
KP9
NK-6
KOM2
KOMSP
KOM1
KP13
PF5
KP10
KP6
KP14
KP16
KP17
KP15
KP11
MC6
KP2
KP1
KP3P
KP4
KP5
KPIP
KP12


GM6
Bul4
BulRd1
Bul2
BulRd4
410
420
430
440
450
460
470
480
490
500
NS3
NS10
NS11
BP6
BP5
NS2
BP4
NS4
NS5
NS1
NS8
NS9
NS7
PFX2
PFX3
AM5
AM10
AM15
AMPc1a
AMPc2
AMP3P
AMIP
AM4
AM1
AMP2P
AM3
AMPc1b
AMPc3
AM2
AM6
AM SL
AM8
DK5
DK8
DK1
NK+8
DK12
DK13

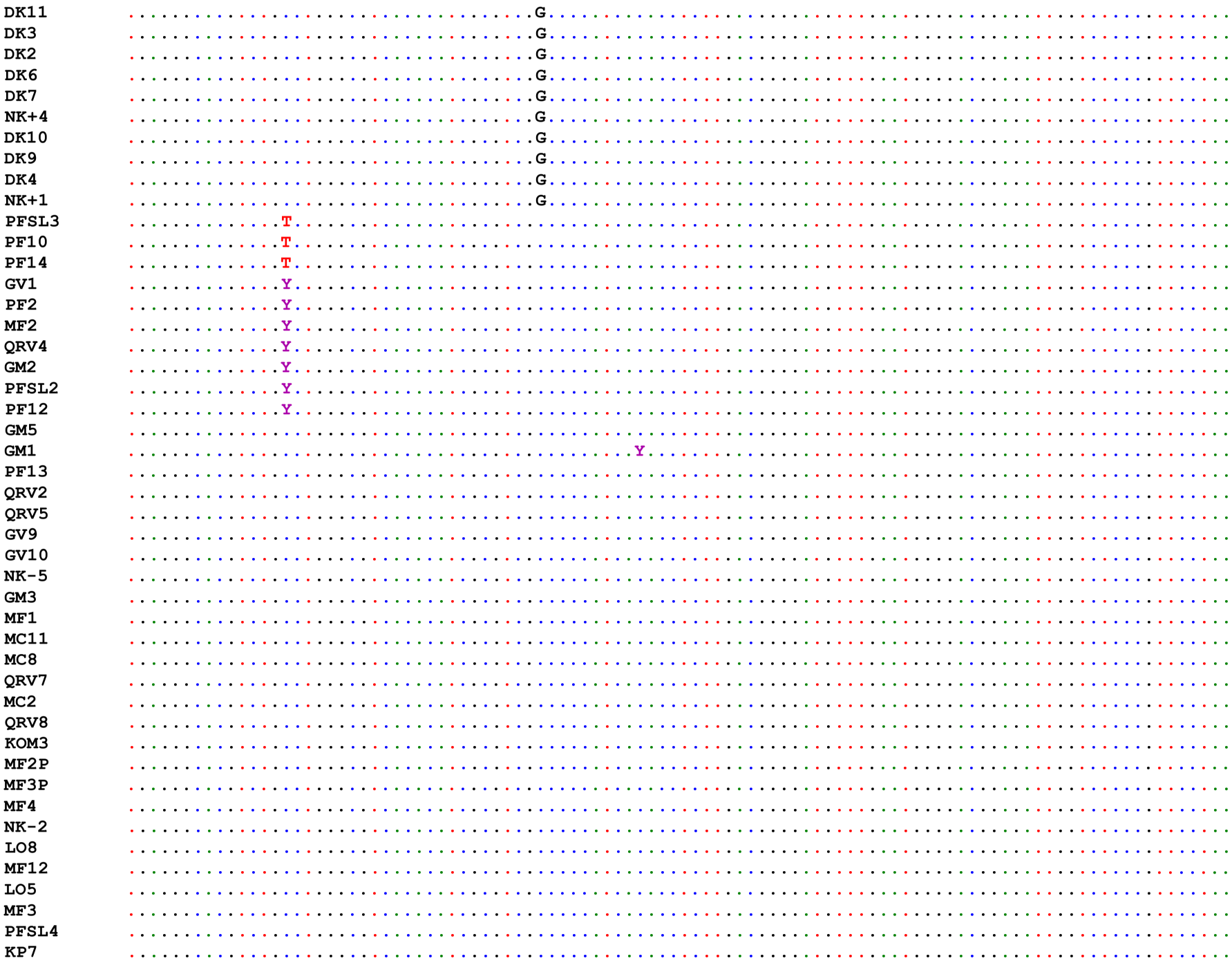
DK11
DK3
DK2
DK6
DK7
NK+4
DK10
DK9
DK4
NK+1
PFSL3
PF10
PF14
GV1
PF2
MF2
QRV4
GM2
PFSL2
PF12
GM5
GM1
PF13
QRV2
QRV5
GV9
GV10
NK-5
GM3
MF1
MC11
MC8
QRV7
MC2
QRV8
KOM3
MF2P
MF3P
MF4
NK-2
LO8
MF12
LO5
MF3
PFSL4
KP7

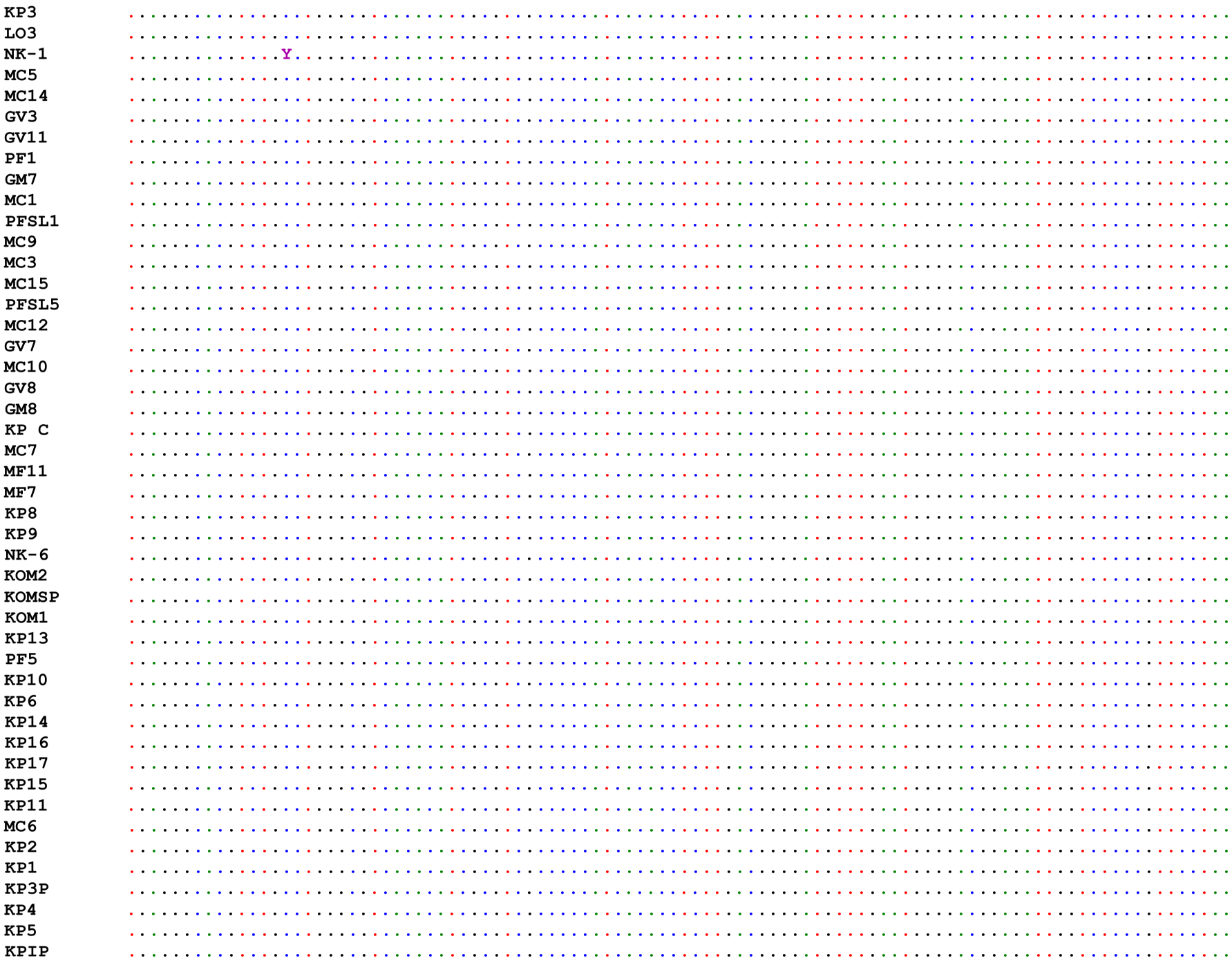
KP3
LO3
NK-1
MC5
MC14
GV3
GV11
PF1
GM7
MC1
PFSL1
MC9
MC3
MC15
PFSL5
MC12
GV7
MC10
GV8
GM8
KP C
MC7
MF11
MF7
KP8
KP9
NK-6
KOM2
KOMSP
KOM1
KP13
PF5
KP10
KP6
KP14
KP16
KP17
KP15
KP11
MC6
KP2
KP1
KP3P
KP4
KP5
KPIP

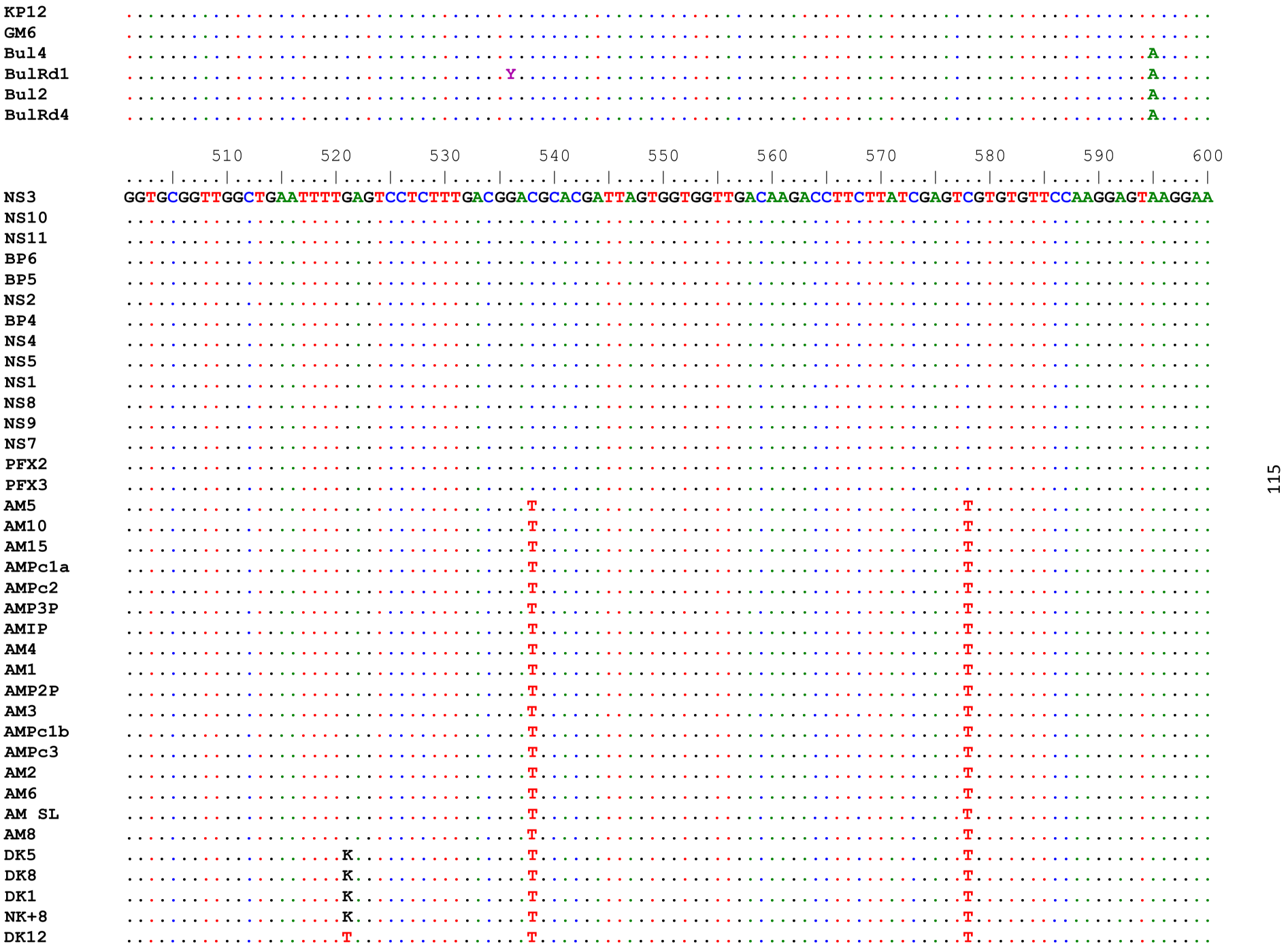
KP12
GM6
Bul4
BulRd1
Bul2
BulRd4
510
520
530
540
550
560
570
580
590
600
NS3
GGTGCGGTTGGCTGAATTTTGAGTCCTCTTTGACGGACGCACGATTAGTGGTGGTTGACAAGACCTTCTTATCGAGTCGTGTGTTCCAAGGAGTAAGGAA
NS10
NS11
BP6
BP5
NS2
BP4
NS4
NS5
NS1
NS8
NS9
NS7
PFX2
PFX3
AM5
AM10
AM15
AMPc1a
AMPc2
AMP3P
AMIP
AM4
AM1
AMP2P
AM3
AMPc1b
AMPc3
AM2
AM6
AM SL
AM8
DK5
DK8
DK1
NK+8
DK12

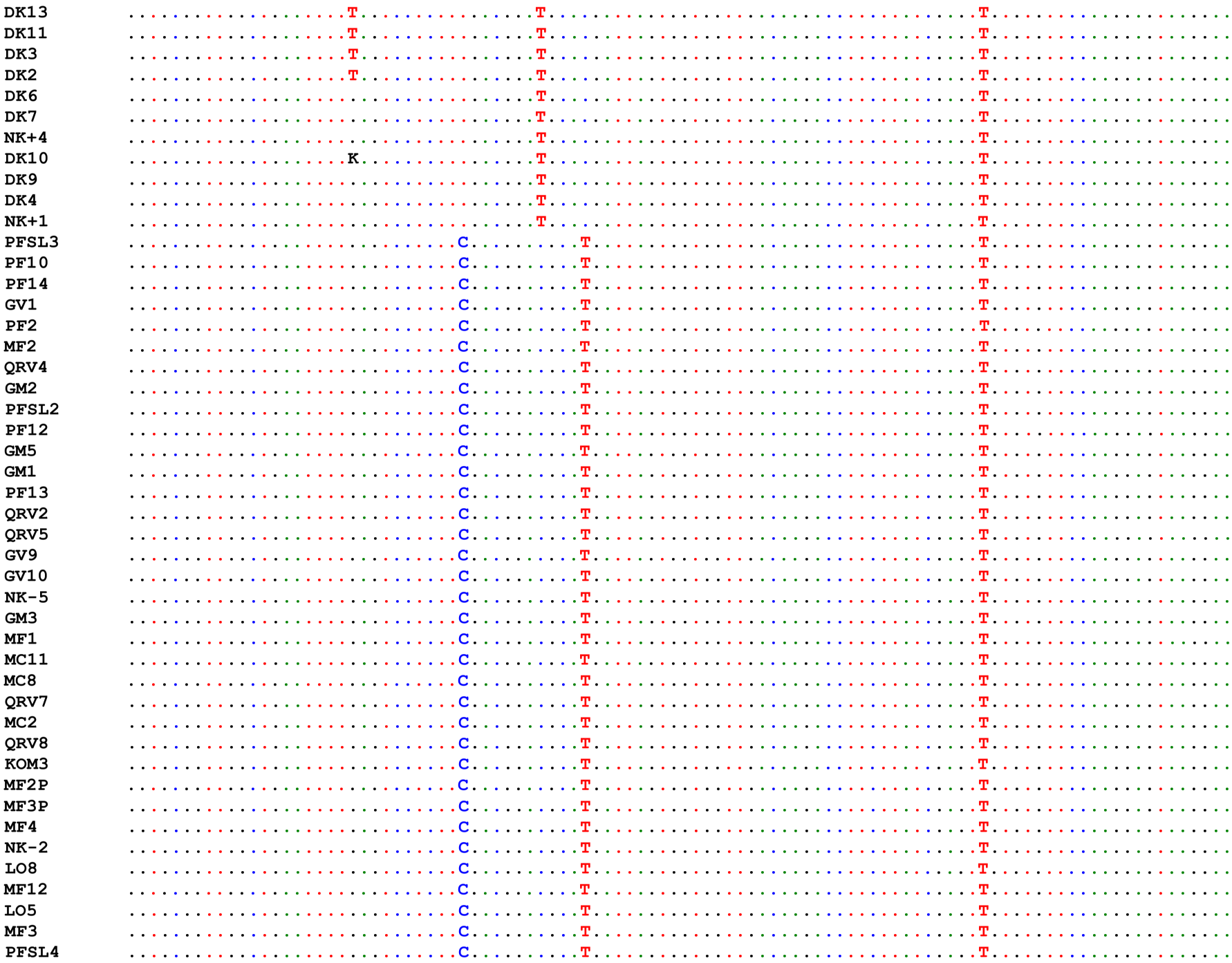
DK13
DK11
DK3
DK2
DK6
DK7
NK+4
DK10
DK9
DK4
NK+1
PFSL3
PF10
PF14
GV1
PF2
MF2
QRV4
GM2
PFSL2
PF12
GM5
GM1
PF13
QRV2
QRV5
GV9
GV10
NK-5
GM3
MF1
MC11
MC8
QRV7
MC2
QRV8
KOM3
MF2P
MF3P
MF4
NK-2
LO8
MF12
LO5
MF3
PFSL4

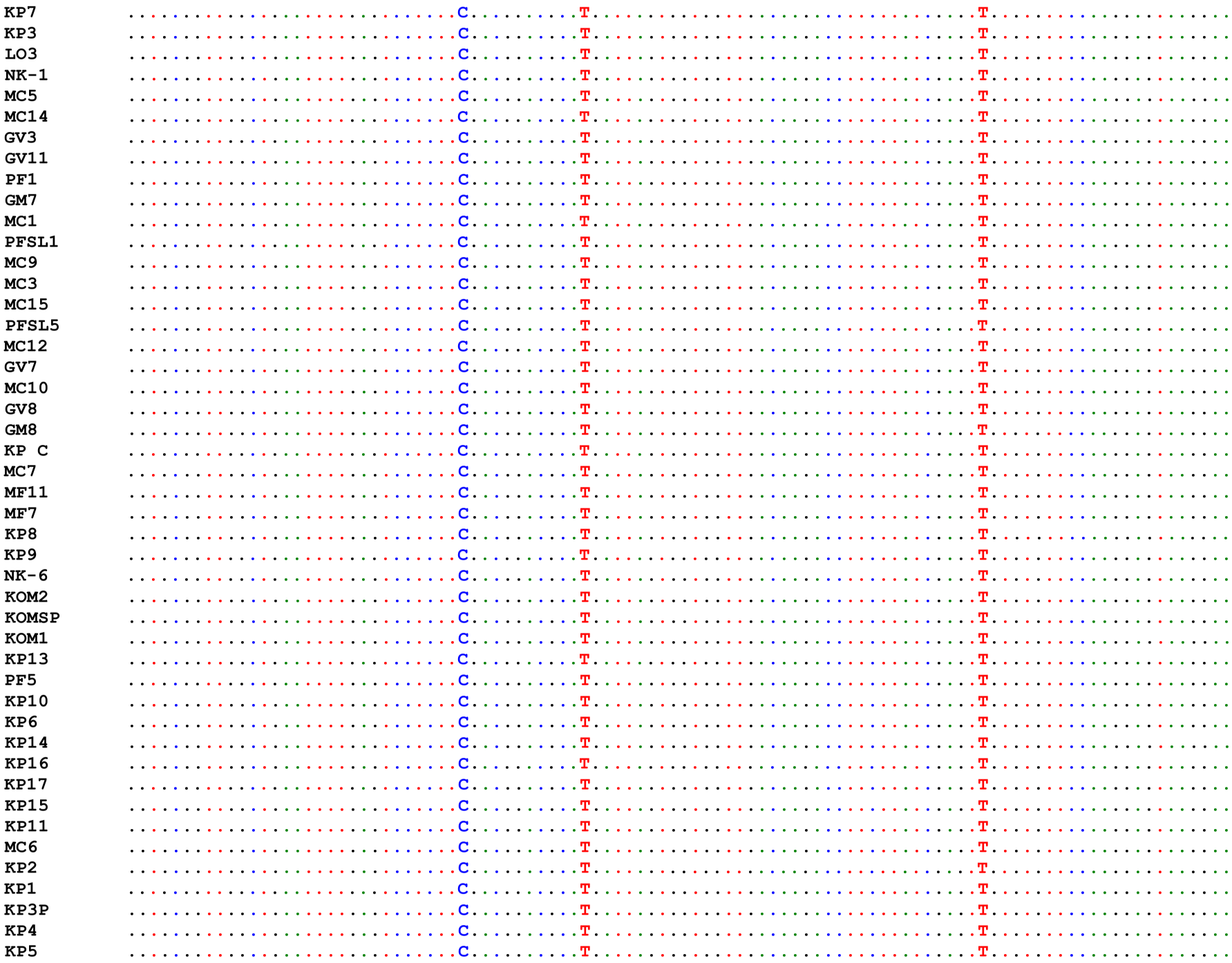
KP7
KP3
LO3
NK-1
MC5
MC14
GV3
GV11
PF1
GM7
MC1
PFSL1
MC9
MC3
MC15
PFSL5
MC12
GV7
MC10
GV8
GM8
KP C
MC7
MF11
MF7
KP8
KP9
NK-6
KOM2
KOMSP
KOM1
KP13
PF5
KP10
KP6
KP14
KP16
KP17
KP15
KP11
MC6
KP2
KP1
KP3P
KP4
KP5

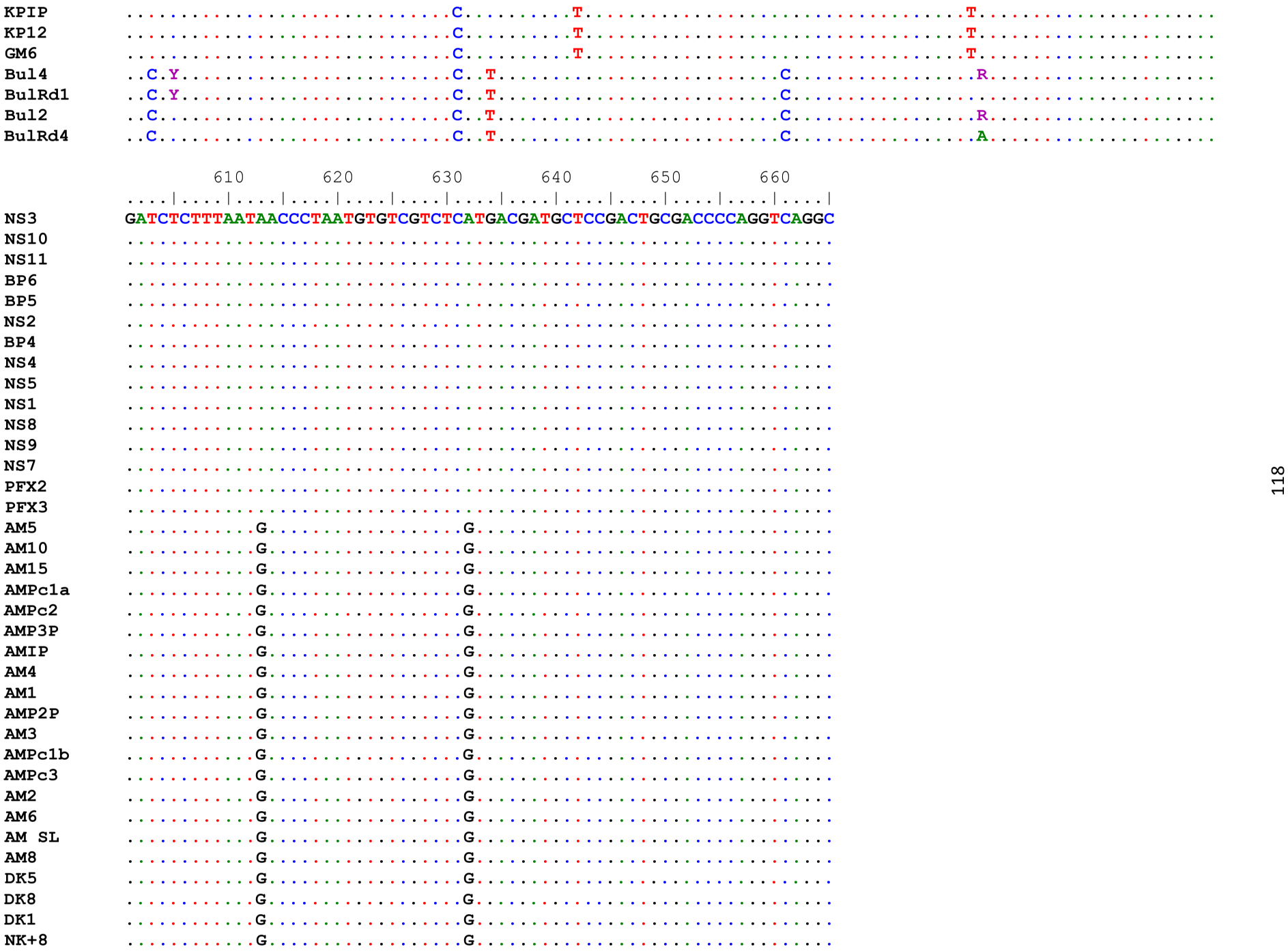
KPIP
KP12
GM6
Bul4
BulRd1
Bul2
BulRd4
610
620
630
640
650
660
NS3
GATCTCTTTAATAACCCTAATGTGTCGTCTCATGACGATGCTCCGACTGCGACCCCAGGTCAGGC
NS10
NS11
BP6
BP5
NS2
BP4
NS4
NS5
NS1
NS8
NS9
NS7
PFX2
PFX3
AM5
AM10
AM15
AMPc1a
AMPc2
AMP3P
AMIP
AM4
AM1
AMP2P
AM3
AMPc1b
AMPc3
AM2
AM6
AM SL
AM8
DK5
DK8
DK1
NK+8

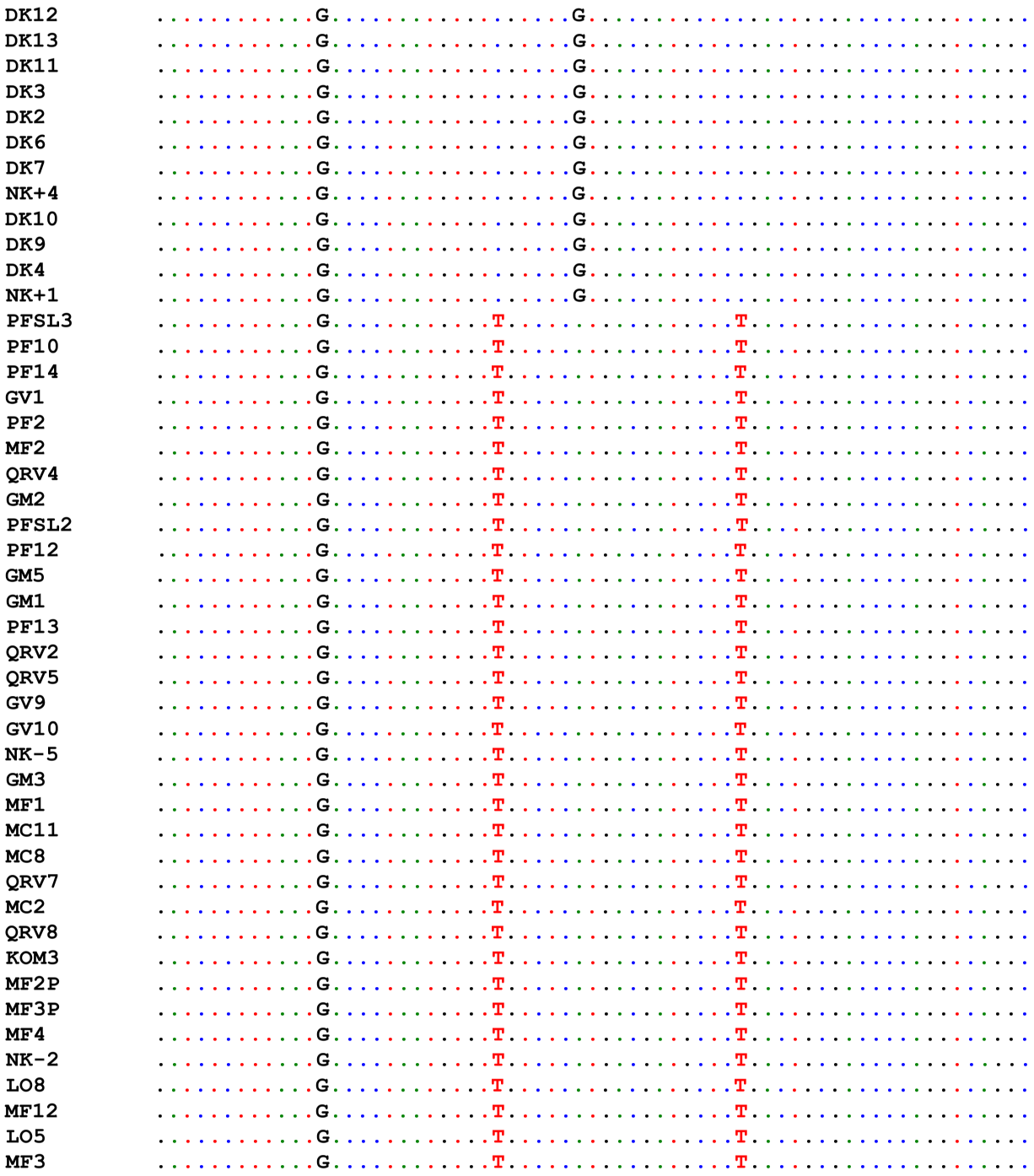
DK12 ..........G..................G.....
DK13 ..........G..................G.....
DK11 ..........G..................G.....
DK3 ..........G..................G.....
DK2 ..........G..................G.....
DK6 ..........G..................G.....
DK7 ..........G..................G.....
NK+4 ..........G..................G.....
DK10 ..........G..................G.....
DK9 ..........G..................G.....
DK4 ..........G..................G.....
NK+1 ..........G..................G.....
PFSL3 ..........G............T..................T.....
PF10 ..........G............T..................T.....
PF14 ..........G............T..................T.....
GV1 ..........G............T..................T.....
PF2 ..........G............T..................T.....
MF2 ..........G............T..................T.....
QRV4 ..........G............T..................T.....
GM2 ..........G............T..................T.....
PFSL2 ..........G............T..................T.....
PF12 ..........G............T..................T.....
GM5 ..........G............T..................T.....
GM1 ..........G............T..................T.....
PF13 ..........G............T..................T.....
QRV2 ..........G............T..................T.....
QRV5 ..........G............T..................T.....
GV9 ..........G............T..................T.....
GV10 ..........G............T..................T.....
NK-5 ..........G............T..................T.....
GM3 ..........G............T..................T.....
MF1 ..........G............T..................T.....
MC11 ..........G............T..................T.....
MC8 ..........G............T..................T.....
QRV7 ..........G............T..................T.....
MC2 ..........G............T..................T.....
QRV8 ..........G............T..................T.....
KOM3 ..........G............T..................T.....
MF2P ..........G............T..................T.....
MF3P ..........G............T..................T.....
MF4 ..........G............T..................T.....
NK-2 ..........G............T..................T.....
LO8 ..........G............T..................T.....
MF12 ..........G............T..................T.....
LO5 ..........G............T..................T.....
MF3 ..........G............T..................T.....

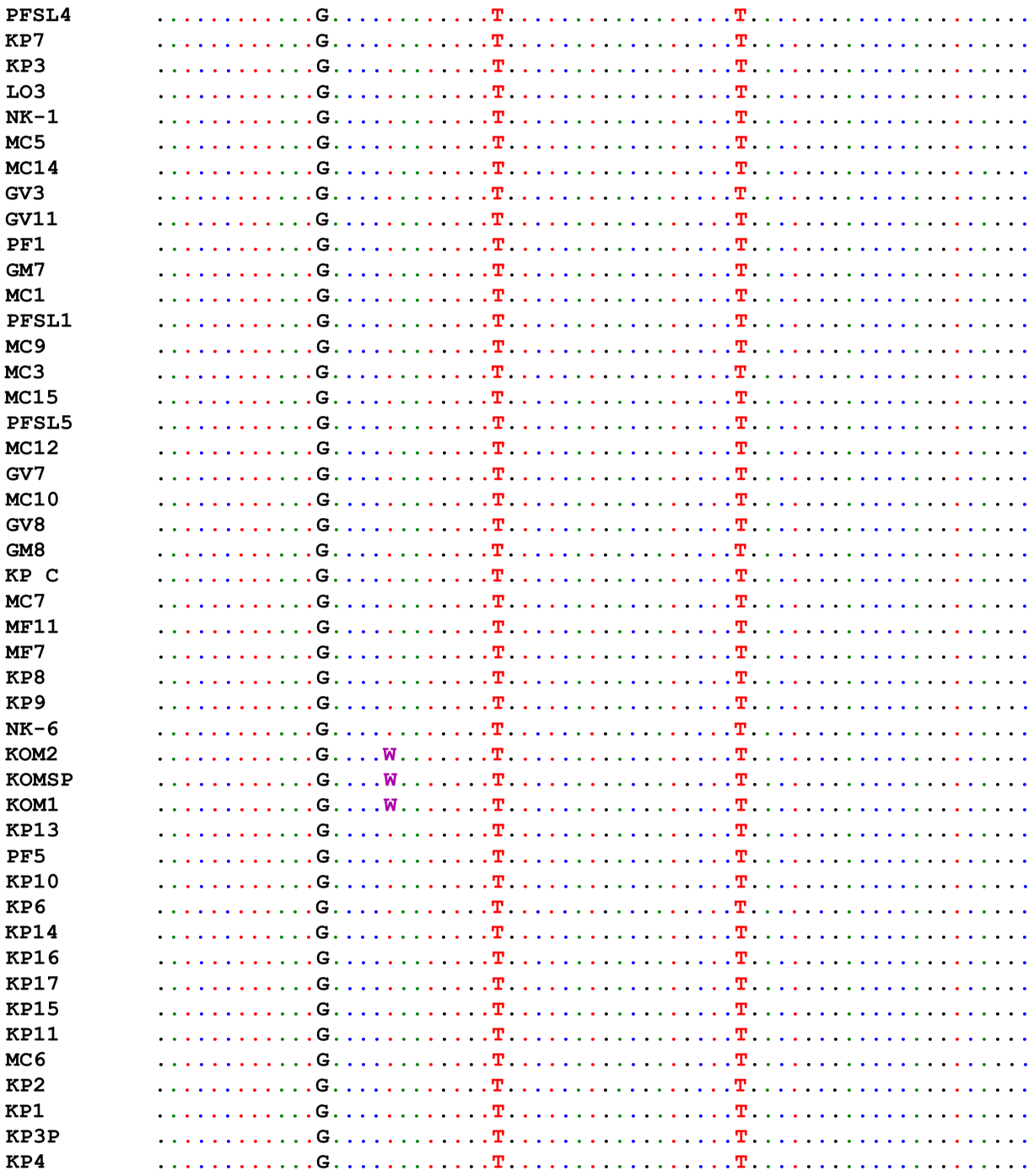
PFSL4 ..........G..........T..................T..................
KP7 ..........G..........T..................T..................
KP3 ..........G..........T..................T..................
LO3 ..........G..........T..................T..................
NK-1 ..........G..........T..................T..................
MC5 ..........G..........T..................T..................
MC14 ..........G..........T..................T..................
GV3 ..........G..........T..................T..................
GV11 ..........G..........T..................T..................
PF1 ..........G..........T..................T..................
GM7 ..........G..........T..................T..................
MC1 ..........G..........T..................T..................
PFSL1 ..........G..........T..................T..................
MC9 ..........G..........T..................T..................
MC3 ..........G..........T..................T..................
MC15 ..........G..........T..................T..................
PFSL5 ..........G..........T..................T..................
MC12 ..........G..........T..................T..................
GV7 ..........G..........T..................T..................
MC10 ..........G..........T..................T..................
GV8 ..........G..........T..................T..................
GM8 ..........G..........T..................T..................
KP C ..........G..........T..................T..................
MC7 ..........G..........T..................T..................
MF11 ..........G..........T..................T..................
MF7 ..........G..........T..................T..................
KP8 ..........G..........T..................T..................
KP9 ..........G..........T..................T..................
NK-6 ..........G..........T..................T..................
KOM2 ..........G....W.....T..................T..................
KOMSP ..........G....W.....T..................T..................
KOM1 ..........G....W.....T..................T..................
KP13 ..........G..........T..................T..................
PF5 ..........G..........T..................T..................
KP10 ..........G..........T..................T..................
KP6 ..........G..........T..................T..................
KP14 ..........G..........T..................T..................
KP16 ..........G..........T..................T..................
KP17 ..........G..........T..................T..................
KP15 ..........G..........T..................T..................
KP11 ..........G..........T..................T..................
MC6 ..........G..........T..................T..................
KP2 ..........G..........T..................T..................
KP1 ..........G..........T..................T..................
KP3P ..........G..........T..................T..................
KP4 ..........G..........T..................T..................

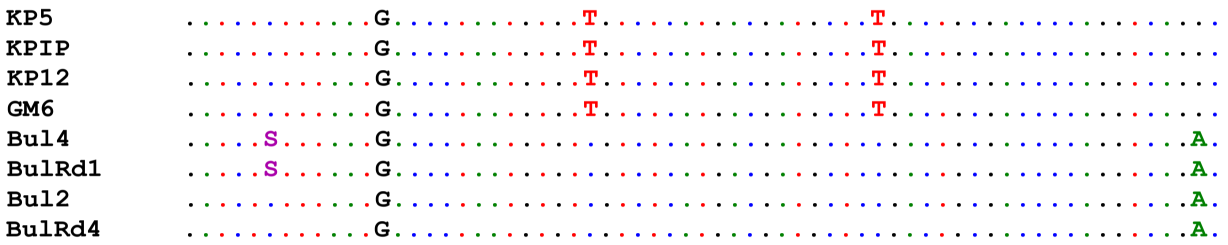
KP5 ..........G..........T..............T..................
KPIP ..........G..........T..............T..................
KP12 ..........G..........T..............T..................
GM6 ..........G..........T..............T..................
Bul4 .....S.....G.....................................A.
BulRd1 .....S.....G.....................................A.
Bul2 ..........G.....................................A.
BulRd4 ..........G.....................................A.

Appendix 2: Nucleotide sequence alignment of 37 TrnfM sequences.

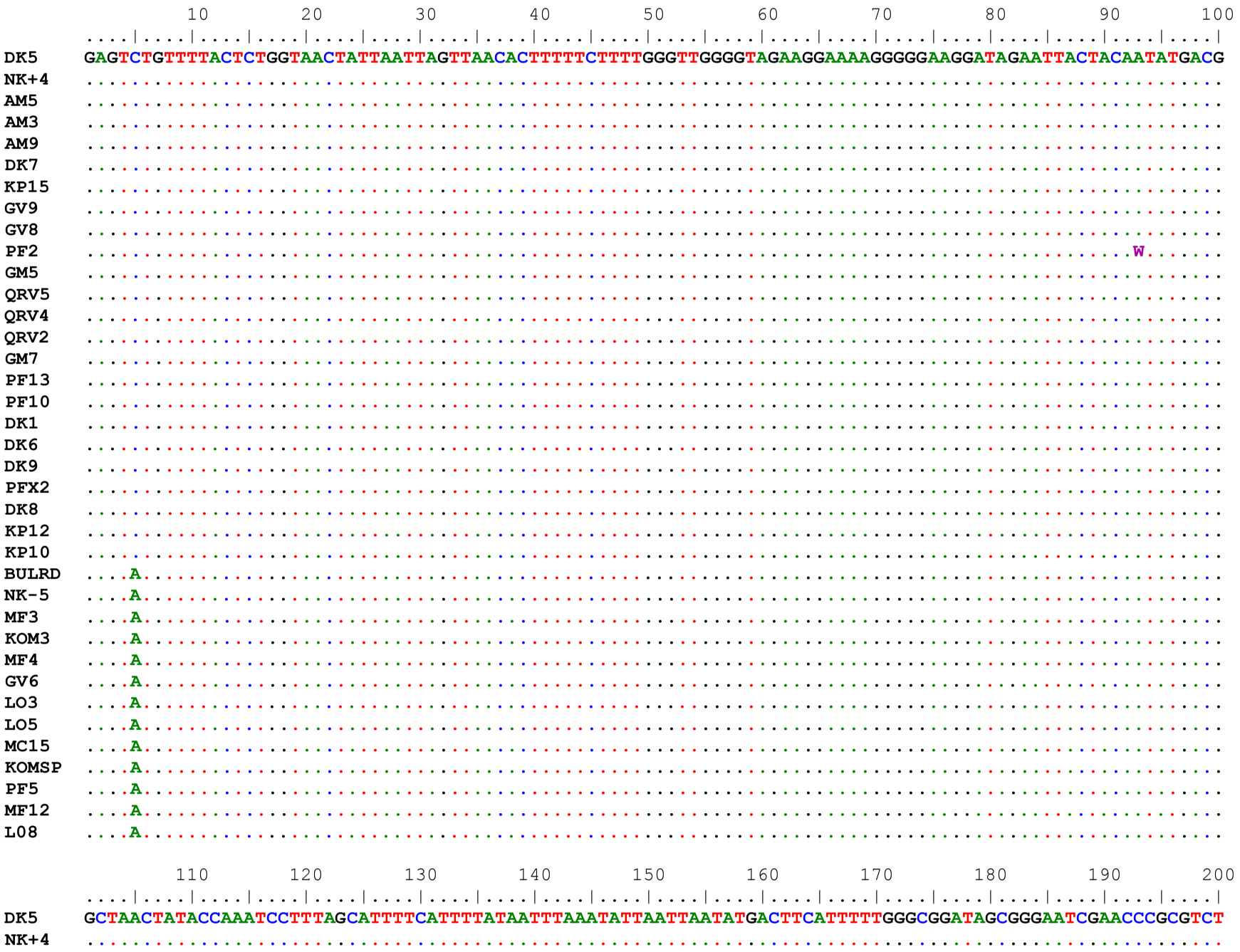

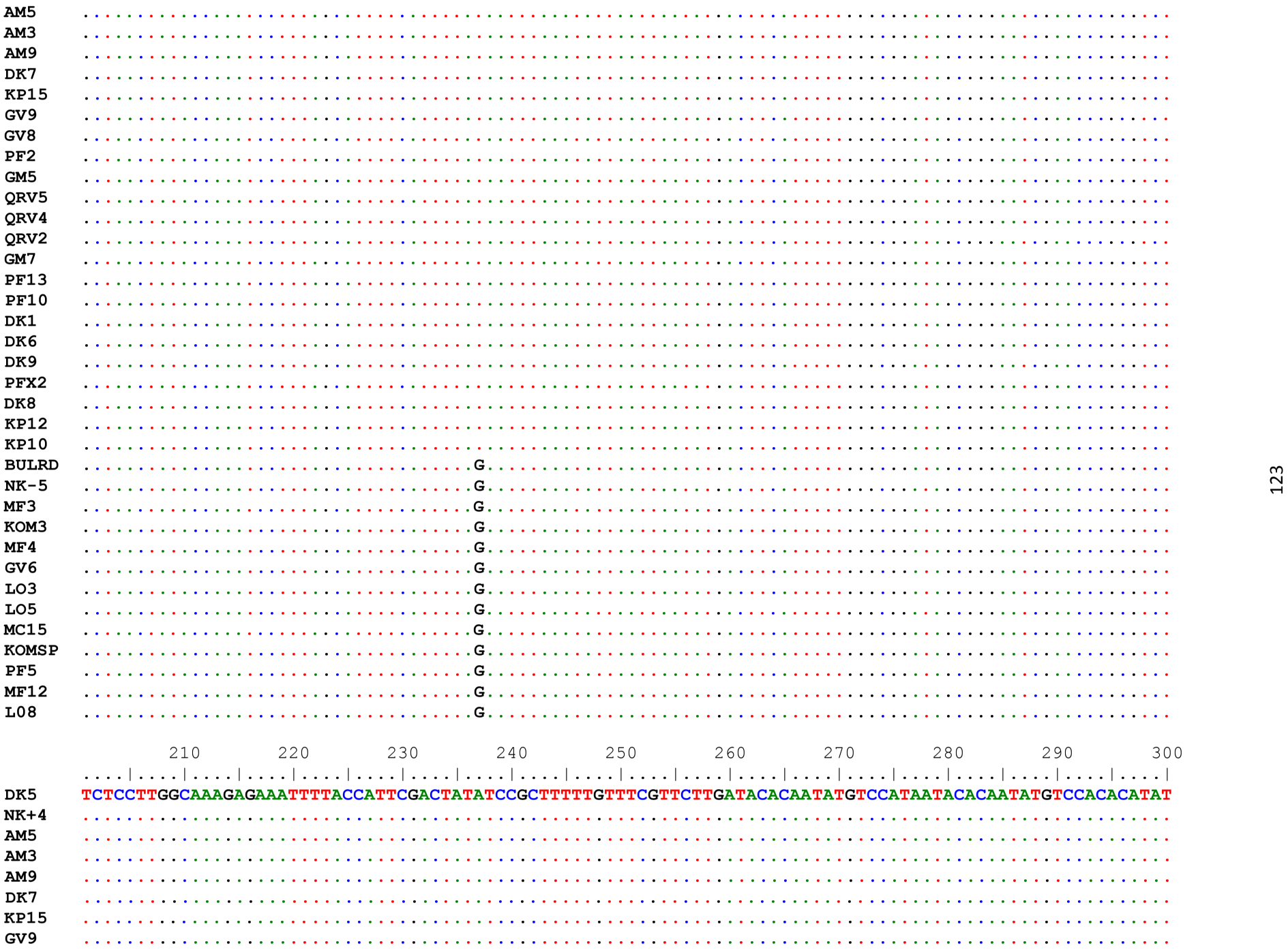
AM5
AM3
AM9
DK7
KP15
GV9
GV8
PF2
GM5
QRV5
QRV4
QRV2
GM7
PF13
PF10
DK1
DK6
DK9
PFX2
DK8
KP12
KP10
BULRD
NK-5
MF3
KOM3
MF4
GV6
LO3
LO5
MC15
KOMSP
PF5
MF12
L08
210
220
230
240
250
260
270
280
290
300
DK5
TCTCCTTGGCAAAGAGAAATTTTACCATTCGACTATATCCGCTTTTTGTTTCGTTCTTGATACACAATATGTCCATAATACACAATATGTCCACACATAT
NK+4
AM5
AM3
AM9
DK7
KP15
GV9


GV8
PF2
GM5
QRV5
QRV4
QRV2
GM7
PF13
PF10
DK1
DK6
DK9
PFX2
DK8
KP12
KP10
BULRD
NK-5
MF3
KOM3
MF4
GV6
LO3
LO5
MC15
KOMSP
PF5
MF12
L08
310
320
330
340
350
360
370
380
390
400
DK5 ATGATATATATGTCTGGAGCATATTTGTGCAGTGCTGGACCGGAGACTCTCTTCAGATTGAGCCAAAATTTTTTATTAATTTTAATTTTTTTTTCAGGAA
NK+4
AM5
AM3
AM9
DK7
KP15
GV9
GV8
PF2
GM5
QRV5
QRV4
QRV2


GM7
PF13
PF10
DK1
DK6
DK9
PFX2
DK8
KP12
KP10
BULRD
NK-5
MF3
KOM3
MF4
GV6
LO3
LO5
MC15
KOMSP
PF5
MF12
L08
410
420
430
440
450
460
470
480
490
500
DK5
CAATAAGTTTGACCCCCCTTCTAATTTTTCTTATATTTATTTGGATTTTGGGAACGTATATTGAATGTGAATGTGTCTCACAACCAAGAATAATTCAGAG
NK+4
AM5
AM3
AM9
DK7
KP15
GV9
GV8
PF2
GM5
QRV5
QRV4
QRV2
GM7
PF13
PF10
DK1
DK6
DK9


PFX2
DK8
KP12
KP10
BULRD
NK-5
MF3
KOM3
MF4
GV6
LO3
LO5
MC15
KOMSP
PF5
MF12
L08
510
520
530
540
550
560
570
580
590
600
DK5 GGTCATTTTGGTTTTTGATCTCGGACAATAGGTTCAAGAGATAAGAGAATTAAGGATACCCACCAAAAAGACTAATCCAATCCATAATGATGTACCTGAA
NK+4
AM5
AM3
AM9
DK7
KP15
GV9
GV8
PF2
GM5
QRV5
QRV4
QRV2
GM7
PF13
PF10
DK1
DK6
DK9
PFX2
DK8
KP12
KP10
BULRD
NK-5

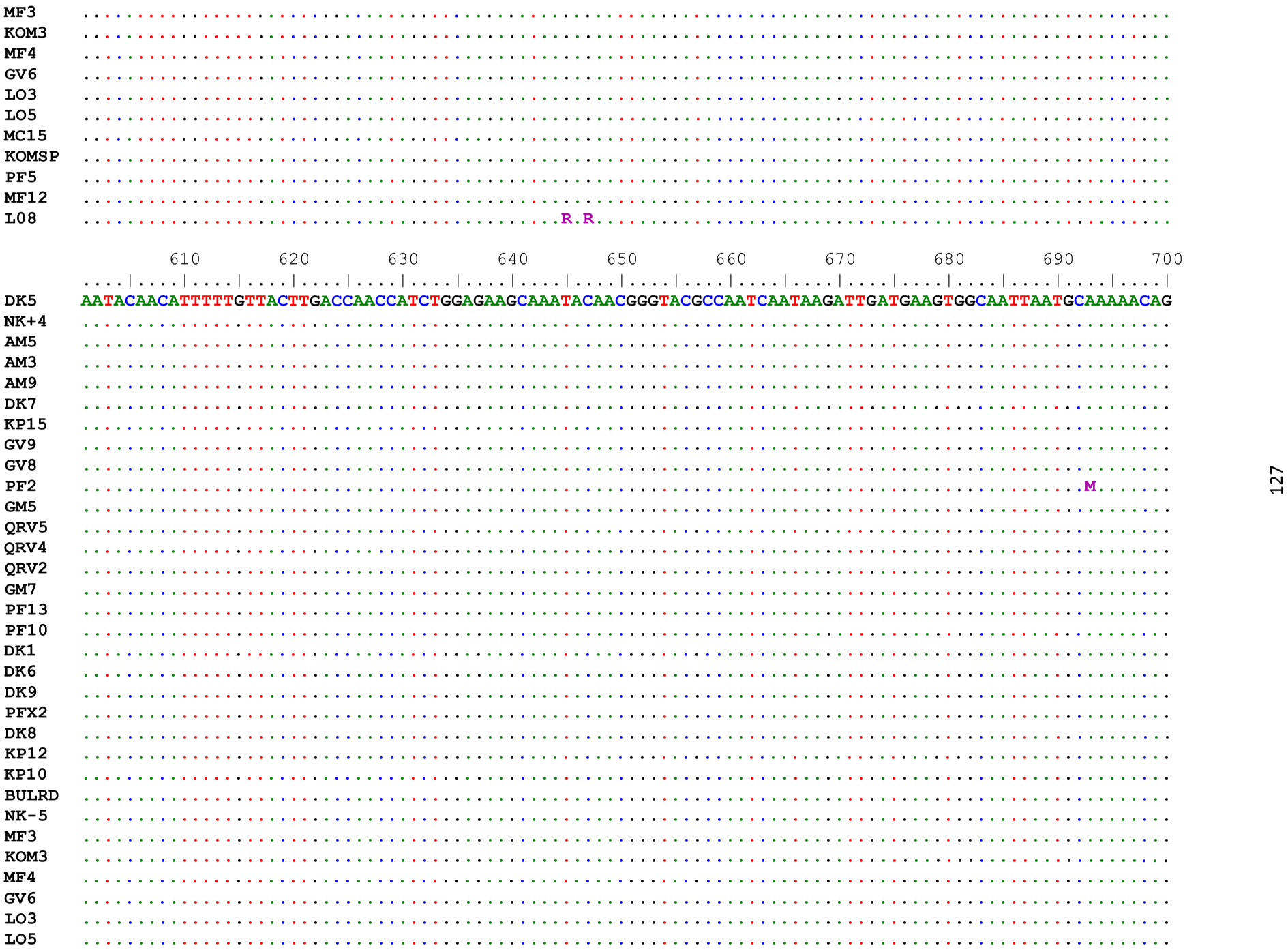
MF3
KOM3
MF4
GV6
LO3
LO5
MC15
KOMSP
PF5
MF12
L08
R R
610 620 630 640 650 660 670 680 690 700
DK5 AATACAACATTTTTGTTACTTGACCAACCATCTGGAGAAGCAAATACAACGGGTACGCCAATCAATAAGATTGATGAAGTGGCAATTAATGCAAAAACAG
NK+4
AM5
AM3
AM9
DK7
KP15
GV9
GV8
PF2
M
GM5
QRV5
QRV4
QRV2
GM7
PF13
PF10
DK1
DK6
DK9
PFX2
DK8
KP12
KP10
BULRD
NK-5
MF3
KOM3
MF4
GV6
LO3
LO5

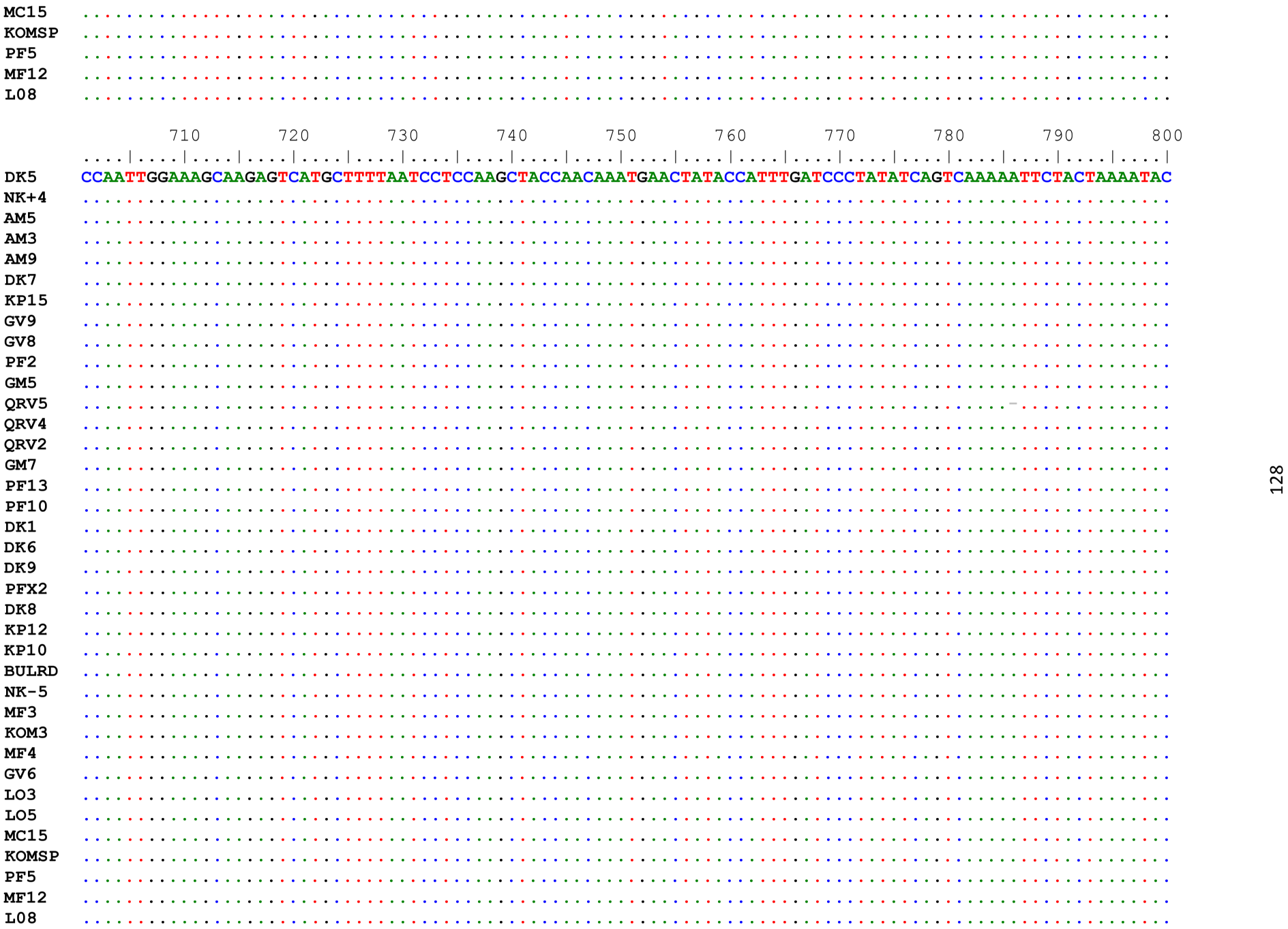
MC15
KOMSP
PF5
MF12
L08
710
720
730
740
750
760
770
780
790
800
DK5 CCAATTGGAAAGCAAGAGTCATGCTTTTAATCCTCCAAGCTACCAACAAATGAACTATACCATTTGATCCCTATATCAGTCAAAAATTCTACTAAAATAC
NK+4
AM5
AM3
AM9
DK7
KP15
GV9
GV8
PF2
GM5
QRV5
QRV4
QRV2
GM7
PF13
PF10
DK1
DK6
DK9
PFX2
DK8
KP12
KP10
BULRD
NK-5
MF3
KOM3
MF4
GV6
LO3
LO5
MC15
KOMSP
PF5
MF12
L08

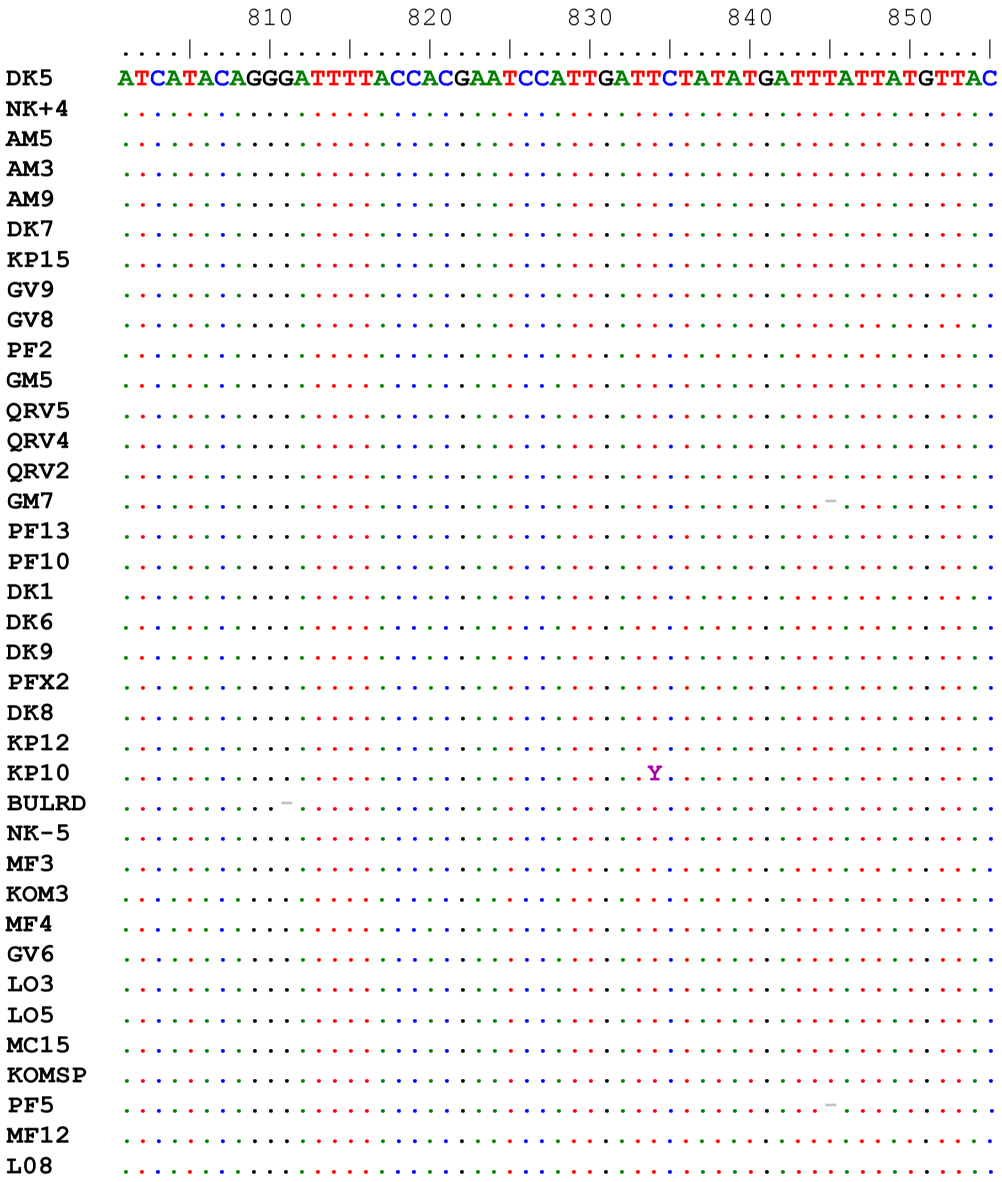
810
820
830
840
850
DK5 ATCATACAGGGATTTTACCACGAATCCATTGATTCTATATGATTTATTATGTTAC
NK+4
AM5
AM3
AM9
DK7
KP15
GV9
GV8
PF2
GM5
QRV5
QRV4
QRV2
GM7
PF13
PF10
DK1
DK6
DK9
PFX2
DK8
KP12
KP10
BULRD
NK-5
MF3
KOM3
MF4
GV6
LO3
LO5
MC15
KOMSP
PF5
MF12
L08

Appendix 3: Ni content in soil samples (n = 3) collected from Kaapsehoop (KP), Agnus Mine (AM), Nkomazi soil around hyperaccumulator occurrence (NK+), Galaxy Mine (GM), Nkomazi soil around non-accumulator occurrence (NK-) and Pullen Farm (PF).

Sample name	Ni content (ppm)	Average Ni (ppm)	Standard deviation
KP	3388	3725.67	412.19
	4185		
	3604		
AM	1682	1789.33	163.08
	1977		
	1709		
NK+	1598	1650	214.13
	1783		
	1569		
GM	915	1196	391.36
	1643		
	1030		
NK-	1097	1166.33	96.86
	1277		
	1125		
PF	130	59.87	62.01
	12.3		
	37.3		

Appendix 4: Ni content in ashed leaf samples collected from Kaapsehoop (KP), Agnus Mine (AM), Nkomazi soil around hyperaccumulator occurrence (NK+), Galaxy Mine (GM), Nkomazi soil around non-accumulator occurrence (NK-) and Pullen Farm (PF).

Sample name	Ni content (ppm)	Average Ni (ppm)	Standard deviation
KP	6231.28	5910.91	753.30
	5050.38		
	6451.08		
AM	4993	6344	1694.33
	5794		
	8245		
NK+	1318.5	4124.37	2560.99
	4718.62		
	6336		
GM	73.5	106.17	28.33
	124		
	121		
NK-	98.1	131.03	29.25
	141		
	154		
PF	2.74	2.92	0.17
	2.97		
	3.06		

Appendix 5: List of unique TrnfM haplotype sequences (n = 15) with respect to sample locality.

Haplotype number	Sample site(s) containing haplotype(s)
1	DK, NK+, AM, KP, PFX
2	AM
3	DK, KP
4	GV, PF, QRV, GM
5	GV
6	GV, PF
7	PF
8	DK, KP, PFX
9	KP
10	BUL
11	GV, PF, LO, MF, KOM, MC, NK-
12	PF, KOM
13	MF
14	LO
15	LO

Appendix 6: The distribution of TrnfM haplotypes across *Senecio coronatus* ecotypes.

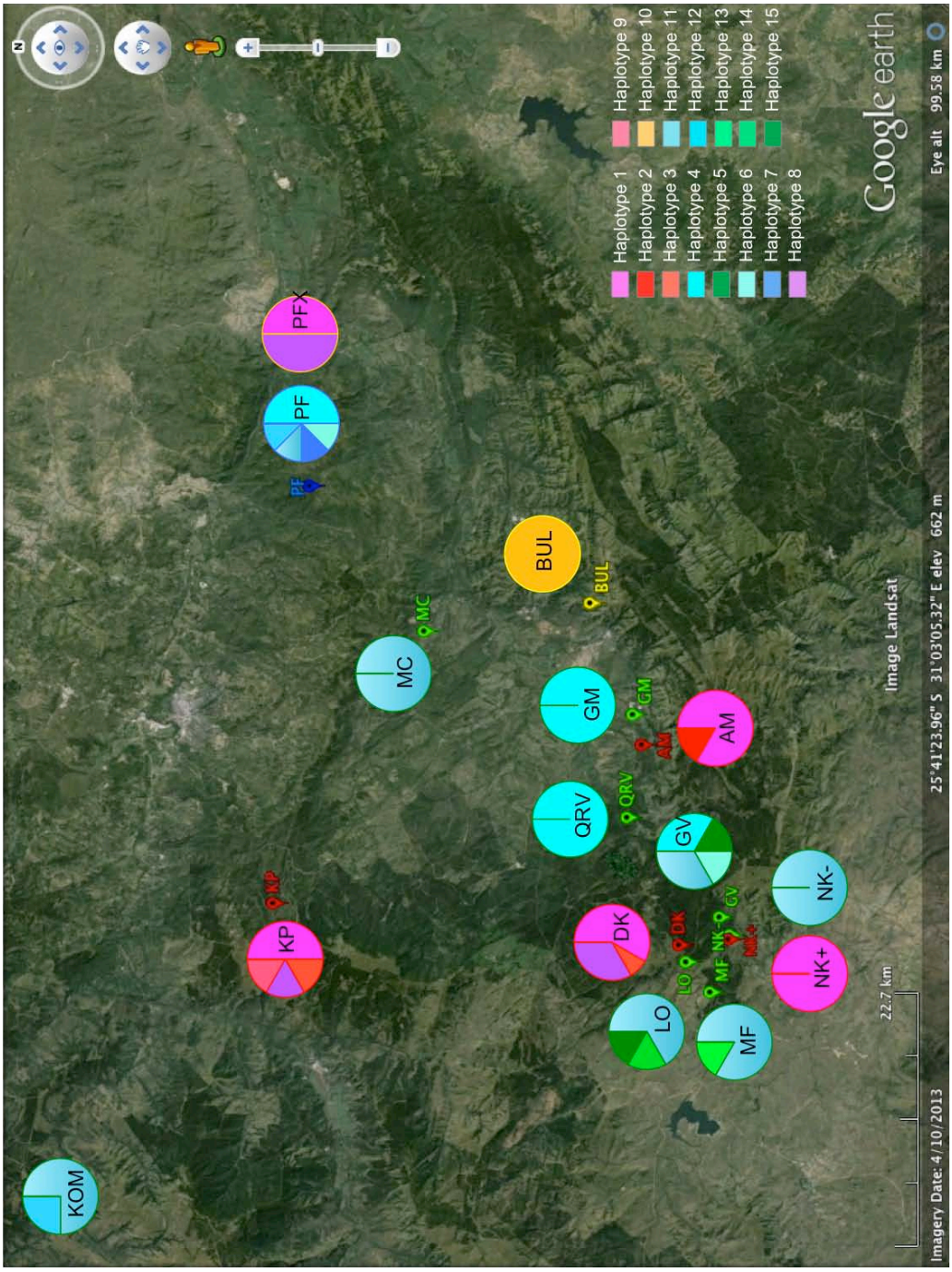

Pie charts represent the presence (by colour) and frequency (%) of a specific haplotype within that population. Sample name indicate Ni hyperaccumulating (red), Ni non-accumulating on serpentine soil (green) and non-accumulating plants on non-serpentine soil (blue), respectively.

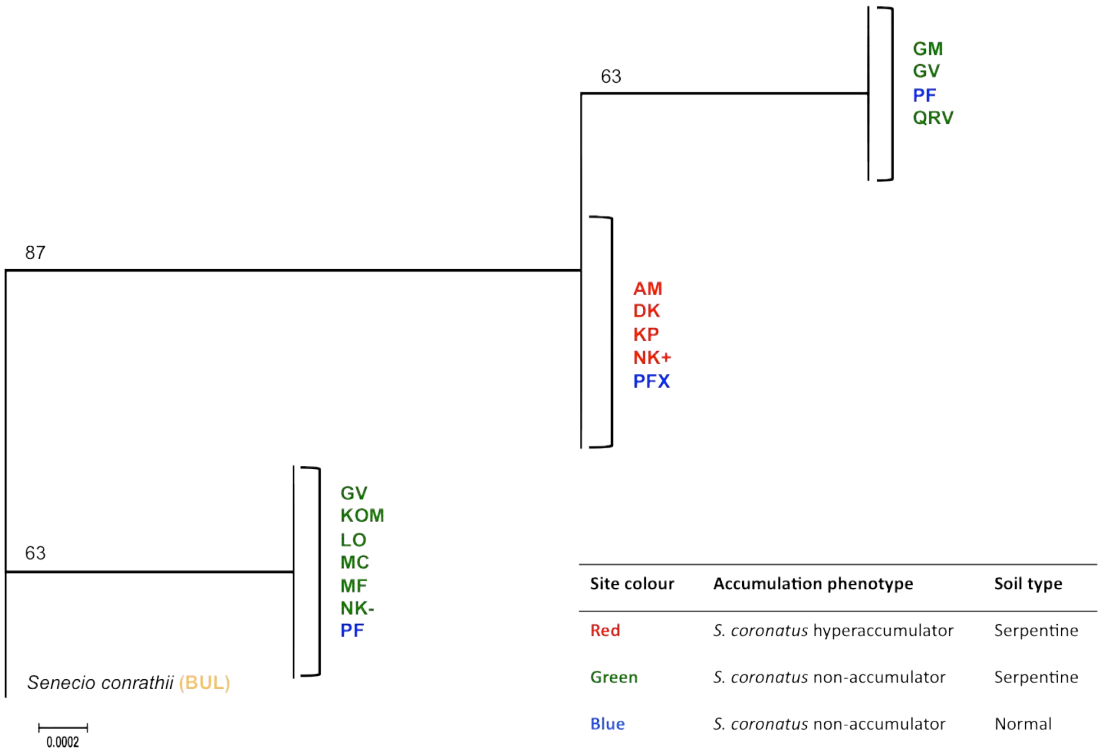

Site colour	Accumulation phenotype	Soil type
Red	*S. coronatus* hyperaccumulator	Serpentine
Green	*S. coronatus* non-accumulator	Serpentine
Blue	*S. coronatus* non-accumulator	Normal
Orange	*S. conrathii* non-accumulator	Normal

Appendix 7: Neighbor-joining phylogram of TrnfM sequences based on Kimura 2-parameter (corrected d-distance). All positions containing gaps or missing data were deleted, resulting in a final data set of 845 positions. The tree is to scale, where branch length is in the same units as those of the evolutionary distances used to infer the phylogenetic tree. The accuracy of the tree generated was evaluated by a bootstrap test (10 000 replicates), where the percentage of replicate trees associated with a given clade is shown at branch nodes. Only bootstrap values over 50% are shown. The tree is rooted with *S. conrathii*. Sample name indicate Ni hyperaccumulating (red), Ni non-accumulating on serpentine soil (green) and non-accumulating plants on non-serpentine soil (blue), respectively.

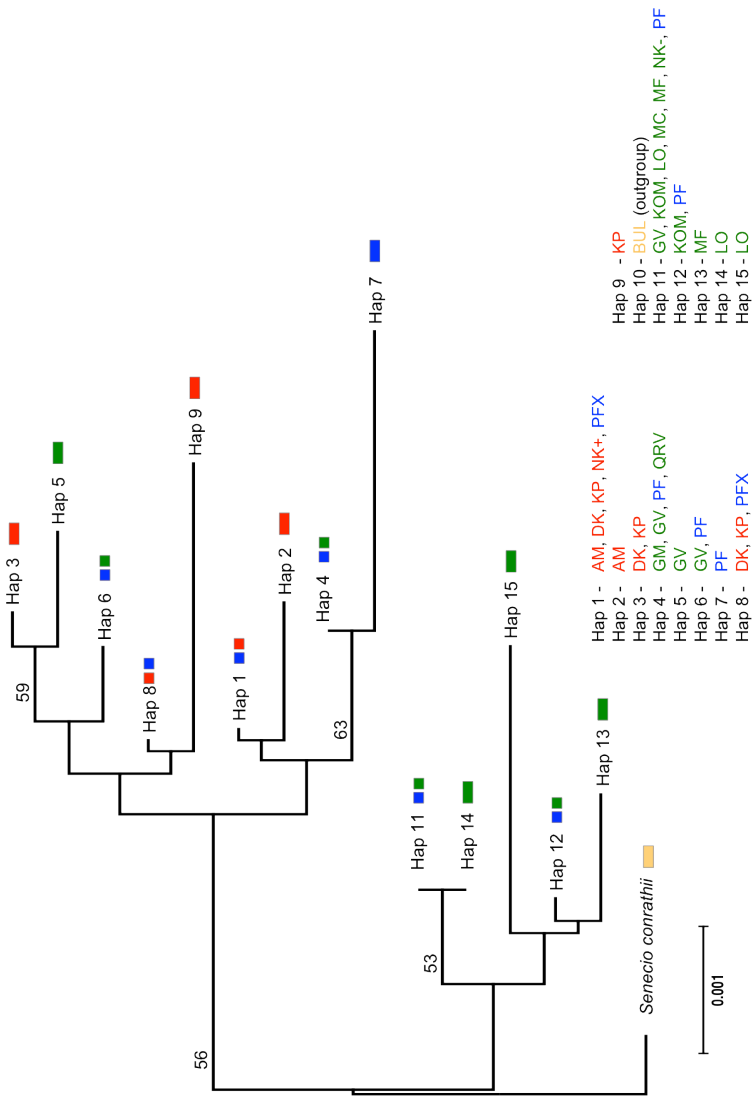

Appendix 8: Neighbor-joining phylogram of unique TrnfM haplotypes. All positions containing gaps or missing data were deleted, resulting in a final data set of 853 positions. The tree is to scale, where branch length is in the same units as those of the evolutionary distances used to infer the phylogenetic tree. The accuracy of the tree generated was evaluated by a bootstrap test (10 000 replicates), where the percentage of replicate trees associated with a given clade is shown at branch nodes. Only bootstrap values over 50% are shown. The tree was rooted with *S. conrathii*.